The Thesis Committee for Parviz Qadir Allahverdiyev
Certifies that this is the approved version of the following thesis:

Improved sweep efficiency through seismic wave stimulation

APPROVED BY
SUPERVISING COMMITTEE:

Supervisor:

Larry W. Lake

Chun Huh

Improved sweep efficiency through seismic wave stimulation

by

Parviz Qadir Allahverdiyev, B.S.

Thesis

Presented to the Faculty of the Graduate School of

The University of Texas at Austin

in Partial Fulfillment

of the Requirements

for the Degree of

Master of Science in Engineering

The University of Texas at Austin

August 2012

Dedication

This thesis is dedicated to my mother, Aytakin Allahverdiyeva, father, Qadir Allahverdiyev, brother, Ilkin Allahverdiyev, and my wife, Antiqa Taghiyeva Allahverdiyeva.

Acknowledgements

I express my deep gratitude to my supervisor and advisor, Dr. Larry W. Lake, for his valuable recommendations and advice throughout my studies in the Petroleum and Geosystems Engineering department at the University of Texas at Austin. It has been my pleasure to work under his supervision.

I wish to thank Dr. Chun Huh for our regular technical meetings, which were extremely useful throughout my studies.

I am also thankful to Dr. Chanseok Jeong for our meetings, and the time he spent on reviewing my work.

Last but not least, I am thankful to my family members, especially my wife Antiqa Taghiyeva Allahverdiyeva for their endless love and support during my studies.

Abstract

Improved sweep efficiency through seismic wave stimulation

Parviz Qadir Allahverdiyev M.S.E.

The University of Texas at Austin, 2012

Supervisor: Larry W. Lake

Enhanced oil recovery as a result of earthquake events has been repeatedly observed and reported. The main advantage of a seismic wave-based EOR is that it is not costly and is easy to deploy. However, the method has not yet been fully investigated; the production enhancement mechanisms need to be identified and confirmed. This thesis shows a possible production mechanism and preliminary estimate of incremental oil recovery due to seismic wave stimulation. The production mechanism is improved sweep efficiency through viscous cross-flow between different permeability layers of a reservoir as a result of fluid pressure oscillations. In this thesis, we studied a possible viscous cross-flow generation between a fracture and a rock matrix of a fractured reservoir model as a result of fluid pressure oscillations. We considered time-harmonic water flooding as a way of sending seismic waves to the reservoir model. To calculate a cross-flow pressure gradient, we investigated oscillatory pressure propagation equations within the rock matrix and the fracture of the reservoir model. According to our results, the volume of the

mobilized oil because of the time-harmonic water flooding during one day of stimulation from the fractured reservoir model is in the order of several barrels.

Table of Contents

List of Tables xi

List of Figures xiii

Chapter 1: Introduction 1

Chapter 2: Literature review 4

2.1 Introduction 4

2.2 Observations 4

2.3 Possible production mechanisms 6

2.4 Laboratory experiments 10

2.5 Field applications 15

2.5.1 Field applications in the US 15

2.5.2 Filed applications in the former USSR area 21

2.5.3 Field applications in China 24

2.5.4 Field application in Indonesia 26

2.5.5 Summary 27

2.6 Conclusions 29

Chapter 3: Viscous cross-flow 30

3.1 Introduction 30

3.2 Defining the problem 31

3.2.1 Reservoir model 31

3.2.2 Time-harmonic water flooding 33

3.2.3 Pressure transient equation for a flow within the fracture 34

3.2.4 Pressure transient equation for a flow within the rock matrix 39

3.3 Derivation of the pressure oscillation equations 41

3.3.1 A review of the derivation procedure 41

3.3.2 The incremental fracture pressure without a cross-flow. 42

3.3.3 The rock matrix fluid pressure 47

3.3.4 The incremental fracture pressure with a cross-flow 49

3.3.5 Volume of mobilized oil 51

3.3.5.1 Cross-flow rate 52
3.3.5.2 Volume of mobilized oil 54
3.3.5.3 Oil fractional flow from the rock matrix to the fracture 54
3.3.6 Summary 56
3.4 Dimensionless analysis 57
3.4.1 Dependent and independent variables 57
3.4.2 Inspectional analysis 58
3.4.3 Summary 64
3.5 Conclusions 65

Chapter 4: Example calculation and sensitivity analysis 66
4.1 Introduction 66
4.2 Example calculation 66
4.2.1 Example calculation steps 66
4.2.2 Incremental fracture pressure distribution 69
4.2.3 Incremental rock matrix pressure distribution 71
4.2.4 Cross-flow rate 74
4.2.5 Volume of the mobilized oil 76
4.3 Sensitivity analysis 76
4.3.1 Stimulation frequency 76
4.3.2 Incremental water injection rate amplitude 79
4.3.3 Fracture dimensions and properties 82
4.3.3.1 Fracture dimensions 82
4.3.3.2 Fracture properties 85
4.3.4 Rock matrix properties 88
4.3.5 Oil viscosity 94
4.3.6 Fractional flow of oil 95
4.4 Comparison with the field data 96
4.5 Conclusions 97

Chapter 5: Conclusion.....99

Appendix A.....101

Appendix B.....107

References.....110

List of Tables

Table 2-1: Summary of the field application of seismic EOR.....28

Table 3-1: Dimensionless groups of the problem.....61

Table 3-2: Scaling factors of the problem.....61

Table 4-1: Data used in the example calculation.....68

Table 4-2: Volume of the mobilized oil for stimulation frequencies of 0.1, 2, 5 and 10 Hz.....79

Table 4-3: Volume of mobilized oil for incremental water injection rate amplitudes of 5, 10, 15, and 20 barrels/day.....81

Table 4-4: Volume of the mobilized oil from the reservoir model of Figure 3-1 for fracture aperture values of 0.0005, 0.001, and 0.005 meters.....84

Table 4-5: Volume of the mobilized oil for fracture absolute permeability values of 50, 100, 400, and 800 Darcy.....88

Table 4-6: Volume of the mobilized oil for total rock matrix compressibility values of 0.0147, 0.147, 0.735, and 1.47 1/GPa.....90

Table 4-7: Volume of the mobilized oil for rock matrix absolute permeability values of 1, 10, 100, and 1,000 md.....92

Table 4-8: Volume of the mobilized oil for rock matrix porosity values of 0.05, 0.1, 0.2, and 0.4.....93

Table 4-9: Volume of the mobilized oil for oil viscosity values of 1, 5, 20, and 50 cp 95

Table 4-10: Volume of the mobilized oil for oil fractional flow values of 0.4, 0.6, 0.8, and 1.....96

Table 4-11: Actual and estimated oil production for 4 field application of seismic EOR. All numbers are approximate.....97

List of Figures

Figure 2-1: TCE production rate versus time for 7 separate experimental runs (from Roberts et al., 2001) 14

Figure 2-2: Oil cut history for operator 1's wells in the Lost Hills reservoir (from Kostrov and Wooden, 2005) 16

Figure 2-3: Oil production rate versus cumulative oil produced for operator 1's wells in the Lost Hills reservoir. The plot was made using the production rate versus time plot given in Kostrov and Wooden (2005) 17

Figure 2-4: Oil production rate and water cut history for the Elk Hills oil field (from Kostrov and Wooden, 2005) 18

Figure 2-5: Oil production rate versus cumulative oil produced for the Elk Hills oil field. The plot was made using the oil production rate history plot given in Kostrov and Wooden, 2005. 19

Figure 2-6: Oil production rate response of the Sharon Ridge field (from Marshall et al., 2011) 20

Figure 2-7: Oil production rate versus cumulative oil produced for the Sharon Ridge field. The plot was made using the oil production rate history plot given in Marshall et al. (2011). 21

Figure 2-8: Oil production rate versus cumulative oil production for 23 wells of the Liaohe field. The plot was made using the oil production rate versus time plot given in Zhu et al. (2005). 25

Figure 2-9: Oil production rate versus cumulative oil produced for the Cha39 area of the Huabei field. The plot was made using the oil production rate history plot given in Zhu et al. (2005). 26

Figure2-10: Oil production rate versus cumulative oil produced for Tilan field. The plot was made using the oil rate history plot given in Barabanov and Pavlov (2009).....27
Figure 2-11: Summary scheme showing types of seismic EOR and possible production mechanisms suggested in the literature 29
Figure 3-1: Schematics of the fractured reservoir model. The fracture width is exaggerated for illustration. 32
Figure 4-1: Absolute value of the one-dimensional incremental fracture pressure distribution 69
Figure 4-2: Change of incremental fracture pressure with time at 1, 5, 10, 20 m from the injector 70
Figure 4-3: Incremental fracture pressure distribution at 1, 2, 3, 6, 7, and 8 seconds of the stimulation.....71
Figure 4-4: Absolute value of the incremental rock matrix pressure amplitude distribution 72
Figure 4-5: Real part of the incremental rock matrix pressure distribution at t=2 seconds.....73
Figure 4-6: Real part of the incremental rock matrix pressure distribution at t=6 seconds.....74
Figure 4-7: Absolute value of the cross-flow rate amplitude distribution with x at the interface of the rock matrix and the fracture.....75
Figure 4-8: Change of cross-flow rate with time at x=1, 5, 10, and 20 meters 75
Figure 4-9: Absolute value of the incremental fracture pressure amplitude distribution for stimulation frequencies of 0.1, 2, 5, and 10 Hz.....77

Figure 4-10: Absolute value of the cross-flow rate amplitude distribution for stimulation frequencies of 0.1, 2, 5, and 10 Hz 78
Figure 4-11: Absolute value of the incremental fracture pressure distribution for incremental water injection rate amplitudes of 5, 10, 15 and 20 barrels/day.....80
Figure 4-12: Absolute value of cross-flow rate amplitude distribution for incremental water injection rates of 5, 10, 15, and 20 barrels/day 81
Figure 4-13: Absolute value of the Incremental fracture pressure amplitude distribution for fracture heights of 3, 5, 10, and 20 meters.....82
Figure 4-14: Absolute value of fracture incremental pressure distribution for fracture aperture values of 0.0005, 0.001, and 0.005 meters 83
Figure 4-15: Cross-flow rate amplitude distribution for fracture apertures of 0.0005, 0.001, and 0.005 meters 84
Figure 4-16: Absolute value of the incremental fracture pressure distribution for total fracture compressibility values of 0.147, 14.7, and 7.35 1/GPa. 85
Figure 4-17: Absolute value of the cross-flow rate amplitude distribution for total fracture compressibility values of 0.147, 1.47, and 7.35 1/GPa 86
Figure 4-18: Absolute value of the incremental fracture pressure distribution for fracture absolute permeability values of 50, 100, 400, and 800 Darcy87
Figure 4-19: Absolute value of the cross-flow rate amplitude distribution for fracture absolute permeability values of 50, 100, 400, and 800 Darcy.....87
Figure 4-20: Absolute value of the incremental rock matrix pressure distribution for total rock matrix compressibility values of 0.0147, 0.147, 0.735, and 1.47 1/GPa.....89

Figure 4-21: Absolute value of the cross-flow rate amplitude distribution for total compressibility values of 0.0147, 0.147, 0.735, and 1.47 1/GPa.....90
Figure 4-22: Absolute value of the incremental rock matrix pressure distribution for rock matrix absolute permeability values of 1, 10, 100, and 1,000 md91
Figure 4-23: Absolute value of the cross-flow rate amplitude distribution for rock matrix absolute permeability values of 1, 10, 100, and 1,000 md 91
Figure 4-24: Absolute value of the incremental fracture pressure amplitude distribution for rock matrix porosities of 0.05, 0.1, 0.2 and 0.4 92
Figure 4-25: Absolute value of the cross-flow rate amplitude distribution for rock matrix porosities of 0.05, 0.1, 0.2, and 0.4 93
Figure 4-26: Absolute value of the incremental fracture pressure amplitude distribution for oil viscosity values of 1, 5, 20, and 50 cp.....94
Figure 4-27: Absolute value of the cross-flow rate amplitude distribution for oil viscosity values of 1, 5, 20, and 50 cp. 95
Figure A-1: Top view of the fracture of Figure 3-1b.....101

Chapter 1: Introduction

Enhanced Oil Recovery (EOR) methods are becoming a popular research area in petroleum engineering. Given that only 20-60% of oil originally in place is recovered using primary and secondary recovery methods, new enhanced oil recovery methods (EOR) are being investigated and developed to increase recovery efficiency.

Despite the availability of several EOR methods mostly CO_2 and thermal EOR methods are being applied in a field scale. A new EOR method is needed that can be applied in a field scale with zero environmental damage and low cost. The method we are proposing in this thesis is EOR through application of elastic waves. The method has no environmental damage and is cheap compared to the other EOR methods. We mostly concentrate on the application of low frequency, seismic EOR.

Interest in the topic began when enhancement of oil production rate was observed during elastic wave generating events such as earthquakes or nearby train passage (Beresnev and Johnson, 1994). Several possible pore scale and reservoir scale production mechanisms were suggested in the literature. The pore scale production mechanisms include coalescence of oil ganglia to form bigger ganglia that are more mobile, detachment of oil ganglia from the pore walls, and destruction of water films blocking pore throats. The possible macro scale production mechanisms include generation of a cross-flow, accelerated degassing of undersaturated reservoirs, changing wettability and relative permeability of a reservoir rock under seismic stimulation.

In this thesis, we concentrate on the idea of the cross-flow generation under seismic wave stimulation that would improve sweep efficiency of highly heterogeneous and fractured reservoirs. The mechanism was first introduced by White et al. (1975) and further investigated by Huh (2006), Jeong et al. (2011), and Jeong (2011). We attempt to investigate a cross-flow pressure gradient generated by the fluid pressure oscillations in a fractured reservoir model, and calculate the volume of mobilized oil because of the stimulation for a given rock matrix, fracture, reservoir fluid properties and stimulation frequency. We use pressure oscillation equations originally given in Jeong et al. (2011) that are solutions of pressure transient equations for a flow in a rock matrix and a fracture for oscillatory fluid pressures.

This thesis consists of 5 chapters. Chapter 1 introduces the seismic stimulation and gives an outline of the thesis. Chapter 2 performs a literature survey on the seismic EOR with more emphasis on the field scale applications of the method.

Chapter 3 investigates the cross-flow generation in a single-fractured reservoir model under seismic wave stimulation. We give a description of the fractured reservoir model along with the derivation of the pressure oscillation equations originally given in Jeong et al. (2011). We also perform inspectional analysis to transform the whole problem into dimensionless form.

Chapter 4 provides an example calculation of the incremental fracture and rock matrix pressures, and cross-flow rate as a result of the seismic wave stimulation using the pressure propagation equations. We also investigate the sensitivity of the incremental fracture pressure and volume of mobilized oil as a result of the seismic wave stimulation

to the reservoir fluid properties, rock matrix properties, fracture properties, fracture dimensions, stimulation frequency, and incremental water injection rate amplitude.

Chapter 5 provides a summary of the thesis, the conclusion, and recommendations for future work.

Chapter 2: Literature review

2.1 Introduction

This chapter reviews publications on elastic wave based EOR with more emphasis on field scale applications of the method. We mostly concentrate on studies of seismic stimulation. We also provide a brief literature survey about high-frequency stimulation. This chapter consists of six sections. The first section gives a brief summary of this chapter. The second section summarizes observations of changes in formation pressure and hydrocarbon production rate as a result of elastic wave generating events. The third section provides information on possible mechanisms that could be influenced by elastic waves to enhance oil recovery. The fourth section talks about results of laboratory experiments studying effects of seismic and ultrasonic waves on oil production rate. The fifth section discusses field scale applications of seismic EOR with oil production rate responses of the fields. The last section gives a summary of this chapter.

2.2 Observations

Interest in elastic wave based EOR originated from observations of oil production rate enhancement during earthquakes, passing of nearby trains and other elastic wave generating events (Beresnev and Johnson 1994). An increase in formation pressure as a result of elastic wave generating events was reported in the US as early as in 1950 by Parker and Stringfield (1950) who reported an increase in the water level of some wells in Florida during earthquakes. They also reported observations about occasional increase

in fluid level of some wells that are close to the railways. Large trains, causing more noise and vibration, affected fluid level of the wells more than the small trains. The fluid level goes down to its original level after the trains passed.

Steinbrugge and Moran (1954) studied the consequences of the California earthquake of July 21, 1952. The study also covers the effects of the earthquake on the oil and gas production rate of the area. Production variations in the Tejon Ranch, Kern River and Fruitvale fields were the greatest. A rise in casing pressure was observed in several wells of Tajon Ranch field. The pressure increases were as large as tenfold, but effects were not permanent. The rise in casing pressures were fast and followed by a slow decline to the approximately 20% below the original value, which then was followed by slow pressure build ups.

Eckel (1970) gives information on the hydrologic effects of the Alaskan earthquake of March 27, 1964. Water levels of many artesian wells changed as a result of the earthquake. In some cases, the level change is as much as 15 feet.

Beresnev and Johnson published a review of early observations of production enhancement as a result of seismic wave generating events, production mechanisms and laboratory studies of seismic wave stimulation. (Beresnev and Johnson, 1994). The following review of the production enhancement observations as a result of earthquakes in Caucasus is from Beresnev and Johnson (1994).

Voytov et al. (1972) reported an increase in oil production rate of the oil fields in Daghestan following the earthquake of May 14, 1970. Osika (1981) reported the effects of the earthquake of 1966 in the Caucasus in the fields of Abino-Ukrainskaya and

Kolodeznoye. Not all wells responded to the earthquake. Smirnova (1968) reported an effect of an earthquake on the oil production rate in the Gudermos field in the northern Caucasus. All of the wells showed an increased oil production rate as a result of an elastic wave generating event or earthquake. The longest effect lasted for a month.

2.3 POSSIBLE PRODUCTION MECHANISMS

White et al. (1975) brought up the idea of cross-flow between rocks of different permeability under low-frequency seismic waves. Their rock model consists of several layers, which were alternately saturated with water and gas. The authors investigated the case of applying seismic waves from the bottom and the top of the rock model. They analytically showed that a cross-flow pressure gradient would be generated between different permeability and fluid saturation layers under seismic wave excitation. The difference between the layer pressures depended on the compressibility of the saturating fluids, and elastic constants of the layers.

Huh (2006) investigated possible production mechanisms of seismic wave stimulation. The author first investigated the possibility of producing residual oil saturation to water flooding by rock stress propagation. Calculation of the recovery of the residual oil saturation is carried out assuming a reservoir model consisting of randomly oriented capillary tubes. He showed that a significant rock displacement is required to produce a small fraction of residual oil saturation. Generating such a rock displacement would be very difficult. Therefore the author suggested improved sweep efficiency to be

dominant production mechanism of the low-frequency wave based EOR rather than mobilizing of residual oil to water flooding.

Huh (2006) also studied the possibility of generating cross-flow between different permeability layers as rock stress propagates through the layers. The author gives analytical solutions for the pressure difference between high and low permeability layers induced by rock stress propagation. The analytical solution that takes into account two-phase flow between the parallel layers shows that the magnitude of the pressure difference between the layers, the cross-flow rate gradient depends on the fluid saturation, permeability and total compressibility of the reservoir rock, and rock elastic modulus. The author also mentioned the possibility of cross-flow generation through fluid pressure oscillations rather than rock stress propagation.

The idea of cross-flow pressure gradient generated by the fluid pressure oscillations was deeply investigated by Jeong et al. (2011) and Jeong (2011). They use time-harmonic water flooding as a way of sending low-frequency waves to a reservoir. Their work includes analytical solution of the pressure transient equations within a one-dimensional fracture and a two-dimensional rock matrix for fluid pressure oscillations.

This thesis concentrates on the pressure oscillation equations originally given by Jeong et al. (2011) to investigate pressure distributions within a rock matrix and a fracture during time-harmonic water flooding of a fractured reservoir model. This work also includes calculation of the viscous cross-flow rate at the interface of the rock matrix and the fracture, and volume of mobilized oil for a given fluid, rock matrix and fracture properties, fracture dimensions, and the stimulation frequency.

The rest of this section summarizes other production mechanisms of elastic wave based EOR suggested in the literature.

Early studies about fluid flow under elastic wave excitation were done by Duhon and Campbell (1965). Several processes that can be enhanced as a result of ultrasonic stimulation were suggested by the authors: cavitation, emulsification, coagulation, and chemical reactions. The cavitation effect of the ultrasonic energy was noted to be the most outstanding.

Cavitation is the formation of bubbles in a liquid as a result of ultrasonic energy. Compression makes bubbles implode which may produce tremendous pressure, on the order of several thousand atmospheres, which might be a major source of fluid flow enhancement under ultrasonic wave excitation. Field scale application of the method may not be feasible, because high frequency waves dampen quickly in a porous medium (Lopukhov and Nikolaevskii, 1995; Huh, 2006).

Kuznetsov et al. (1998) suggested three possible mechanisms to explain the effect of wave energy on fluid flow in porous medium. The first possible mechanism is that periodic movements of oil and water molecules within a porous medium make them more mobile by decreasing their degree of adherence to pore walls. The second possible mechanism is that the variable pressure gradient generated by the elastic wave destructs water films attached to the pore throats. This mechanism could lead to an increase in relative permeability to both oil and water. The authors suggest that the effect is bigger on oil relative permeability, because oil molecules are much larger than water molecules.

The third mechanism suggested by the authors is reduction in the interfacial tension and contact angle between oil and water by elastic waves.

Pride et al. (2008) suggested two conditions under which seismic stimulation would work. The first condition is that when a seismic wave pushes an oil ganglia through a pore throat the radius of the meniscus of downstream of the bubble should be reduced sufficiently to get through the pore throat. The second condition is that oil ganglia should have enough time during one cycle of the stimulation to get through a restriction before seismic wave forces would push it in the other direction.

Kostrov and Wooden (2002) describe two possible production mechanisms of seismic wave-based EOR. The first possible production mechanism is dislodgement of oil droplets from the pore walls making them mobile. This mechanism requires the attraction force of the elastic wave to be greater than adhesion force of oil molecules to the pore walls. The second suggested mechanism is coalescence of oil droplets to form larger droplets that have higher mobility. This mechanism requires the attraction force of elastic waves plus molecular attraction forces between oil molecules to be greater than force of static electrical repulsion of oil molecules.

Barabanov and Pavlov (2009) describe two possible production mechanisms. The first is a change of reservoir rock wettability towards neutrality through application of seismic waves. According to the paper seismic load leads to excitation of electromagnetic fields. This under favorable circumstances can change the wettability of an oil reservoir towards neutrality. The second possible mechanism described in the paper is generation of a vortex flow. They showed that the rock particles have linear trajectory with vertical

polarization very close to the vibration source. At some radial distance from the source the trajectory becomes circular. That distance is very sensitive to the vibration source frequency. In the areas where particles move in a circular trajectory vortex flow of water could be generated. The vortex flow could possibly detach oil films from the pore walls and make them mobile.

Kurlenya and Serdyukov (1999) investigated the impact of seismic waves on fluid properties of Yuzhno-Teterevsky oil reservoir of Russia. The authors observed a decrease in kinematic viscosity, density and an increase in initial boiling point of the produced oil. They suggested two mechanisms that can lead to the change of fluid properties as a result of seismic wave stimulation. The first mechanism is partial degassing of oil and water within the target formation. Serdyukov and Kurlenya (2007) provide more discussion of degassing of oil reservoirs under elastic wave stimulation. The second mechanism is removal of absorbed oil from the pore surface, which would increase the fraction of the heavy components within the oil.

2.4 LABORATORY EXPERIMENTS

Early laboratory experiments of the effect of elastic waves on fluid flow through permeable media were published by Duhon and Campbell (1965). Displacement of oil by water in sandstone core samples under ultrasonic stimulation was investigated. An increase in the oil recovery efficiency as a result of the ultrasonic wave energy was observed. The lower the stimulation frequency, the higher the final oil recovery efficiency was observed. The suggested production mechanisms based on the laboratory

experiments include pressure fluctuations that fracture the sand binding materials to increase number of interconnected flow channels (increased permeability of the core sample), and cavitation. Cavitation is discussed more in Section 2.3.

Hamidi et al. (2011) also studied the effects of ultrasonic waves on oil recovery from Berea sandstone cores. They concluded that high viscosity oil reservoir would benefit more from the ultrasonic wave stimulation than low viscosity oil reservoirs and that ultimate oil recovery does not depend on the ultrasonic stimulation frequency. They also concluded that water-wet low-viscosity reservoirs would benefit more from the ultrasonic wave stimulation than oil-wet low-viscosity reservoirs.

High frequency waves dampen quickly within a porous medium (Lopukhov and Nikolaevskii, 1995; Huh, 2006). Thus ultrasonic stimulation would be an appropriate method for near wellbore treatment rather than reservoir-scale stimulation method. Application of acoustic waves as a near wellbore treatment technique is also discussed in van der Bas et al. (2004).

The following review of the early laboratory experiments of the seismic wave stimulation is from Beresnev and Johnson (1994). Medlin et al. (1983) studied oil displacement by CO_2 in the presence of seismic waves of amplitude as low as 10^{-8} m and a frequency of 100 Hz. The experiment was done using sandstone core samples. During the stimulation the CO_2 flow rate reached its maximum of 0.18 cm^3/hour. The CO_2 flow rate ceased when excitation was turned off and recommenced when excitation was resumed. Ashiepkov (1989) studied oil flow rate through several core samples as a function of seismic wave intensity. Core samples with different permeability showed

different increases in oil production rate as wave intensity increased from 10^{-2} to 10^{3} W/m^2.

Simkin and Surguchev (1991), and Kouznetsov et al. (1998) studied the effects of seismic waves on gravitational separation rate, degassing of fluids in porous media, displacement of oil by gas-free water, and displacement of oil by CO_2 saturated water. In all laboratory experiments the frequency of the elastic wave stimulation was between 100-200Hz. Several observations were reported by the authors: enhancement of gravitational separation, degassing of fluids, change in relative permeability, and enhancement of oil displacement efficiency by gas-free and CO_2-saturated water. Each is reviewed below:

Enhancement of gravitational separation. A cylindrical sandpack was saturated with water and then the water was displaced by kerosene. Water was again injected into the sandpack until the kerosene saturation reached 50%. The sandpack was set vertically to observe gravitational separation of kerosene and water in the absence and presence of elastic waves. The gravitational separation under the elastic waves was 500 times faster than that in the absence of the elastic waves.

Degassing of fluids in the sandpack and change in relative permeability. Laboratory results of degassing of the CO_2 saturated water in the presence of the elastic waves was also reported by Simkin and Surguchev (1991), and Kouznetsov et al. (1998). The experiment was done using a sandstone sandpack. According to the results, elastic wave stimulation enhances degassing of the CO_2 saturated water. This process could affect oil and water relative permeability of the sandpack, because gas bubbles released

from the liquid may plug some pore throats and change the relative permeability to oil and water. Another experimental result reported by Simkin and Surguchev (1991) and Kouznetsov et al. (1998) investigated change in relative permeability to oil and water at gas saturations of 0% and 10%. . According to the results, at lower water saturations (0-40%), the presence of the gas lowers oil relative permeability, whereas at water saturations of above 50%, the presence of gas increases oil relative permeability.

Oil displacement by gas-free and CO_2-saturated water. Another experiment reported by Simkin and Surguchev (1991) and Kouznetsov et al. (1998) investigates oil displacement by gas-free water and CO_2-saturated water under elastic wave stimulation. Sandstone sandpack was used to perform the experiment. In both cases the presence of the elastic waves enhanced oil recovery from the sandpack.

Roberts et al. (2001) studied enhanced dense, nonaqueous-phase liquid (DNAPL) transport in a sand core under low frequency wave stimulation. The stimulation was performed using a specifically designed apparatus capable of providing dynamic stresses to the core sample at a certain frequency. The sand core was evacuated, then fully saturated with water and then with 7 ml of trichloroehylene (TCE). Water was injected through the core and produced at the outlet. The TCE concentration of the produced water was measured to calculated TCE production rate. The apparatus was turned on and off periodically to observe change in TCE production rate with and without the stimulation. Each run is numbered in Figure 2-1, which shows the TCE production rate versus time. All production peaks were caused by the stimulation, except for the peak near the end of run 2. The stimulation frequency was 20-100Hz.

Increased core permeability as a result of dynamic stress stimulation was observed. The authors explain the permeability increase as mobilization and production of fine grains that were plugging pore throats and reducing permeability of the core. Fine grained sand production was observed at the outlet of the core, which supports the idea.

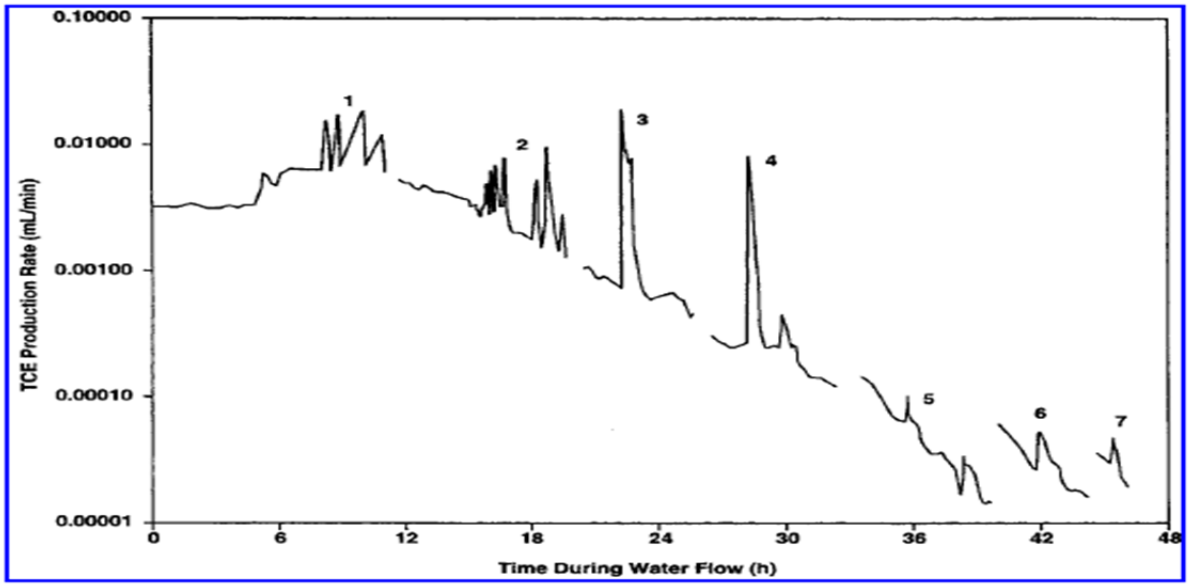

Figure 2-1: TCE production rate versus time for 7 separate experimental runs (from Roberts et al., 2001)

Roberts et al. (2003) investigated changes of fluid pressure within Berea sandstone core under dynamic stress stimulation. The same apparatus as for the previous work is used in this study. Mechanical stress was provided at a frequency of 25 Hz. Steady-state experiments were conducted by injecting two phases (oil and brine) simultaneously. The liquids were injected into the core at different rates to provide different oil cut at the outlet of the core. Dynamic stress stimulation caused an increase in

fluid pressure drops for any oil cut. The magnitude of the fluid pressure drop changes proportionally with applied oil cut.

2.5 FIELD APPLICATIONS

This section gives a review of the field applications of seismic EOR. All given field applications showed increased oil production rate as a result of the stimulation. We do not remark about economic successfulness of any of the projects.

2.5.1 Field applications in the US

Kostrov and Wodden (2005) published results of two field applications of seismic stimulation in the US. The stimulations were done using the Applied Seismic Research (ASR) hydro-impact tool. A more detailed description of the tool can be found in Kostrov and Wooden (2008). ASR stimulated several formations that have 0.1-2000 md permeability, 10-50% porosity, 11-38 degree API oil gravity and 20-5000 scf/stb GOR. They observed that oil gravity and GOR were the properties that most affect efficiency of seismic stimulation. They concluded that any formation having by-passed oil-bearing productive layers with a 17 degree API or greater oil gravity and a GOR of less than 2000scf/stb would benefit from the stimulation.

Lost Hills. The first field application is the Lost Hills field of the Central Valley of California. The formation is diatomite with porosity of 45-55% and permeability of 0.1-2 md. The productive layers are located at a depth of 2,200-3,700 feet. The ASR hydro-impact tool was placed inside a borehole at a depth of approximately 812 ft. The stimulation area was divided into two parts: operator 1's and operator 2's area. Seismic

stimulation in operator 2's area was done continuously between October 2001 and May 2002. Stimulation in operator 1's area started in September 2003. Figure 2-2 and 2-3 show oil production and oil cut response of operator 1's wells. 92 wells are operating in operator 1's area. As a result of seismic stimulation the total oil cut of the 92 wells was increased and the total water cut was decrease. There was no overall increase in total fluid production rate. The dashed line of Figure 2-2 shows the decline rate in oil cut without the stimulation, and the dashed line of Figure 2-3 shows the decline rate in oil production rate without the stimulation. Stimulation in operator 2's wells has an impact on operator 1's wells.

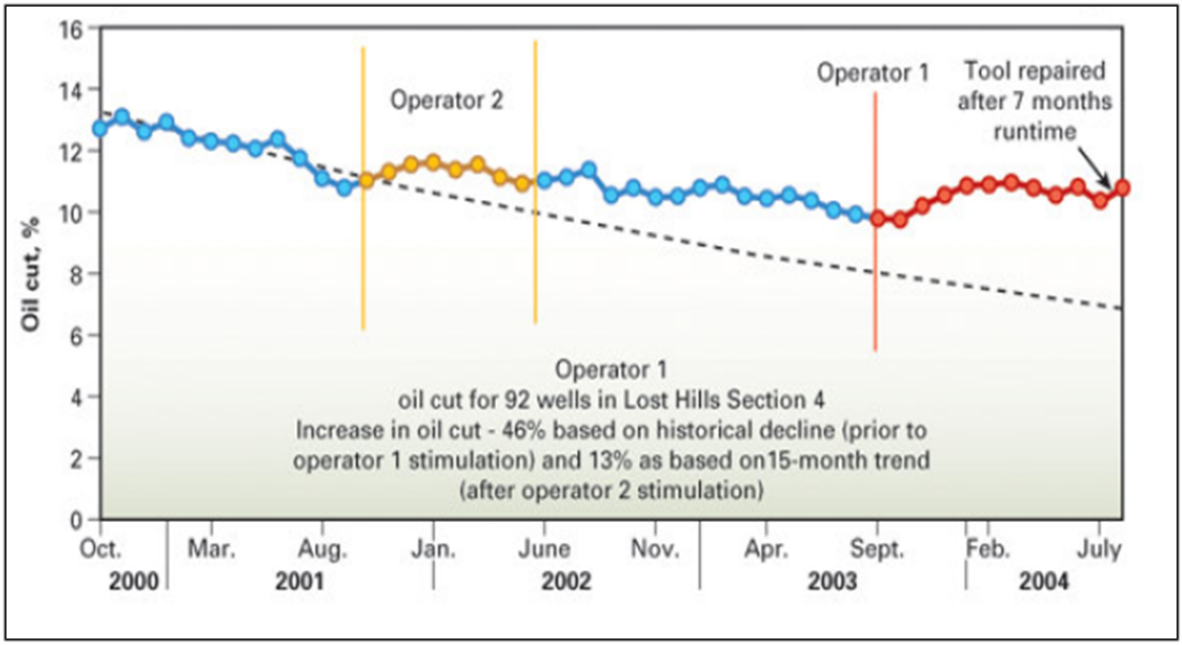

Figure 2-2: Oil cut history for operator 1's wells in the Lost Hills reservoir (from Kostrov and Wooden, 2005)

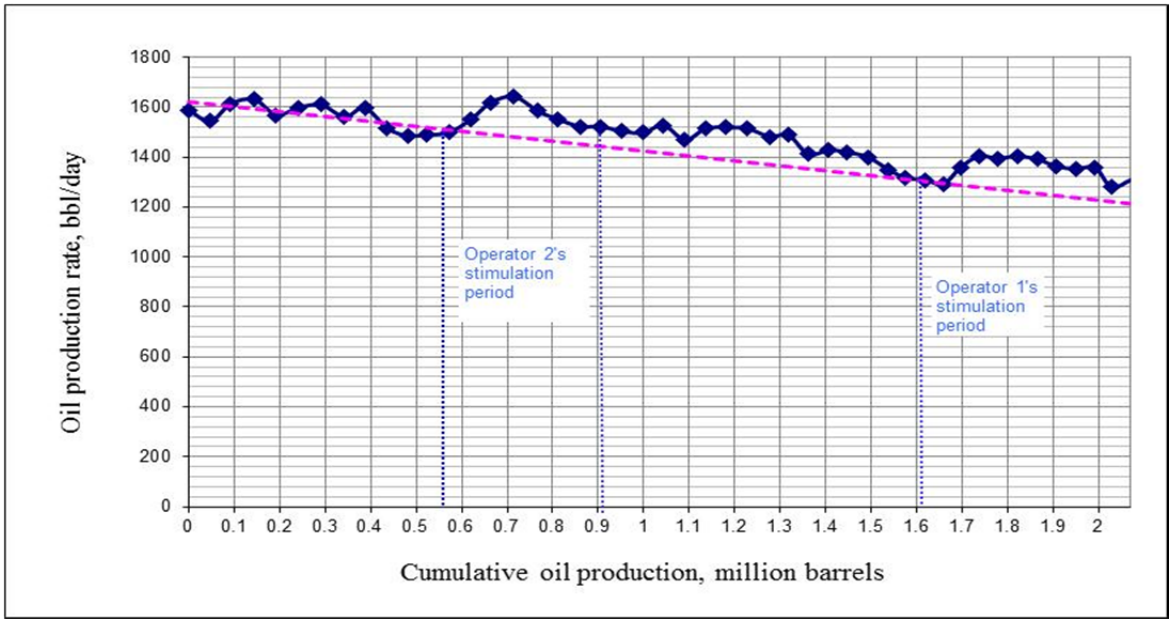

Figure 2-3: Oil production rate versus cumulative oil produced for operator 1's wells in the Lost Hills reservoir. The plot was made using the production rate versus time plot given in Kostrov and Wooden (2005)

Elk Hills. The second field application reported by Kostrov and Wooden (2005) is the Elk Hills formation also located in California, US. The sandstone formation has average porosity of 32-39% and average permeability of 30-400 md with the productive layers located at a depth of 2,800-3,100 feet. Two Hydro-Impact tools were installed to stimulate the field. The affected area has approximately 0.5 mile radius. There are 73 wells operating in the area. As a result of seismic stimulation the average oil production rate increased from 1,556 to 2,212 bbl/d and the oil cut increased from an average of 16.8 to 21.6%. The water production rate response was not stable. Figures 2-4 and 2-5 show oil cut and oil production rate response of the field to the seismic wave stimulation. The

dashed lines of Figures 2-4 and 2-5 represents the predicted decline rate of oil cut and oil production rate without the stimulation.

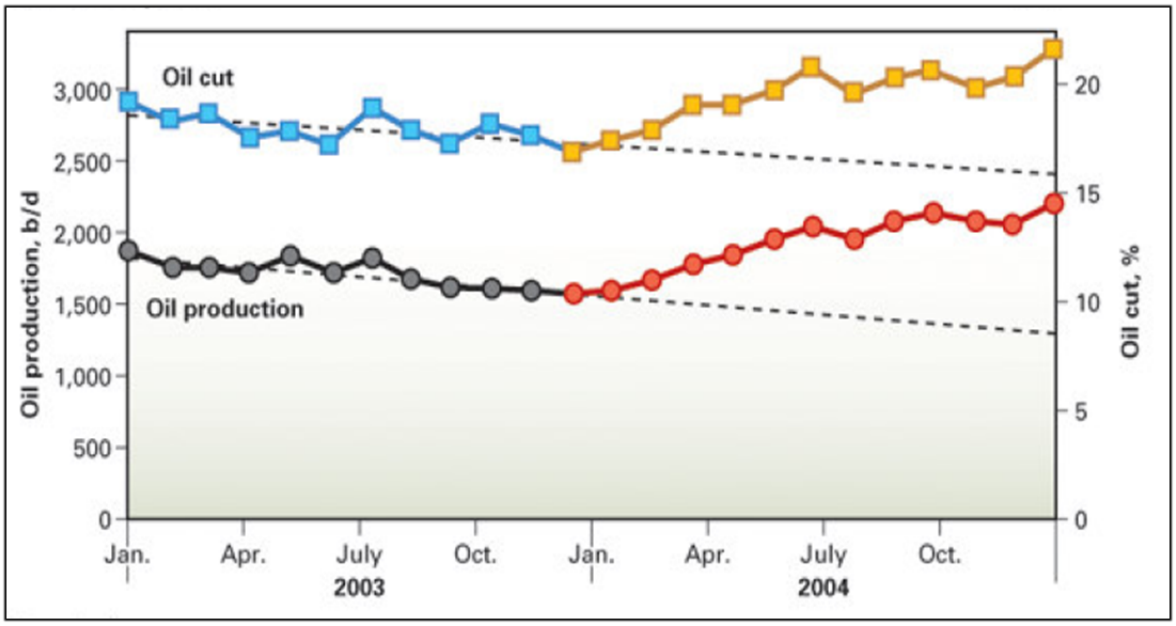

Figure 2-4: Oil production rate and water cut history for the Elk Hills oil field (from Kostrov and Wooden, 2005)

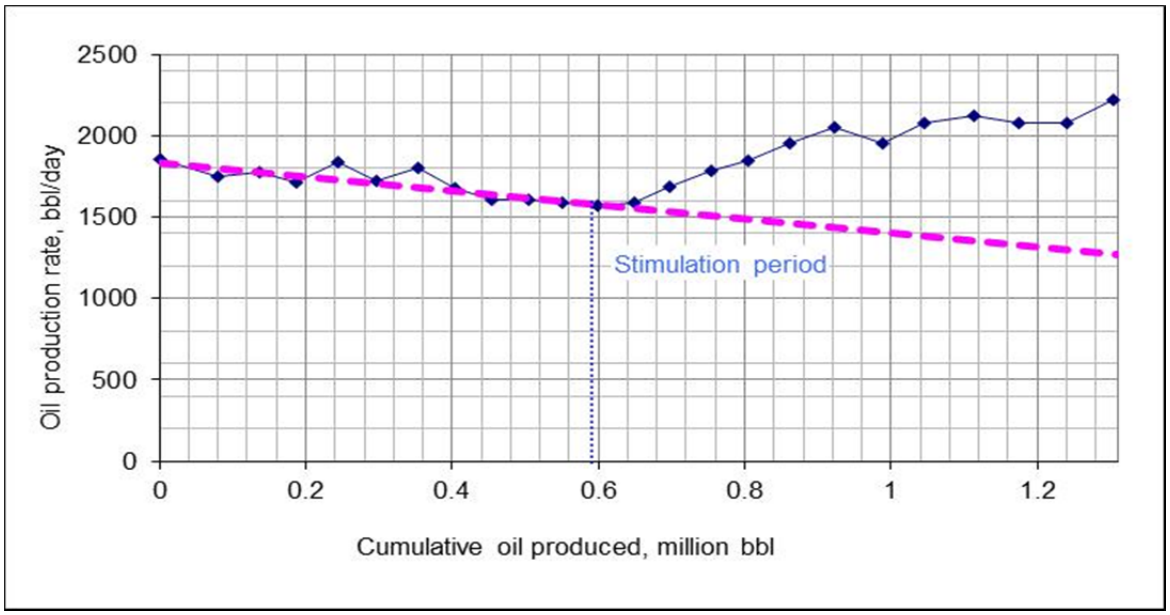

Figure 2-5: Oil production rate versus cumulative oil produced for the Elk Hills oil field. The plot was made using the oil production rate history plot given in Kostrov and Wooden, 2005.

Sharon Ridge. Another field application of the seismic EOR was performed in the Sharon Ridge field of Texas, US. The geology of the field and the results of the stimulation is in Marshall et al. (2011).

The Glorietta and the Clearfork intervals of the reservoir are being produced. The interval is dolomite with some anhydrite and sand layers. The sand layers have porosity of 13-20%, and permeability of 10 md. The dolomitic layers have porosity of 13% and permeability of 1 md. The Clearfork interval is dolomitic. The stimulation was performed using ASR's tool.

Figures 2-6 and 2-7 show the impact of the stimulation on the oil production rate history. The solid line of Figure 2-7 and the solid line of Figure 2-6 shows oil production decline rate before the stimulation.

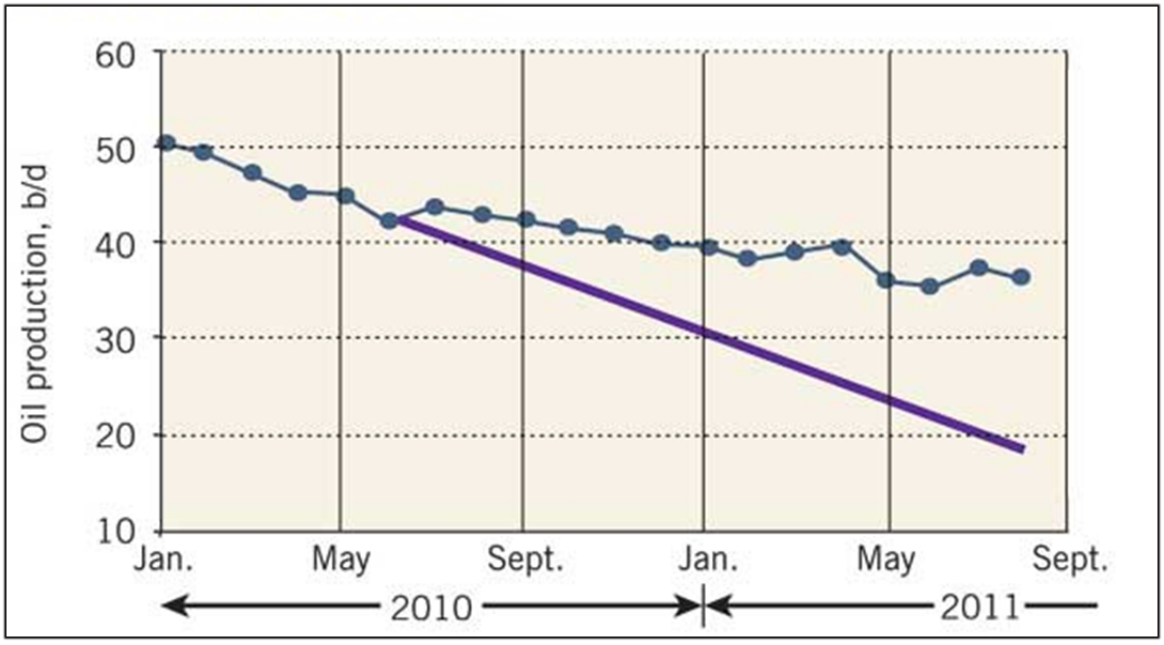

Figure 2-6: Oil production rate response of the Sharon Ridge field (from Marshall et al., 2011)

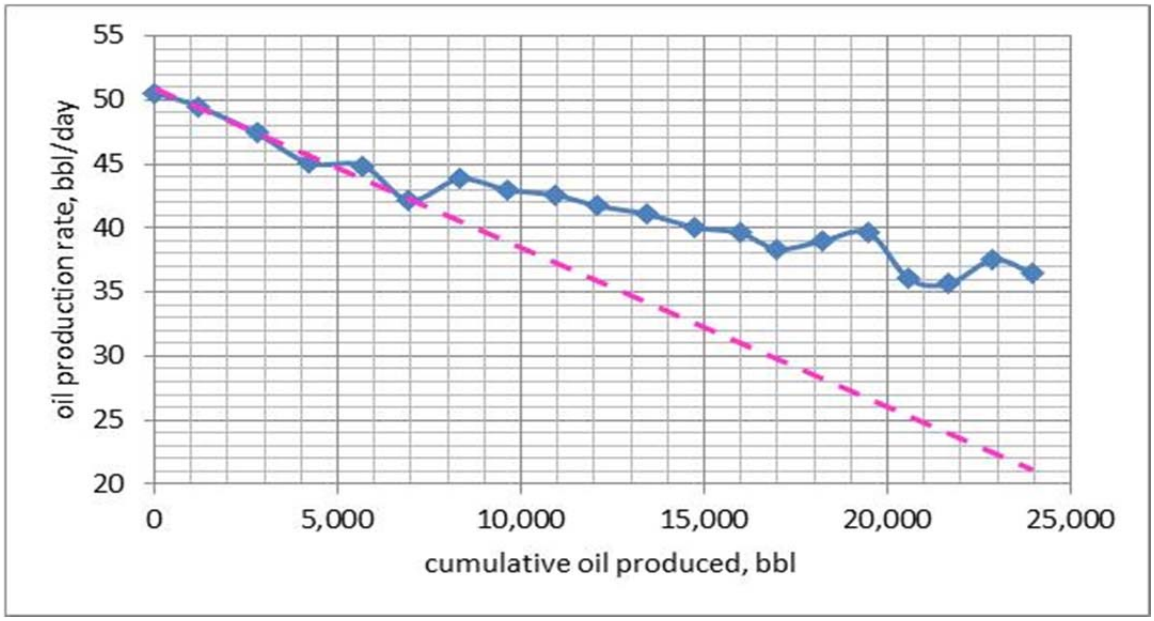

Figure 2-7: Oil production rate versus cumulative oil produced for the Sharon Ridge field. The plot was made using the oil production rate history plot given in Marshall et al. (2011).

2.5.2 Filed applications in the former USSR area

The following review of the Abuzy, Changirtash, and Jirnovskiy oil field applications are from Simkin and Surguchev (1991), Nikolaevskiy et al. (1996), and Kouznetsov et al. (1998).

Abuzy oilfield. The first field experiment of elastic wave stimulation using surface vibrators was performed in the Abuzy field, in the Krasnodar region of Russia in 1987. The stimulation was performed using 2 surface vibrators each having 50 MW power. The test lasted for 37 days. The depth of the oil bearing formation is 4920 ft. The oil cut at the beginning of the stimulation was less than 10%. As a result of seismic stimulation the oil cut increased by up to 20-25%. Besides a change in oil cut, compositional changes were also observed in the produced hydrocarbons. Methane

content in the well annulii increased. These are signs of accelerated degassing of oil under seismic stimulation. A 10-100 times increase of the hydrocarbon concentration in the air samples taken from special geochemical wells at the depth of 650-820 feet was observed (Simkin and Surguchev, 1991).

Changirtash oilfield. Another experiment was performed in the Changirtash oilfield in Kirgizstan in 1988. Changirtash is one of the oldest oilfields of Kirgizstan where oil production started in 1939. The formation is fine grained sandstone with shale layers. The sandstone formation has 30 md average permeability and 10-23% average porosity. A total of 89 wells are operating in this field, 25 of them are water injectors. The experiment was conducted in two areas of the field.

The first study area has dimensions of 1,970×1,970 ft. The oil bearing formation has 35 degrees dip with pay zone of 59-82 feet thickness and 35 cp oil viscosity. 6 producers were operating in this area. The water cut before seismic stimulation was around 69%. Two surface vibrators were located at the center of the area 66 feet apart. Each of the vibrators has power of 50 kW and generated elastic waves continuously over one month, October 1988. Vibrators were hummer type vibrators. The hummers created 55 stress pulses per minute generating a seismic wave of 20Hz frequency. As a result of the stimulation the water cut decreased by 25-30 % and more than 300 tonnes of incremental oil were recovered. Gas samples were taken before and after stimulation. A considerable increase in the content of light components was reported in the gas samples.

The second experimental area was larger (4,920×4,920 ft). 16 producers were operating in this area. The water cut before stimulation was around 89%. The surface

vibrators used to stimulate the reservoir were the same as in the first pilot area. The incremental oil production exceeded 1,000 tonnes, a 1.6 fold increase in the average daily production. At the same time with seismic stimulation air was injected into the lower part of the pay zone. The fluid was produced from the upper part of the layer. Thus the incremental oil production is a result of the seismic stimulation and the air injection.

Jirnovski oilfield. The field is located in the Volgogradskiy region of Russia. The formation is sandstone. Surface vibrators were used to stimulate the field. The water cut before stimulation was more than 90%. The experiment was performed in two stages. The first stage of the experiment was performed between October 20 and December 15, 1991. The second stage of the test was conducted between May 18 and July 13, 1992. The duration of the stimulation was the same as the first stage (one month). The average oil production rate was increased by 54% and the average water production rate was decreased by 6% in average as a result of the first stage.

Samotlor oilfield. Samatlor is an oil field located in Western Siberia, Russia. The following review of the Samatlor field application is from Kostrov and Wooden (2002). The formation has porosity of 21-28% and permeability of 100-2,000 md. The crude oil gravity is 34 degree API. The oil cut before stimulation was 90%. The field was stimulated using in-situ stimulator intermittently during 7 months. 340,000 barrels of incremental oil was recovered as a result of the stimulation. The production rates of the wells within the 1-1.5 mile radius of the stimulated well were affected by the stimulation.

Mancharov oilfield. Another seismic stimulation was done in the Mancharov oil field of Bashkortostan Republic of Russia in 1995 (Belonenko et al., 1996). The

stimulation affected two productive formations. The first is the Bobrikovsky formation, which has 0.2-1 D average permeability and 25-30% porosity. The average water cut before the stimulation was 97-98.5%. . The second productive formation, the Turneisky, has 0.01-0.015 D average permeability and 15% average porosity. Each well's response to the stimulation was different. In some wells the water cut decreased 1.4-2.8 times and oil production increased 8.5-34.5 times. 11,750 tonnes of incremental oil was recovered as a result of the seismic stimulation.

2.5.3 Field applications in China

Applications of elastic wave stimulation in Chinese oil fields were reviewed from Zhu et al. (2005).

Liaohe oilfield. Seismic stimulation was applied to the Liaohe oilfield, a heavy oil field in China, in 1997. The layer has an average depth 4,950-5,400 feet with the pay zone that is around 222 feet in thickness and has 24% porosity, and 2,420 md porosity. The crude oil viscosity is 500 cp at reservoir conditions, and 3,000 to 4,000 cp at the surface conditions. The oil specific gravity is 0.946 with an asphaltene content of 37.52%.

Seismic stimulation was conducted using in-situ vibrators. The vibrating system was lowered to a depth of 1,916 feet in one of the boreholes. 26 wells within 2,600 feet radius of the stimulated well were affected by the stimulation. Calculations were carried out on the production data from 23 wells that effectively influenced by the stimulation. The maximum oil production rate was increased from 36 tons/day to 47 tons/day. Total

water cut decreased from 63% to 58% from those 23 wells. Figure 2-8 shows the oil production rate versus cumulative oil production before and during seismic stimulation for the 23 wells of Liaohe oil field.

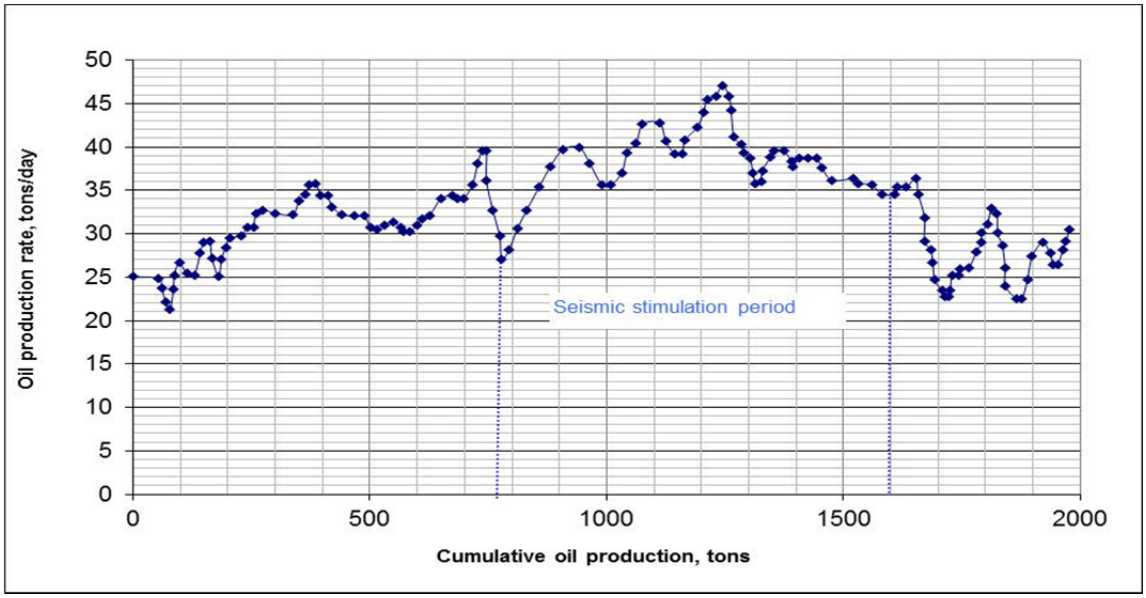

Figure 2-8: Oil production rate versus cumulative oil production for 23 wells of the Liaohe field. The plot was made using the oil production rate versus time plot given in Zhu et al. (2005).

Huabei oilfield. Seismic stimulation was applied to Huabei oil field in 1999 using the same in-situ stimulation tool as for the Liaohe field. There are 58 wells operating within 3,280 feet of the stimulated well. The total oil production rate of the 58 wells was increased by 27.5% and total water oil ratio decreased by an average of 48.4%. Figure 2-9 shows the oil production rate versus cumulative oil produced for the Cha39 area of the field. The dashed lines of the figure show decline rate before and after the stimulation.

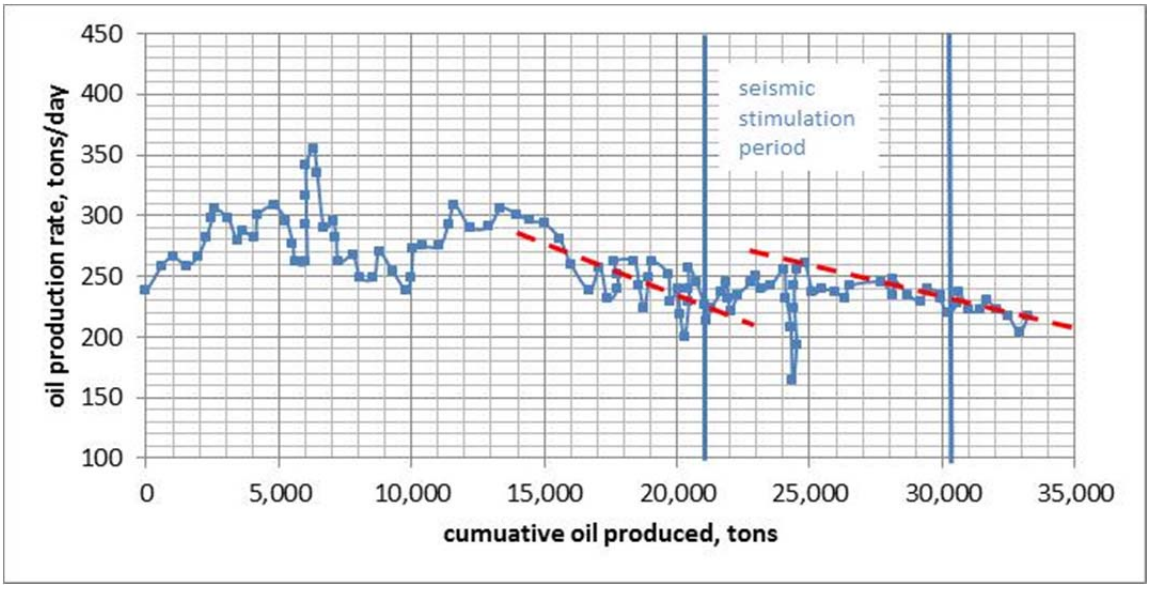

Figure 2-9: Oil production rate versus cumulative oil produced for the Cha39 area of the Huabei field. The plot was made using the oil production rate history plot given in Zhu et al. (2005).

Shengli oilfield. Seismic stimulation in the Shengli field was carried out using the same in-situ stimulation tool as for Liaohe field. The producing layers are located between 3,180-9,710 feet depth and consist of 15 major sandstone layers and 74 mini layers. The radius of study area was 0.93 mile with 23 wells operating within it. As a result of the seismic stimulation the average surface viscosity of crude oil was reduced by 21 %., which led to an increased recovery factor from 18.2 to 41.8 %. High frequency stimulation was also performed in this field. A detailed description of the stimulation and the results can be found in Guo et al. (2004).

2.5.4 Field application in Indonesia

Tilan oilfield. Another seismic stimulation was performed in the Tilan oilfield of Indonesia (Barabanov and Pavlov, 2009).The seismic stimulation lasted for 100 days.

The average water cut before stimulation was 96%. The oil production rate was increased by 75% of the oil production rate before the stimulation. Figure 2-10 shows that effect of the seismic stimulation persisted after the end of the stimulation.

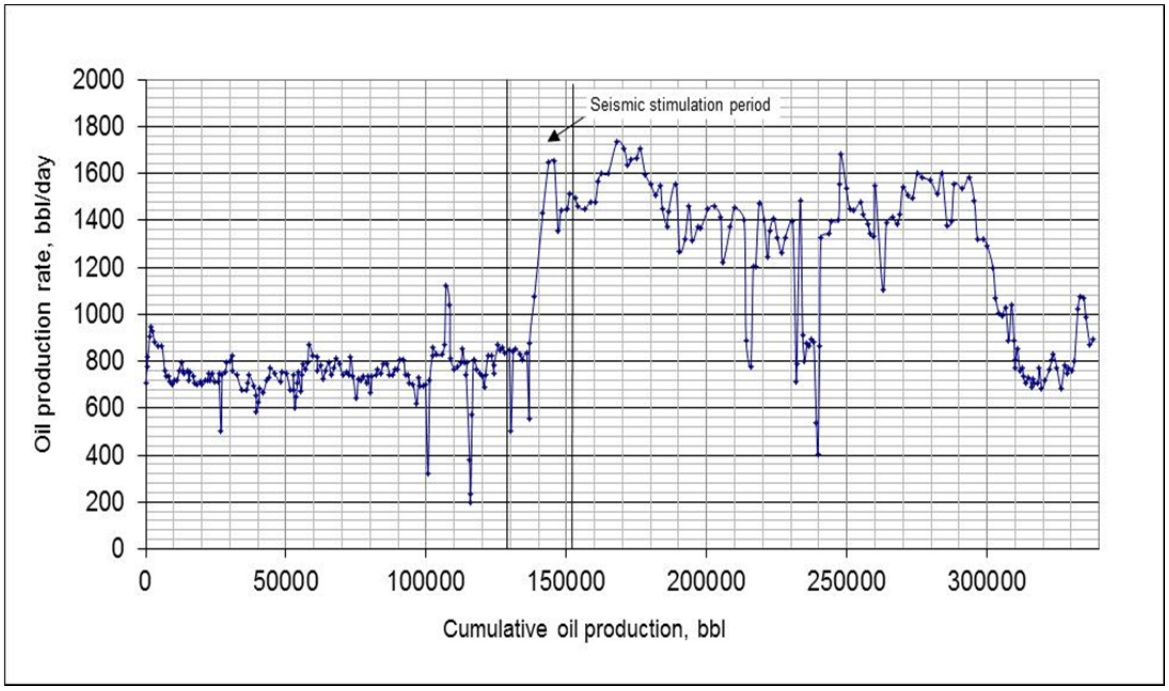

Figure2-10: Oil production rate versus cumulative oil produced for Tilan field. The plot was made using the oil rate history plot given in Barabanov and Pavlov (2009).

2.5.5 Summary

All field applications presented in this section showed increased oil production rate. Most production rate enhancements are obvious from the oil production rate history plots. In some cases, oil production rate enhancement is not sharp (Lost Hills). Table 2-1 summarizes all mentioned field examples. More analysis needed to investigate the economic feasibility of the seismic EOR.

Location	Field Name	Reservoir rock type	Approximate depth of productive layers, feet	Permeability (md)	Porosity, (%)	Type of Seismic EOR	oil production response	Water production response
USA	Lost Hills	Diatomite	2,200-3,700	0.1-2	45-55	In-situ	Oil cut increased	Water cut decreased
	Elk Hills	Sandstone	2,800-3,100	30-400	32-39	In-situ	Average oil production rate increased from 1,556 to 2,212 bbl/day.	Increasing, declining and constant water production rate periods were observed.
	Sharon Ridge	Dolomite	2,300-3,100	-	-	In-situ	4,100 barrels of incremental oil recovered by August, 2011.	-
former USSR area	Abuzy	Sandstone	4,920	-	-	Surface	Oil cut increased by up to 25 % of oil cut before stimulation.	Water cut was 20-25% less than before stimulation.
	Changirtash Test 1	Sandstone	790-1,470	0.1-30	23-Oct	Surface	300 tonness of incremental oil produced.	Water cut was 25-30% less than before stimulation.
	Changirtash Test 2	Sandstone	790-1,470	0.1-30	23-Oct	Surface	1000 tonness of incremental oil produced (combined with air injection).	Water cut was 20-25% less than before stimulation (combined)with the air injection).
	Jirnovskiy	Sandstone	3,280	100-5,000	18-35	Surface	Oil production rate was 54% greater than before stimulation.	Water cut was 6 % less than before the stimulation.
	Mancharov	-	-	10-1,000	15-30	Surface	11,750 tonnes of incremental oil recovered.	Water cut of some wells decreased by 1.4-2.8 times than before the stimulation.
	Samatlor	Sandstone	5,700-7,500	100-2,000	21-28	In-situ	340,000 bbls of incremental oil or 40% of total oil production from affected part.	-
China	Liaohe	Sandstone	4,950-5,400	2420, (average)	24 (average)	In-situ	Oil prodaction rate was 30.5% greater than before stimulation.	Water cut was 8% less than before stimulation.
	Huabai	Sandstone	-	-	-	In-situ	Oil production rate was 27.5% greater than before stimulation.	WOR was 48.4% less than before stimulation.
	Shengli	Sandstone	3,180-9,710	-	-	In-situ	Recovery factor increased by 130%.	-
Indonesia	Tilan	Sandstone	-	10-1,000	10-20	-	Oil production rate was 75% greater than before stimulation.	-

Table 2-1: Summary of the field application of seismic EOR

2.6 CONCLUSIONS

Early observations of the oil production rate increment during earthquakes and other elastic wave generating events motivated scientists and the oil industry to investigate elastic wave based EOR as a new method. The positive changes in oil production rate as a result of field-scale application of the seismic EOR gives a promise of the feasibility of the method. The dominant production mechanisms of the seismic EOR have not been proven yet. Several pore-scale and reservoir-scale production mechanisms were suggested in the literature. Figure 2-11 summarizes the application type (surface or in-situ) and possible production mechanisms suggested in the literature. In this thesis we concentrate on the possible cross-flow generation between a fracture and a rock matrix of a fractured reservoir model as a result of the seismic wave application.

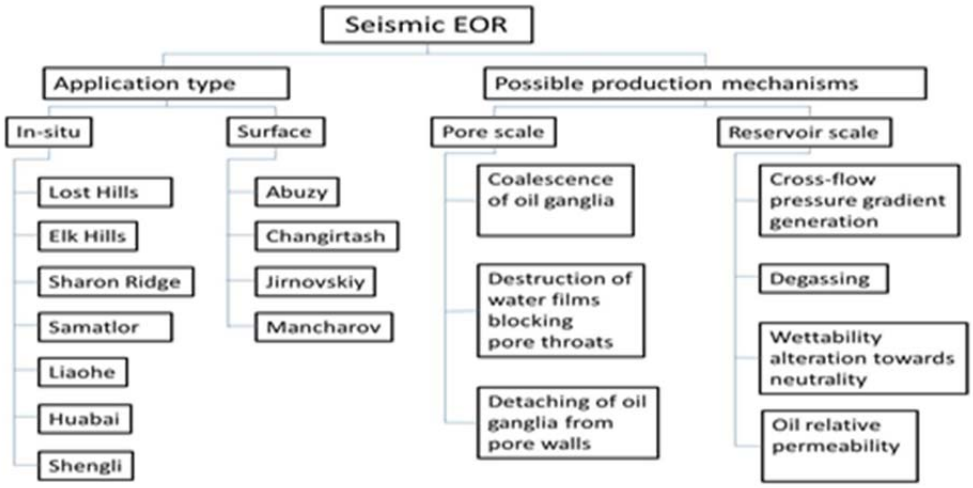

Figure 2-11: Summary scheme showing types of seismic EOR and possible production mechanisms suggested in the literature

Chapter 3: Viscous cross-flow

3.1 INTRODUCTION

Huh (2006) showed that a significant rock displacement is needed to produce residual oil saturation of a reservoir. Bersenev (2006) also showed that we need large amplitude of acceleration fields of rock matrix to mobilize trapped oil droplets. It is shown that generating such displacements using seismic waves would be very difficult (Huh (2006), Jeong (2011) and Jeong et al. (2011)). Huh suggested improved sweep efficiency through fluid cross-flow generation to be a dominant production mechanism of seismic EOR.

This chapter investigates the cross-flow pressure gradient at an interface between a rock matrix and a fracture of a fractured reservoir model, which is caused by the fluid pressure oscillations. The possibility of cross-flow generation by rock stress propagation is ignored throughout this work.

This chapter consists of 5 sections. The first section gives an outline of the chapter. The second section describes the reservoir model and defines the problem, describing the pressure propagation equations within a rock matrix and a fracture with their boundary and initial conditions. The third section of this chapter solves pressure propagation equations for fluid pressure oscillations. The solutions are originally given by Jeong et al. (2011). The fourth section performs inspectional analysis to transform the problem into dimensionless form and to develop dimensionless groups of the problem. The purposes of the inspectional analysis are to minimize the number of free parameters

in the problem and to be able to apply the results to any geometrically similar system. The last section gives conclusions of each section of this chapter.

3.2 DEFINING THE PROBLEM

3.2.1 Reservoir model

Figure 3-1a shows a schematic of the simplified fractured reservoir model we employ in our study. Figure 3-1b shows a portion of the fractured reservoir model between the injector and one of the producers. The model has 3 wells, 2 producers and an injector. In Figure 3-1b, the x coordinate is parallel to the 1-D fracture: the y coordinate is parallel to the interface plane between the fracture and the rock matrix. The distances between the injector and each of the producers are the same. The length of the fracture of Figure 3-1b is equal to the distance between the injector and one of the producers of the Figure 3-1a. We assume that initial oil saturation within the fracture is equal to the residual oil saturation (S_{or}) of the reservoir and initial oil saturation of the rock matrix is equal to the initial oil saturation of the reservoir ($1-S_{wr}$): S_{wr} denotes residual water saturation of the reservoir. We also assume that the fracture pressure before the stimulation is equal to a steady-state pressure solution, and the rock matrix pressure before the stimulation is equal to the initial reservoir pressure. We also assume that the reservoir is undersaturated, and the capillary entry pressure of the rock matrix is zero.

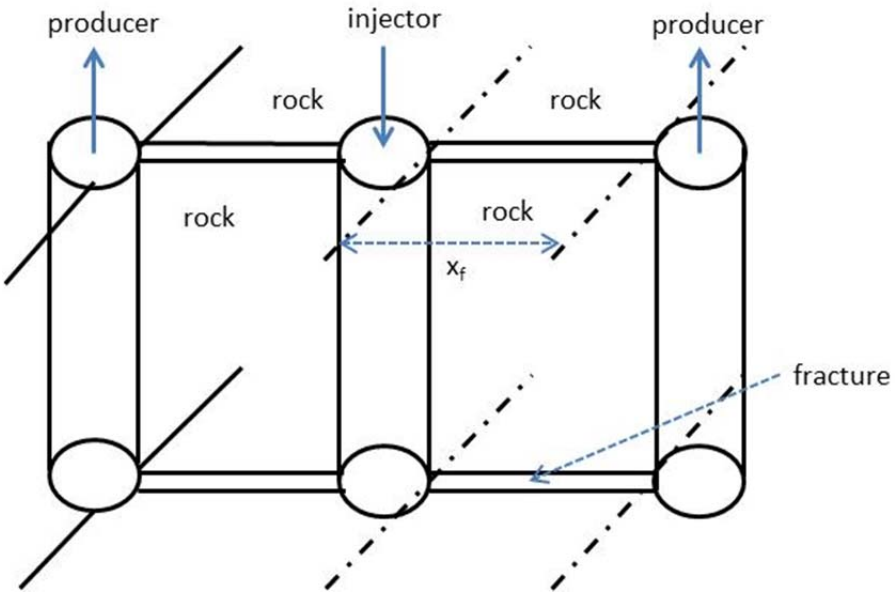

a. Schematic of the fractured reservoir model.

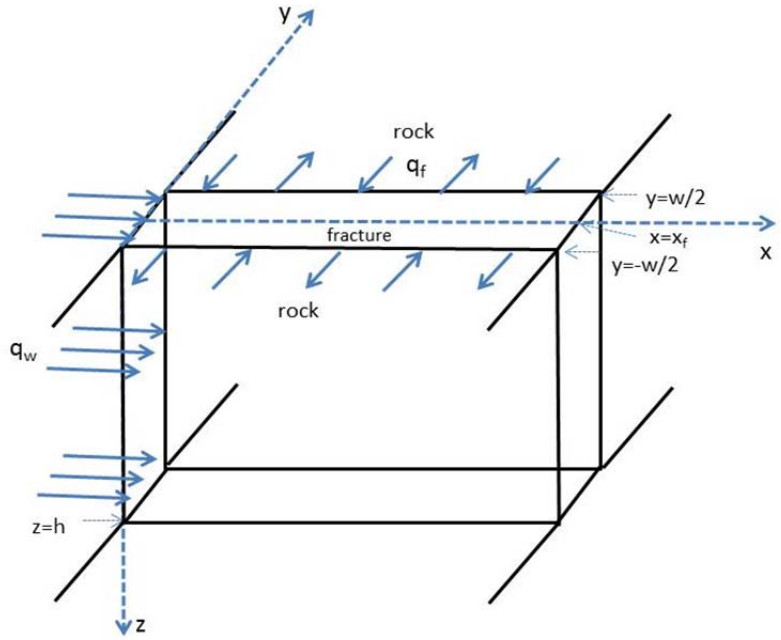

b. Dashed part of the fractured reservoir model.

Figure 3-1: Schematics of the fractured reservoir model. The fracture width is exaggerated for illustration.

3.2.2 Time-harmonic water flooding

Time-harmonic water flooding is taken as a way of delivering seismic waves to the reservoir to generate fluid pressure oscillations (Jeong et al., 2011). The fluid pressure oscillations generate a rock matrix pressure gradient in y direction (normal to the fracture faces), which is the driving force for the cross-flow. Mathematical expression of the time harmonic water flooding is given below:

$$q_w(t) = \hat{q}_w e^{i\omega t} \tag{3.1}$$

where $q_w(t)$ is incremental water injection rate at the injection well, $\hat{q}_w$ is the injection rate amplitude, ω is angular frequency of the stimulation, and i is imaginary unit. A positive $q_w(t)$ implies that the water injection rate was increased by $q_w(t)$ from its steady-state value before the stimulation, whereas a negative $q_w(t)$ means that the water injection rate was decreased from its steady-state value. Mathematical expressions for the fluid pressure oscillations within the fracture and the rock matrix can be written as follows:

$$P_f(x,t) = \hat{P}_f(x) e^{i\omega t} \tag{3.2}$$

$$P_r(x,y,t) = \hat{P}_r(x,y) e^{i\omega t} \tag{3.3}$$

where $P_f(x,t)$ is the fluid pressure inside the fracture, $\hat{P}_f(x)$ is the incremental fracture pressure amplitude, $P_r(x,y,t)$ is the fluid pressure in the rock matrix, and $\hat{P}_r(x,y)$ is the incremental rock matrix pressure amplitude. The oscillatory fluid pressures in the fracture and rock matrix are discussed more in Sections 3.2.3 and 3.2.4. The angular frequency of the stimulation is defined by the following equation:

$$\omega = 2\pi n \tag{3.4}$$

where n is the stimulation frequency in Hz.

We employ a complex-valued solution for solving the one-dimensional incremental fracture pressure transient equation, which is a partial differential equation and given in Section 3.2.3. By doing so, here, we are able to get rid of the time dependence of the PDE. Thus, we can transform the PDE into an ordinary differential equation (ODE) only in terms of the space x, which is much easier to solve than the PDE. Despite the aforementioned benefit of a complex-valued solution, it is hard to visualize or understand it. As such, at Sections 3.3.2-3.3.5, we will show the real-valued solution converted from the complex-valued solution.

3.2.3 Pressure transient equation for a flow within the fracture

The stimulated fracture pressure, $P_{fs}(x,t)$ is defined by the following equation:

$$P_{fs}(x,t) = P_{ss}(x) + P_f(x,t) \tag{3.5}$$

where $P_{fs}(x,t)$ is the stimulated fracture pressure, $P_{ss}(x)$ is a steady-state solution for the fracture pressure without the stimulation, and $P_f(x,t)$ is the incremental fracture pressure generated by the stimulation. A positive $P_f(x,t)$ means that the total fracture pressure was increased by $P_f(x,t)$ from the steady-state fracture pressure, whereas a negative $P_f(x,t)$ means that the total fracture pressure was decreased by the modulus of $P_f(x,t)$ from the steady-state fracture pressure. The steady-state fracture pressure, $P_{ss}(x)$ can be calculated by solving the diffusivity equation within the fracture for a steady-state flow, which is given below:

$$\frac{d^2 P_{ss}(x)}{dx^2} = 0 \qquad 3.6$$

Equation 3.6 assumes that only one phase is flowing through the one-dimensional fracture, the flow is steady-state, the fracture is homogeneous and properties in it are isotropic, and there is no cross-flow at the interface of the fracture and the rock matrix. We solve Equation 3.6 using the following boundary conditions.

$$P_{ss}(x) = P_{inj} \text{ at } x = 0 \qquad 3.7$$

$$P_{ss}(x) = P_p \text{ at } x = x_f \qquad 3.8$$

where P_{inj} is the bottom hole pressure of the injector, and P_p is the bottom hole pressure of the producers. The solution of Equation 3.6 using the boundary conditions 3.7 and 3.8 is given below:

$$P_{ss}(x) = \left(\frac{P_p - P_{inj}}{x_f} \right) x + P_{inj} \qquad 3.9$$

We can calculate the incremental fracture pressure generated by the stimulation, $P_f(x,t)$ by solving the pressure transient equation for a flow within a one-dimensional fracture with a cross-flow term as described in Section3.3. The one-dimensional fracture pressure transient equation with a cross-flow term is given below (Cinco et al., 1978). Derivation of Equation 3.10 is given in Appendix A.

$$\frac{\phi_f c_{tf}}{\lambda_f} \frac{\partial P_f(x,t)}{\partial t} = \frac{\partial^2 P_f(x,t)}{\partial x^2} - \frac{1}{\lambda_f wh} q_f(x,t)\big|_{y=w/2} \qquad 3.10$$

where φ_f is the fracture porosity, c_{tf} is the total fracture compressibility, λ_f is the mobility of the flowing liquid, which is in fact a mixture of oil and water within the fracture,

$q_f(x,t)$ is the cross-flow rate (volumetric flow rate per unit length of the fracture) evaluated at the interface between the rock matrix and the fracture, where y=w/2 and $0 \leq x \leq x_f$. $P_f(x,t)$ is the incremental fracture pressure generated by the stimulation. Equation 3.10 has the following assumptions:

1. Only one phase is flowing. We assume that capillary pressure is equal to zero; there is no difference between oil and water phase pressures. Thus, we can use a one phase flow solution for the fracture pressure and apply it to calculate the cross flow rate at the fracture and the rock matrix interface, which is in reality a two-phase flow problem.
2. We assume that mobility of the flowing liquid through the fracture, λ_f is constant and equal to the water mobility within the fracture at residual oil saturation. λ_f is defined by the following equation:

$$\lambda_f = \frac{k_f k_{rw}^{\circ}}{\mu_w} \qquad 3.11$$

where k_f is the fracture absolute permeability, k_{rw}° is the water end point relative permeability of the fracture, and μ_w is water viscosity.

3. The fracture is homogeneous and properties in it are isotropic.
4. The incremental fracture pressure gradient induced by the stimulation vanishes at the end of the fracture ($x=x_f$). This assumption is mathematically expressed in Equation 3.17 as a boundary condition. However, the steady-state fracture pressure is not subject to this boundary condition.

We can calculate the stimulated fracture pressure using Equation 3.5; the steady-state fracture pressure without the stimulation is calculated using Equation 3.9, and the incremental fracture pressure due to the stimulation is calculated using the solution of Equation 3.10 for fluid pressure oscillations. The solution of Equation 3.10 for fluid pressure oscillations is originally given by Jeong et al. (2011) and again in Section 3.3.

$q_f(x,t)|_{y=w/2}$ in Equation 3.9 is cross-flow rate evaluated at the interface between the fracture and the rock matrix. $q_f(x,t)|_{y=-w/2}$ is also a notation for the cross-flow rate evaluated at the interface of the fracture and rock matrix. We use the first notation throughout this work. $q_f(x,t)|_{y=w/2}$ is volumetric flow rate per unit length of the fracture and defined by the following equation:

$$q_f(x,t) = -2h\lambda_r \left.\frac{\partial P_r(x,y,t)}{\partial y}\right|_{y=w/2} \tag{3.12}$$

where $P_r(x,y,t)$ is the incremental pressure of the two-dimensional rock matrix, w is the aperture of the fracture, and h is the height of the fracture (Figure 3.1 b). $P_r(x,y,t)$ is discussed more in the next section. λ_r is mobility of the cross-flow liquid within the rock matrix. We assume that mobility of the cross-flow liquid within the rock matrix is equal to the mobility of oil within the rock matrix at irreducible water saturation and it is constant throughout the stimulation. λ_r is defined by the following equation:

$$\lambda_r = \frac{k_r k_{ro}^{\circ}}{\mu_o} \tag{3.13}$$

where k_r is the absolute permeability of the rock matrix, k^o_{ro} is the oil end point relative permeability of the rock matrix, and μ_o is the oil viscosity. Substituting the cross-flow rate and the mobility of the flowing liquid within the rock matrix and the fracture of Equation 3.10 with Equations 3.11-3.13 gives the following expression for the incremental fracture pressure transient equation:

$$\frac{\phi_f \mu_w c_{tf}}{k_f k^{\circ}_{rw}} \frac{\partial P_f(x,t)}{\partial t} = \frac{\partial^2 P_f(x,t)}{\partial x^2} + \frac{2k_r k^{\circ}_{ro} \mu_w}{w k_f k^o_{rw} \mu_o} \frac{\partial P_r(x,y,t)}{\partial y}\bigg|_{y=w/2} \tag{3.14}$$

The solution of Equation 3.14 is originally given by Jeong et al. (2011) and again in Section 3.3.

The following initial and boundary conditions are used:

$$P_f(x,t) = 0 \quad \text{, at} \quad t = 0 \tag{3.15}$$

$$\frac{\partial P_f(x,t)}{\partial x} = -\frac{\mu_w q_w}{2whk_f k^o_{rw}} = -\frac{\mu_w \hat{q}_w e^{i\omega t}}{2whk_f k^o_{rw}}, \text{ at } x = 0 \tag{3.16}$$

$$\frac{\partial P_f(x,t)}{\partial x} = 0 \ , \ \text{at} \ x = x_f \tag{3.17}$$

where q_w is the volumetric water injection rate and defined by Equation 3.1. Since $P_f(x,t)$ is the incremental fracture pressure generated by the stimulation, the boundary condition 3.17 does not mean that there is no flow at the end of the fracture ($x=x_f$). The boundary condition 3.17 implies that the stimulation does not affect the gradient of the fracture incremental pressure in the x direction at the end of the fracture, $x=x_f$.

3.2.4 Pressure transient equation for a flow within the rock matrix

The stimulated rock matrix pressure can be calculated using the following equation:

$$P_{rs}(x,y,t) = P_i + P_r(x,y,t) \tag{3.18}$$

where $P_{rs}(x,y,t)$ is the stimulated rock matrix pressure, P_i is the initial (before the stimulation) pressure of the reservoir, and $P_r(x,y,t)$ is the rock matrix incremental pressure generated by the stimulation. We assume that the rock matrix was not swept before the stimulation. Thus the rock matrix pressure before the stimulation is approximated to be equal to the initial reservoir pressure, P_i.

We can calculate $P_r(x,y,t)$ by solving the two-dimensional incremental rock matrix pressure transient equation, which is given below:

$$\frac{\varphi_r c_{tr}}{\lambda_r}\frac{\partial P_r(x,y,t)}{\partial t} = \frac{\partial^2 P_r(x,y,t)}{\partial x^2} + \frac{\partial^2 P_r(x,y,t)}{\partial y^2} \tag{3.19}$$

where $P_r(x,y,t)$ is the incremental rock matrix pressure generated by the stimulation, c_{tr} is the total rock matrix compressibility, φ_r is the rock matrix porosity, and λ_r is mobility of the liquid flowing through the rock matrix. Equation 3.19 has the following assumptions:

1. Only one phase is flowing. We also assume that capillary pressure is equal to zero; there is no difference between oil and water phase pressures. Thus we can use a one-phase flow solution for the rock matrix pressure and apply it to calculate the cross flow rate at the fracture and the rock matrix interface, which is, otherwise, a two-phase flow problem.

2. The rock matrix is homogeneous and its properties are isotropic.
3. We also assume that mobility of the flowing liquid through the rock matrix is time-independent. That is, it remains the mobility of oil within the rock matrix at initial oil saturation, which is defined by Equation 3.13.

Substituting the mobility term of Equation 3.19 with Equation 3.13 gives the following expression for the incremental rock matrix pressure transient equation:

$$\frac{\varphi_r \mu c_{tr}}{k_r k_{ro}^{\circ}} \frac{\partial P_r(x,y,t)}{\partial t} = \frac{\partial^2 P_r(x,y,t)}{\partial x^2} + \frac{\partial^2 P_r(x,y,t)}{\partial y^2} \qquad 3.20$$

The initial and boundary conditions used are given below.

$$P_r(x,y,t) = 0 \quad \text{, at} \quad t = 0 \qquad 3.21$$

$$P_r = P_f \text{ , at } \quad y = w/2 \qquad \text{and} \quad 0 \le x \le x_f \qquad 3.22$$

Complex number expression of the oscillatory fracture and the rock matrix pressures, Equations 3.2 and 3.3 do not satisfy the initial conditions given in Sections 3.2.3 and 3.2.4. We use the complex number expression to solve the incremental fracture and the rock matrix pressure transient equations for the incremental fracture and the rock matrix pressure amplitudes. Once we have an expression for the incremental fracture and the rock matrix pressure amplitudes, we use real-valued trigonometric expression of the fluid pressure oscillations to carry out our calculations. The trigonometric expressions satisfy the initial conditions.

3.3 DERIVATION OF THE PRESSURE OSCILLATION EQUATIONS

3.3.1 A review of the derivation procedure

This section shows the solution procedures of the rock matrix and the fracture pressure transient equations, Equations 3.14 and 3.20 for oscillatory fluid pressures. The solutions are originally given by Jeong et al. (2011). We additionally give derivation steps of the pressure oscillation equations and analytical expressions for calculating cross-flow rate at the interface of the rock matrix and the fracture and volume of mobilized oil as a result of the stimulation.

We first solve the diffusivity equation for a flow within the fracture, Equation 3.14 assuming that there is no cross-flow at the interface of the rock matrix and the fracture, which means that the rock matrix incremental pressure gradient in the y direction, i.e., the direction perpendicular to the interface is equal to zero. Then we will use boundary condition 3.22 to express the rock matrix incremental pressure in terms of the fracture incremental pressure. The next step is to substitute the rock matrix incremental pressure term of Equation 3.14 with the expression obtained in the previous step and solve the fracture incremental pressure transient equation with the cross-flow term retored, Equation 3.14. We can use the solution of Equation 3.14 with the cross-flow term restored to compute the incremental rock matrix pressure caused by the stimulation and subsequently cross-flow rate at the fracture and the rock matrix interface.

3.3.2 The incremental fracture pressure without a cross-flow.

The incremental fracture pressure equation with no cross-flow can be obtained by setting the incremental rock matrix pressure gradient term of Equation 3.14 to zero. Equation 3.14 with no cross-flow becomes

$$\frac{\partial^2 P_f(x,t)\big|_{q_f=0}}{\partial x^2} - \frac{\phi_f \mu_w c_{tf}}{k_f k_{rw}^o} \frac{\partial P_f(x,t)\big|_{q_f=0}}{\partial t} = 0 \qquad 3.23$$

where $P_f(x,t)|_{q_f=0}$ is the incremental fracture pressure with no cross-flow (q_f=0). We seek a solution for the fracture incremental pressure equation with no cross-flow in a time-harmonic form. The mathematical expression of the $P_f(x,t)|_{q_f=0}$ is given below:

$$P_f(x,t)\big|_{q_f=0} = \hat{P}_f(x,t)\big|_{q_f=0} e^{i\omega t} \qquad 3.24$$

where $P_f(x,t)|_{q_f=0}$ is the complex-valued fracture incremental pressure amplitude assuming that there is no cross-flow, ω is the angular frequency of the stimulation, and i is imaginary unit.

The first order derivative of $P_f(x,t)|_{q_f=0}$ with respect to time is the following:

$$\frac{\partial P_f(x,t)\big|_{q_f=0}}{\partial t} = i\omega \hat{P}_f(x)\big|_{q_f=0} e^{i\omega t} \qquad 3.25$$

The second order derivative of $P_f(x,t)|_{q_f=0}$ with respect to position, x is given below:

$$\frac{\partial^2 P_f(x,t)\big|_{q_f=0}}{\partial x^2} = \frac{\partial^2 \hat{P}_f(x)\big|_{q_f=0}}{\partial x^2} e^{i\omega t} \qquad 3.26$$

Substituting Equations 3.25 and 3.26 into Equation 3.23 gives the following ordinary differential equation for the incremental fracture pressure transient equation with no cross-flow:

$$\frac{d^2 \hat{P}_f(x)\Big|_{q_f=0}}{dx^2} - D_f^2 \hat{P}_f(x)\Big|_{q_f=0} = 0 \qquad 3.27$$

where D_f^2 expresses the liquid flow ability through the fracture with no cross-flow. D_f^2 is defined by the following expression:

$$D_f^2 = \frac{i\omega\phi_f \mu_w c_{tf}}{k_f k_{rw}^o} \qquad 3.28$$

The solution of Equation 3.27 is given below:

$$\hat{P}_f(x)\Big|_{q_f=0} = C_1 e^{D_f x} + C_2 e^{-D_f x} \qquad 3.29$$

Equation 3.29 expresses the amplitude of the fracture incremental pressure, induced by the stimulation under the assumption that there is no cross-flow. The form of Equation 3.29 will help us to approximate the rock matrix incremental pressure distribution with the cross-flow.

The first term of Equation 3.29, $C_1 e^{D_f x}$ represents pressure wave motion in the negative x direction, and the second term, $C_2 e^{-D_f x}$ represents pressure wave motion in the positive x direction.

The initial condition 3.15 for the no cross-flow case becomes

$$P_f(x,t)\Big|_{q_f=0} = 0 \text{ at } t = 0 \qquad 3.30$$

Boundary conditions 3.16 and 3.17 for the no cross-flow case become as followings:

$$\left.\frac{\partial P_f(x,t)}{\partial x}\right|_{q_f=0} = -\frac{\mu_w \hat{q}_w e^{i\omega t}}{2whk_f k_{rw}^o}, \text{ at } x=0 \qquad 3.31$$

$$\left.\frac{\partial P_f(x,t)}{\partial x}\right|_{q_f=0} = 0 \ , \text{ at } x = x_f \qquad 3.32$$

We must apply boundary conditions 3.31 and 3.32 to evaluate C_1 and C_2 of Equation 3.29. Substituting the time-harmonic solution for $P_f(x,t)|_{q_f=0}$, Equation 3.24 into boundary condition 3.31 gives the following:

$$\left.\frac{d\hat{P}_f(x)}{dx}\right|_{q_f=0} = -\frac{\mu_w \hat{q}_w}{2whk_f k_{rw}^o} \quad \text{at} \quad x=0 \qquad 3.33$$

Differentiating Equation 3.29 with respect to x and equating to Equation 3.33 gives

$$\left.\frac{d\hat{P}_f(x)}{dx}\right|_{q_f=0} = C_1 D_f e^{D_f x} - C_2 D_f e^{-D_f x} = -\frac{\mu_w \hat{q}_w}{2whk_f k_{rw}^o} \quad \text{at x=0} \qquad 3.34$$

At x=0 Equation 34 becomes

$$C_1 - C_2 = -\frac{\mu_w \hat{q}_w}{2whk_f k_{rw}^o D_f} \qquad 3.35$$

or

$$C_1 - C_2 = -\frac{R_f}{D_f} \qquad 3.36$$

where R_f is defined by the following expression:

$$R_f = \frac{\mu_w \hat{q}_w}{2whk_f k_{rw}^o} \tag{3.37}$$

Substituting time-harmonic solution for $P_f(x,t)|_{q_f=0}$, Equation 3.24 into boundary condition 3.32 and equating to the derivative of Equation 3.29 with respect to x gives the following equation

$$C_1 D_f e^{D_f x} - C_2 D_f e^{-D_f x} = 0 \quad \text{at } x = x_f \tag{3.38}$$

or

$$C_1 = C_2 e^{-2D_f x_f} \tag{3.39}$$

Upon solving Equations 3.36 and 3.39 we get the following expressions for C_1 and C_2:

$$C_1 = \frac{R_f}{D_f} \frac{e^{-2D_f x_f}}{1 - e^{-2D_f x_f}} \tag{3.40}$$

$$C_2 = \frac{R_f}{D_f} \frac{1}{1 - e^{-2D_f x_f}} \tag{3.41}$$

Substituting C_1 and C_2 into the original Equation 3.29 gives the following result:

$$\hat{P}_f(x) = \frac{R_f}{D_f}\left(\frac{e^{D_f x - 2D_f x_f} + e^{-D_f x}}{1 - e^{-2D_f x_f}}\right) = \frac{R_f}{D_f}\left(\frac{2e^{-D_f x_f}}{1 - e^{-2D_f x_f}}\right)\left(\frac{e^{-D_f(x_f - x)} + e^{-D_f(x_f - x)}}{2}\right) \tag{3.42}$$

Recall hyperbolic sine and cosine functions:

$$\sinh(D_f x_f) = \frac{1 - e^{-2D_f x_f}}{2e^{-D_f x_f}} \tag{3.43}$$

$$\cosh\left[D_f(x_f - x)\right] = \frac{e^{D_f(x_f - x)} + e^{-D_f(x_f - x)}}{2} \tag{3.44}$$

Substituting Equations 3.43 and 3.44 into Equation 3.42 gives the following expression for the incremental fracture pressure amplitude assuming there is no cross-flow at the interface of the fracture and the rock matrix.

$$\hat{P}_f(x)\Big|_{q_f=0} = \frac{R_f}{D_f}\frac{\cosh\left[D_f(x-x_f)\right]}{\sinh\left[D_f x_f\right]} \tag{3.45}$$

where D_f and R_f are defined by Equations 3.28 and 3.37, respectively.

Equation 3.45 defines the one-dimensional incremental fracture pressure amplitude with no cross-flow, $\widehat{P}_f(x)\big|_{q_f=0}$ at any distance from the injector. D_f is a complex number, which makes $\widehat{P}_f(x)\big|_{q_f=0}$ to be complex-valued as well. The actual value of the incremental fracture pressure amplitude with no cross-flow is defined as the absolute value of $\widehat{P}_f(x)\big|_{q_f=0}$. The real-valued incremental fracture pressure distribution, in terms of both space and time, for no cross-flow case is defined below:

$$P_f(x,t)\Big|_{q_f=0} = \left|\hat{P}_f(x)\Big|_{q_f=0}\right|\sin(\omega t+\eta) \tag{3.46}$$

where η is a phase shift between real and imaginary values of the fracture incremental pressure amplitude, and $\left|P_f(x,t)|_{q_f=0}\right|$ is the absolute value of the incremental fracture pressure amplitude assuming that there is no cross-flow. η is defined by the following equation:

$$\eta = \tan^{-1}\left\{\frac{imag\left[\hat{P}_f(x)\Big|_{q_f=0}\right]}{real\left[\hat{P}_f(x)\Big|_{q_f=0}\right]}\right\} \tag{3.47}$$

η changes with the distance from the injector and it is equal to zero when t=0.

Equation 3.46 defines the real-valued incremental fracture pressure distribution assuming there is no cross-flow at the rock matrix and the fracture interface.

3.3.3 The rock matrix fluid pressure

To calculate the cross-flow rate, we must solve the incremental pressure propagation equation within the rock matrix. We seek a solution for the rock matrix equation that is in the form of Equation 3.29. Equation 3.29 has two terms; the first term represents wave motion in the negative x direction, and the second term represents wave motion in the positive x direction within the fracture. Because the fracture has finite length, wave motions are in both directions within the fracture. i.e., the propagating and reflecting waves. In contrary, within the rock matrix, wave propagates in only one direction (the positive y direction) from the interface, because we assume that the rock matrix is of an infinite size. Following is the approximated solution for the incremental rock matrix pressure:

$$P_r(x,y,t) = P_r(x,t)\big|_{y=w/2}\, e^{-D_r y} \tag{3.48}$$

where D_r expresses ability of the liquid to flow through the rock matrix. D_r is expressed with the following equation:

$$D_r^2 = \frac{\varphi_r \mu_o c_{tr} \omega}{k_r k_{ro}^o} i \tag{3.49}$$

$P_r(x,y,t)|_{y=w/2}$ is the rock matrix incremental pressure distribution at the interface of the fracture and the rock matrix, where y=w/2 and $0 \le x \le x_f$. The time-harmonic solution for

the incremental rock matrix pressure, $P_r(x, y, t)$ is defined by Equation 3.3. Substituting $P_r(x, y, t)$ of Equation 3.48 with Equation 3.3 gives the following expression for the incremental rock matrix pressure distribution:

$$P_r(x, y, t) = \hat{P}_r(x)\Big|_{y=w/2} e^{-D_r y} e^{i\omega t} \tag{3.50}$$

where $\hat{P}_r(x)\Big|_{y=w/2}$ is the incremental rock matrix pressure amplitude evaluated at the interface between the fracture and the rock matrix.

According to the boundary condition 3.22, $P_r = P_f$ at y=w/2 and $0 \le x \le x_f$. Thus the incremental pressure distribution within the two-dimensional rock matrix becomes

$$P_r(x, y, t) = \hat{P}_f(x) e^{-D_r y} e^{i\omega t} \tag{3.51}$$

or

$$\hat{P}_r(x, y) = \hat{P}_f(x) e^{-D_r y} \tag{3.52}$$

where $P_r(x, y, t)$ is the two-dimensional rock matrix incremental pressure, $\hat{P}_r(x, y)$ is the incremental rock matrix pressure amplitude, and $\hat{P}_f(x)$ is the one-dimensional incremental fracture pressure amplitude with the cross-flow. We can obtain $\hat{P}_f(x)$ by solving Equation 3.14, which is given in the next section. We show in the next section that $\hat{P}_f(x)$ is complex-valued, which makes $\hat{P}_r(x, y)$ to be complex-valued as well. The real-valued two-dimensional rock matrix incremental pressure can be calculated using the following equation:

$$P_r(x, y, t) = \left|\hat{P}_r(x, y)\right| \sin(\omega t + \theta) \tag{3.53}$$

where $\left|\hat{P}_r(x,y)\right|$ is the absolute value of $\hat{P}_r(x,y)$, and θ is a phase shift between the real and imaginary values of $\hat{P}_r(x,y)$. θ is equal to zero when t=0 and defined by the following equation:

$$\theta = \tan^{-1}\left\{\frac{imag\left[\hat{P}_r(x,y)\right]}{real\left[\hat{P}_r(x,y)\right]}\right\} \tag{3.54}$$

3.3.4 The incremental fracture pressure with a cross-flow

In this section we solve Equation 3.14 to obtain the incremental fracture pressure amplitude distribution, $\hat{P}_f(x)$ with the existence of the cross-flow. Once calculated, we (a) apply Equations 3.52 and 3.53 to obtain the incremental rock matrix pressure distribution, (b) then apply Equation 3.12 to obtain cross-flow rate at the interface between the fracture and the rock matrix, and (c) evaluate the volume of the mobilized oil.

The first order derivative of the rock matrix incremental pressure with respect to y coordinate evaluated at the rock matrix and the fracture interface can be obtained from Equation 3.51.

$$\left.\frac{\partial P_r(x,y,t)}{\partial y}\right|_{y=w/2} = -D_r\hat{P}_f(x)e^{i\omega t}e^{-\frac{D_r w}{2}} \tag{3.55}$$

The second order derivative of $P_r(x,y,t)$ with respect to x coordinate, and the first order derivative of $P_r(x,y,t)$ with respect to time are similar to Equations 3.25 and 3.26; they are obtained from Equation 3.2. Substituting the second order derivative of $P_r(x,y,t)$ with respect to x, the first order derivative of $P_r(x,y,t)$ with respect to time, and

Equation 3.55 into Equation 3.14 gives the following ordinary differential equation for the incremental fracture pressure propagation equation:

$$\frac{d^2\hat{P}_f(x)}{dx^2} - \left(\frac{2k_r k_{ro}^o D_r \mu_w e^{-\frac{D_r w}{2}}}{k_f k_{rw}^o w \mu_o} + \frac{\phi_f \mu_w c_{tf} \omega}{k_f k_{rw}^o} i \right) \hat{P}_f(x) = 0 \qquad 3.56$$

or

$$\frac{d^2\hat{P}_f(x,t)}{dx^2} - \bar{D}_f^2 \hat{P}_f(x) = 0 \qquad 3.57$$

where $\bar{D}_f^2$ expresses liquid flow ability through the fracture when there is a cross-flow. $\bar{D}_f^2$ is constant and defined by the following expression:

$$\bar{D}_f^2 = \frac{2k_r k_{ro}^o D_r \mu_w e^{-\frac{D_r w}{2}}}{k_f k_{rw}^o w \mu_o} + \frac{\phi_f \mu_w c_{tf} \omega}{k_f k_{rw}^o} i \qquad 3.58$$

Solution of Equation 3.56 is in the following form:

$$\hat{P}_f(x) = A_1 e^{\bar{D}_f x} + A_2 e^{-\bar{D}_f x} \qquad 3.59$$

We evaluate the constants A_1 and A_2 using the boundary conditions 3.16 and 3.17. The procedure is exactly the same as evaluating the constants for the no cross-flow case (Section 3.3.2). Upon evaluating the integration constants we get the following equation.

$$\hat{P}_f(x) = \frac{R_f}{\bar{D}_f} \frac{\cosh\left[\bar{D}_f (x - x_f)\right]}{\sinh\left[\bar{D}_f x_f\right]} \qquad 3.60$$

Equation 3.60 defines the one-dimensional incremental fracture pressure amplitude generated by the time-harmonic water flooding. $\bar{D}_f$ is a complex number, which makes $\hat{P}_f(x)$ to be complex-valued as well. The actual value of the incremental

fracture pressure amplitude is the absolute value of $\hat{P}_f(x)$. Substituting $\hat{P}_f(x)$ into complex number expression of the rock matrix pressure oscillations (Equation 3.2) gives complex-valued incremental fracture pressure, which satisfies boundary conditions 3.16 and 3.17 that we used to derive $\hat{P}_f(x)$. As mentioned earlier, the complex number approach of expressing oscillatory fluid pressures does not satisfy initial condition. Therefore, we also give analytical expression for real-valued incremental fracture pressure distribution that satisfies initial condition 3.15. The real-valued fracture incremental pressure distribution can be calculated using the following equation:

$$P_f(x,t) = \left|\hat{P}_f(x)\right| \sin(\omega t + \alpha) \tag{3.61}$$

where $\left|\hat{P}_f(x)\right|$ is the absolute value of the incremental fracture pressure, and α is the phase shift between the real and imaginary values of $\hat{P}_f(x)$. α is equal to zero when t=0 and defined below:

$$\alpha = \tan^{-1}\left\{\frac{imag\left[\hat{P}_f(x)\right]}{real\left[\hat{P}_f(x)\right]}\right\} \tag{3.62}$$

3.3.5 Volume of mobilized oil

In the above subsections, it was shown that by carrying out time-harmonic water flooding of small amplitude, an exchange of fluid between the fracture and rock matrix can be induced. Such a fluid exchange may be a way of extracting the oil from the rock matrix to the fracture. In this section we provide an analytical solution for calculating the total cross flow rate, and the volume of mobilized oil because of the stimulation assuming

that (a) the rock matrix was not swept before the stimulation (b) the oil extracted out of the rock matrix does not flow back when the direction of the cross-flow reverses.

3.3.5.1 Cross-flow rate

The total cross-flow rate of the oil and water mixture is calculated using Equation 3.12. λ_r of Equation 3.12 is mobility of the cross-flow liquid within the rock matrix. We assume that λ_r is constant and equal to the oil mobility within the rock matrix at initial oil saturation. λ_r is defined by Equation 13, and $\left.\frac{\partial P_r(x,y,t)}{\partial y}\right|_{y=w/2}$ of Equation 3.12 is defined by Equation 3.55. Substituting Equations 3.13 and 3.55 into Equation 3.12 gives the following expression for the cross-flow rate at the fracture and the rock matrix interface.

$$q_f(x,t)\Big|_{y=w/2} = \frac{2hk_r k_{ro}^{\circ} D_r \hat{P}_f(x)}{\mu_o} e^{-\frac{D_r w}{2}} e^{iwt} \qquad 3.63$$

where $q_f(x,t)|_{y=w/2}$ is the volumetric cross-flow rate per unit length of the fracture evaluated at the interface of the rock matrix and the fracture.

The fluid pressure oscillations make cross-flow rate to be oscillatory. The mathematical expression for the cross-flow rate oscillations is given below:

$$q_f(x,t)\Big|_{y=w/2} = \hat{q}_f(x)\Big|_{y=w/2} e^{i\omega t} \qquad 3.64$$

where $q_f(x,t)|_{y=w/2}$ is the cross-flow rate amplitude evaluated at the interface of the fracture and the rock matrix. Substituting the cross-flow term of Equation 3.63 with Equation 3.64 gives the following expression for the cross-flow rate amplitude evaluated at the interface of the fracture and the rock matrix:

$$\hat{q}_f(x)\Big|_{y=w/2} = \frac{2hk_r k_{ro}^{\circ} D_r \hat{P}_f(x)}{\mu_o} e^{-\frac{D_r w}{2}} \tag{3.65}$$

The cross-flow rate amplitude evaluated at the rock matrix and the fracture interface at any distance x from the injector (Figure 3.1) is calculated using Equation 3.65. D_r and $\hat{P}_f(x)$ are complex numbers, which makes $q_f(x,t)|_{y=w/2}$ to be complex-valued as well. The actual cross-flow rate amplitude is the absolute vale of $q_f(x,t)|_{y=w/2}$. The real-valued cross-flow rate distribution with time and x can be calculated using the following equation:

$$q_f(x)\Big|_{y=w/2} = \left|\hat{q}_f(x)\Big|_{y=w/2}\right| \sin(\omega t + \beta) \tag{3.66}$$

where $\left|q_f(x,t)|_{y=w/2}\right|$ is the absolute value of the cross-flow rate amplitude evaluated at the fracture and the rock matrix interface, and β is phase shift between real and imaginary parts of the cross-flow rate amplitude, $\hat{q}_f(x)|_{y=w/2}$. β equals to zero when t=0 and defined by the following equation:

$$\beta = \tan^{-1}\left\{\frac{imag\left[\hat{q}_f(x)\Big|_{y=w/2}\right]}{real\left[\hat{q}_f(x)\Big|_{y=w/2}\right]}\right\} \tag{3.67}$$

$q_f(x,t)|_{y=w/2}$ of Equation 3.66 is real valued. The cross-flow rate can be negative or positive. Liquid flows from the rock matrix to the fracture when the rock matrix pressure increases in the direction of the positive y axis, whereas the liquid flows from the fracture to the rock matrix when the rock matrix pressure decreases in the direction of the positive

y axis. We call the flow from the rock matrix to the fracture a negative flow, and the flow from the fracture to the rock matrix a positive flow.

3.3.5.2 Volume of mobilized oil

The volume of mobilized oil is the integral of the cross flow rate over time and distance from the injector, x.

$$V = \int\int \left(q_f^+(x,t)\Big|_{y=w/2} f^+ - q_f^-(x,t)\Big|_{y=w/2} f^- \right) dxdt \qquad 3.68$$

where $q_f^-(x,t)\Big|_{y=w/2}$ is the cross-flow rate from the rock matrix to the fracture, $q_f^+(x,t)\Big|_{y=w/2}$ is the cross-flow rate from the fracture to the rock matrix, f^- is the fractional flow of oil from the rock matrix to the fracture, and f^+ is the fractional flow of oil from the fracture to the rock matrix. As mentioned earlier, we assume that fractional flow of oil from the fracture to the rock matrix is negligible ($f^+=0$). This assumption is based on relative permeability hysteresis. Thus Equation 3.68 becomes:

$$V = \int\int \left(q_f^-(x,t)\Big|_{y=w/2} f^- \right) dxdt \qquad 3.69$$

The oil fractional flow from the rock matrix to the fracture, f^- is discussed in the next section.

3.3.5.3 Oil fractional flow from the rock matrix to the fracture

The fractional flow of oil from the rock matrix to the fracture is a function of the oil saturation of the rock matrix. The following equation expresses the change of oil saturation of the rock matrix with time:

$$\frac{\partial S_o(x,y,t)}{\partial t} = \frac{k_r k_{ro}}{\varphi_r \mu_o}\left(\frac{\partial^2 P_r(x,y,t)}{\partial x^2} + \frac{\partial^2 P_r(x,y,t)}{\partial y^2}\right) \tag{3.70}$$

where $S_o(x,y,t)$ is the oil saturation of the rock matrix, $P_r(x,y,t)$ is the rock matrix incremental pressure, k_r is the rock matrix absolute permeability, k_{ro} is the oil relative permeability of the rock matrix, φ_r is the rock matrix porosity and μ_o is oil viscosity. The derivation of Equation 3.70 is given in Appendix B.

$P_r(x,y,t)$ is defined by Equation 3.51. Taking the second order derivative of $P_r(x,y,t)$ with respect to x and y coordinates and substituting in Equation 3.70 gives the following expression for the change of oil saturation of the rock matrix with time:

$$\frac{\partial S_o(x,y,t)}{\partial t} = \frac{k_r k_{ro} e^{-\frac{D_r w}{2}} e^{i\omega t}}{\varphi_r \mu_o}\left(\frac{d^2 \hat{P}_f(x)}{dx^2} + D_r^2 \hat{P}_f(x)\right) \tag{3.71}$$

where D_r represents flow ability of the cross-flow liquid through the rock matrix and defined by Equation 3.49. $\hat{P}_f(x)$ is the one-dimensional incremental fracture pressure generated by the stimulation. The second derivative of $\hat{P}_f(x)$ with respect to x coordinate is given below:

$$\frac{d^2 \hat{P}_f}{dx^2} = R_f \bar{D}_f \frac{\cosh\left[\bar{D}_f (x - x_f)\right]}{\sinh\left[\bar{D}_f x_f\right]} \tag{3.72}$$

or

$$\frac{d^2 \hat{P}_f}{dx^2} = \bar{D}_f^2 \hat{P}_f(x) \tag{3.73}$$

where $\overline{D}_f$ represents liquid flow ability through the fracture with the cross-flow and defined by Equation 3.58. Substituting Equations 3.49, 3.58 and 3.73 into Equation 3.72 gives

$$\frac{\partial S_o(x,y,t)}{\partial t} = \frac{k_r k_{ro} \hat{P}_f(x) e^{-D_r y} e^{i\omega t}}{\varphi_r \mu_o} \left(\frac{2k_r k_{ro}^o \mu_w}{k_f k_{rw}^o w \mu_o} \sqrt{\frac{\varphi_r \mu_o c_{tr} \omega}{k_r k_{ro}^o}} i + \frac{\phi_f \mu_w c_{tf} \omega}{k_f k_{rw}^o} i + \frac{\varphi_r \mu_o c_{tr} \omega}{k_r k_{ro}^o} i \right) \quad 3.74$$

Under the small compressibility assumption the right side of Equation 3.74 is small. We realize that $\frac{\partial S_o(x,y,t)}{\partial t}$ is not actually zero, because we are producing rock matrix oil through the cross-flow. However, we also know that we produce very small fraction of the rock matrix oil during short period of time because of a small cross-flow pressure gradients generated by the time-harmonic water flooding. This supports the assumption of insignificant change in the rock matrix oil saturation during short periods of time. In the example calculation (Chapter 4), we therefore assume that the fractional flow of oil from the rock matrix to the fracture, $\bar{f}$ that is directly proportional to the oil saturation of the rock matrix, remains constant during one day of stimulation.

3.3.6 Summary

Section 3.3 gives derivation of the equations, which are originally given by Jeong et al. (2011). The real-valued incremental pressure distribution within a fracture can be calculated using Equation 3.61, where the incremental fracture pressure amplitude and the phase shift between the real and imaginary parts of the fracture pressure amplitude are calculated using Equation 3.60 and 3.62 respectively. The real-valued incremental rock

matrix pressure is calculated using Equation 3.53, where the incremental rock matrix pressure amplitude and the phase shift between the real and imaginary parts of the rock matrix pressure amplitude can be calculated using Equations 3.52 and 3.54. The real-valued cross-flow rate can be calculated using Equation 3.66, where the cross-flow rate amplitude and the phase shift between the real and imaginary parts of the cross-flow rate amplitude can be calculated using Equations 3.65 and 3.67. The volume of mobilized oil is calculated using Equation 3.69. An example calculation is given in Chapter 4.

3.4 DIMENSIONLESS ANALYSIS

The purposes of the dimensionless analysis are to minimize the number of free parameters of the problem, to transform it to the dimensionless form so that it would be applicable to any geometrically similar system, and to develop dimensionless groups that will have some physical significance. There are two methods of transforming the problem into dimensionless form: dimensional analysis and inspectional analysis. We perform the method of inspectional analysis in this chapter.

3.4.1 Dependent and independent variables

The problem has 3 independent variables, which are x, y, and t. The dependent variables of the problem are $P_f(x,t)$ and $P_r(x,y,t)$. There are 15 free variables that are k_r, k_f, k_{ro}°, k_{rw}°, φ_r, φ_f, c_{tr}, c_{tf} w, h, x_f, μ_o, μ_w, $\hat{q}_w$, ω. There are total of 18 parameters (3 independent and 15 free variables) that are required to define the problem.

$$P_r, P_f = f(x, y, t; k_r, k_f, k_{ro}^{\circ}, k_{rw}^{\circ}, \varphi_r, \varphi_f, c_{tr}, c_{tf}, w, h, x_f, \mu_o, \mu_w, \hat{q}_w, \omega) \qquad 3.75$$

3.4.2 Inspectional analysis

Inspectional analysis is done using the procedures shown in Shook et al. (1992). The following linear transformations for dependent and independent variables are used:

$$t = t_1^* t_D + t_2^* \tag{3.76}$$

$$x = x_1^* x_D + x_2^* \tag{3.77}$$

$$y = y_1^* y_D + y_2^* \tag{3.78}$$

$$P_f(x,t) = P_{f1}^* P_{fD} + P_{f2}^* \tag{3.79}$$

$$P_r(x,y,t) = P_{r1}^* P_{rD} + P_{r2}^* \tag{3.80}$$

Where t_D, x_D, y_D, P_{fD}, and P_{rD} are dimensionless time, dimensionless x coordinate, dimensionless y coordinate, dimensionless incremental fracture pressure and dimensionless incremental rock matrix pressure, respectively. $t_1^*, t_2^*, x_1^*, x_2^*, y_1^*, y_2^*, P_{r1}^*$, P_{r2}^*, P_{f1}^*, and P_{f2}^* are scaling factors.

The chain rule is used to transform the incremental fracture and the rock matrix pressure derivatives with respect to x and y coordinates, and time to the dimensionless form.

$$\frac{\partial P_f}{\partial x} = \frac{\partial P_f}{\partial P_{fD}} \frac{\partial P_{fD}}{\partial x_D} \frac{\partial x_D}{\partial x} \tag{3.81}$$

Equations 3.77 and 3.79 gives the followings:

$$\frac{\partial P_f}{\partial P_{fD}} = P_{f1}^* \tag{3.82}$$

$$\frac{\partial x_D}{\partial x} = \frac{1}{x_1^*} \tag{3.83}$$

Thus, the transformation of the first and second order incremental fracture pressure derivative with respect to x coordinate to the dimensionless form is given below.

$$\frac{\partial P_f}{\partial x} = \frac{\partial P_f}{\partial P_{fD}} \frac{\partial P_{fD}}{\partial x_D} \frac{\partial x_D}{\partial x} = \frac{P_{f1}^*}{x_1^*} \frac{\partial P_{fD}}{\partial x_D} \tag{3.84}$$

$$\frac{\partial^2 P_f}{\partial x^2} = \frac{P_{f1}^*}{x_1^*} \frac{\partial^2 P_{fD}}{\partial x_D^2} \frac{\partial x_D}{\partial x} = \frac{P_{f1}^*}{\left(x_1^*\right)^2} \frac{\partial^2 P_{fD}}{\partial x_D^2} \tag{3.85}$$

The incremental fracture pressure derivative with respect to time becomes

$$\frac{\partial P_f}{\partial t} = \frac{\partial P_f}{\partial P_{fD}} \frac{\partial P_{fD}}{\partial t_D} \frac{\partial t_D}{\partial t} = \frac{P_{f1}^*}{t_1^*} \frac{\partial P_{fD}}{\partial t_D} \tag{3.86}$$

The incremental rock matrix pressure derivative with respect to x and y coordinates become

$$\frac{\partial^2 P_r}{\partial x^2} = \frac{P_{r1}^*}{\left(x_1^*\right)^2} \frac{\partial^2 P_{rD}}{\partial x_D^2} \tag{3.87}$$

$$\frac{\partial P_r}{\partial y} = \frac{P_{r1}^*}{y_1^*} \frac{\partial P_{rD}}{\partial y_D} \tag{3.88}$$

$$\frac{\partial^2 P_r}{\partial y^2} = \frac{P_{r1}^*}{\left(y_1^*\right)^2} \frac{\partial^2 P_{rD}}{\partial y_D^2} \tag{3.89}$$

The incremental rock matrix pressure derivative with respect to time become

$$\frac{\partial P_r}{\partial t} = \frac{P_{f1}^*}{t_1^*} \frac{\partial P_{rD}}{\partial t_D} \tag{3.90}$$

Substituting Equations 3.85, 3.86 and 3.88 in Equation 3.14 and dividing both sides of the equation by $\frac{P_1^*}{(x_1^*)^2}$ gives the following dimensionless form of the fracture equation:

$$\underbrace{\left(\frac{\phi_f \mu_w c_{tf}}{k_f k_{rw}^o}\frac{(x_1^*)^2}{t_1^*}\right)}_{1}\frac{\partial P_{fD}}{\partial t_D} = \frac{\partial^2 P_{fD}}{\partial x_D^2} + \underbrace{\left(\frac{2k_r k_{ro}^o \mu_w}{w k_f k_{rw}^o \mu_o}\frac{(x_1^*)^2}{P_{f1}^*}\frac{P_{r1}^*}{y_1^*}\right)}_{2}\frac{\partial P_{rD}}{\partial y_D} \tag{3.91}$$

Substituting Equation 3.87, 3.89 and 3.90 into Equation 3.20 and dividing both sides of the equation by $\frac{P_{r1}^*}{\left(x_1^*\right)^2}$ gives the following dimensionless form of the rock matrix pressure transient equation:

$$\underbrace{\left(\frac{\varphi_r \mu_o c_{tr}}{k_r k_{ro}^o}\frac{(x_1^*)^2}{t_1^*}\right)}_{3}\frac{\partial P_{rD}}{\partial t_D} = \frac{\partial^2 P_{rD}}{\partial x_D^2} + \underbrace{\left(\frac{x_1^*}{y_1^*}\right)^2}_{4}\frac{\partial^2 P_{rD}}{\partial y_D^2} \tag{3.92}$$

Equations 3.91 and 3.92 are dimensionless forms of the pressure transient equations within the fracture and the rock matrix respectively. Dimensionless forms of the initial conditions are given below

$$P_{fD} = \underbrace{-\frac{P_{f2}^*}{P_{f1}^*}}_{5}, \text{ at } \quad t_D = \underbrace{-\frac{t_2^*}{t_1^*}}_{6} \tag{3.93}$$

$$P_{rD} = \underbrace{-\frac{P_{r2}^*}{P_{r1}^*}}_{7}, \text{ at } \quad t_D = -\frac{t_2^*}{t_1^*} \tag{3.94}$$

The boundary conditions become

$$\frac{\partial P_{fD}}{\partial x_D} = -\left(\frac{\mu_w \hat{q}_w}{2whk_f k_{rw}^o} \frac{x_1^*}{P_{f1}^*} \right) e^{i\omega t}, \text{ at } x_D = -\frac{x_2^*}{x_1^*} \qquad 3.95$$

8 9

$$\frac{\partial P_{fD}}{\partial x_D} = 0 \text{ , at } x_D = \left(\frac{x_f - x_2^*}{x_1^*} \right) \qquad 3.96$$

10

$$P_{rD} = \frac{P_f - P_{r2}^*}{P_{r1}^*}, \text{ at } y_D = \frac{w - 2y_2^*}{2y_1^*} \text{ and } -\frac{x_2^*}{x_1^*} \le x_D \le \frac{x_f - x_2^*}{x_1^*} \qquad 3.97$$

11 12

There are 12 dimensionless groups and 10 scaling factors of the problem. The dimensionless groups and scaling factors are numbered and also summarized in Tables 3-1 and 3-2.

Dimensionless groups											
1	2	3	4	5	6	7	8	9	10	11	12
$\frac{\phi_f \mu_w c_{tf}}{k_f k_{rw}^o} \frac{(x_1^*)^2}{t_1^*}$	$\frac{2k_f k_{ro}^o \mu_w}{wk_f k_{rw}^o \mu_o} \frac{(x_1^*)^2}{P_{f1}^*} \frac{P_{r1}^*}{y_1^*}$	$\frac{\varphi_r \mu_o c_{tr}}{k_r k_{ro}^o} \frac{(x_1^*)^2}{t_1^*}$	$\left(\frac{x_1^*}{y_1^*}\right)^2$	$\frac{P_{f2}^*}{P_{f1}^*}$	$\frac{t_2^*}{t_1^*}$	$\frac{P_{r2}^*}{P_{r1}^*}$	$\frac{\mu_w \hat{q}_w}{2whk_f k_{rw}^o} \frac{x_1^*}{P_{f1}^*}$	$\frac{x_2^*}{x_1^*}$	$\frac{x_f - x_2^*}{x_1^*}$	$\frac{P_f - P_{r2}^*}{P_{r1}^*}$	$\frac{w - 2y_2^*}{2y_1^*}$

Table 3-1: Dimensionless groups of the problem

Scaling factors									
1	2	3	4	5	6	7	8	9	10
x_1^*	x_2^*	y_1^*	y_2^*	t_1^*	t_2^*	P_{f1}^*	P_{f2}^*	P_{r1}^*	P_{r2}^*

Table 3-2: Scaling factors of the problem

We need to set the dimensionless groups to be equal to one or zero to be able to evaluate the scaling factors. Equating the dimensionless groups to one or zero is arbitrary provided that multiplicative scaling factors do not disappear and we do not change the original form of Equations 3.14 and 3.20. Setting groups 5-7, 9, and 12 to be equal to zero gives the followings for the additive scaling factors:

$$x_2^* = 0 \tag{3.98}$$

$$y_2^* = w/2 \tag{3.99}$$

$$t_2^* = 0 \tag{3.100}$$

$$P_{f2}^* = 0 \tag{3.101}$$

$$P_{r2}^* = 0 \tag{3.102}$$

Setting groups 1, 2, 4, 8, and 10 to be equal to one gives the following expressions for the multiplicative scaling factors:

$$x_1^* = x_f \tag{3.103}$$

$$y_1^* = x_f \tag{3.104}$$

$$P_{r1}^* = \frac{\mu_o \hat{q}_w}{4hk_r k_{ro}^o} \tag{3.105}$$

$$P_{f1}^* = \frac{\mu_w \hat{q}_w x_f}{2whk_f k_{rw}^o} \tag{3.106}$$

$$t_1^* = \frac{\varphi_f \mu_w c_{tf} x_f^2}{k_f k_{rw}^o} \tag{3.107}$$

The dimensionless form of the fracture equation becomes:

$$\frac{\partial P_{fD}}{\partial t_D} = \frac{\partial^2 P_{fD}}{\partial x_D^2} + \left.\frac{\partial P_{rD}}{\partial y_D}\right|_{y_D=0} \tag{3.108}$$

The dimensionless form of the rock matrix equation becomes:

$$\left(\frac{k_f k_{rw}^o \phi_r c_{tr} \mu_o}{k_r k_{ro}^o \phi_f c_{tf} \mu_w}\right)\frac{\partial P_{rD}}{\partial t_D} = \frac{\partial^2 P_{rD}}{\partial x_D^2} + \frac{\partial^2 P_{rD}}{\partial y_D^2} \tag{3.109}$$

Dimensionless boundary and initial conditions become:

$$P_{fD} = 0 \text{, at } \quad t_D = 0 \tag{3.110}$$

$$P_{rD} = 0 \text{, at } \quad t_D = 0 \tag{3.111}$$

$$\frac{\partial P_{fD}}{\partial t_D} = -e^{i\omega t} = -\frac{q_w(t)}{\hat{q}_w} = -q_{wD} \text{, at } x_D = 0 \tag{3.112}$$

$$\frac{\partial P_{fD}}{\partial x_D} = 0 \text{ , at } x_D = 1 \tag{3.113}$$

$$P_{rD} = \frac{4hk_r k_{ro}^o}{\mu_o \hat{q}_w} P_f(x,t) \text{, } \quad \text{at } y_D = 0 \text{ and } 0 \le x_D \le 1 \tag{3.114}$$

where q_{wD} is dimensionless incremental water injection rate and defined by the following equation:

$$q_{wD} = \frac{q_w(t)}{\hat{q}_w} \tag{3.115}$$

The dimensionless dependent and independent variables are defined by the following equations:

$$x_D = \frac{x}{x_f} \tag{3.116}$$

$$y_D = \frac{2y - w}{2x_f} \tag{3.117}$$

$$t_D = \frac{k_f k_{rw}^o}{\phi_f \mu_w c_{tf} x_f^2} t \tag{3.118}$$

$$P_{fD} = \frac{2whk_f k_{rw}^o}{\mu_w x_f \hat{q}_w} P_f(x,t) \tag{3.119}$$

$$P_{rD} = \frac{4hk_r k_{ro}^o}{\mu_o \hat{q}_w} P_r(x,y,t) \tag{3.120}$$

The dimensionless angular frequency of the stimulation is defined below

$$\omega_D = \frac{\phi_f \mu_w c_{tf} x_f^2 \omega}{k_f k_{rw}^o} \tag{3.121}$$

3.4.3 Summary

The rock matrix and the fracture incremental pressures in any geometrically similar system are a function of the dimensionless free variables, dimensionless stimulation frequency, dimensionless incremental water injection rate, and the dimensionless group of the problem.

$$P_{fD}, P_{rD} = f\left[t_D, x_D, y_D; \omega_D, q_{wD}\left(\frac{k_f k_{rw}^o \varphi_r c_{tr} \mu_o}{k_r k_{ro}^o \varphi_f c_{tf} \mu_w}\right)\right] \tag{3.122}$$

where, t_D, x_D, y_D are dimensionless independent variables, ω_D and q_{wD} are the dimensionless stimulation frequency and incremental water injection rate respectively. $\frac{k_f k_{rw}^o \varphi_r c_{tr} \mu_o}{k_r k_{ro}^o \varphi_f c_{tf} \mu_w}$ is the dimensionless group of the problem that represents the time scaling factor difference between a flow within the rock matrix and the fracture.

3.5 CONCLUSIONS

Description of the fractured reservoir model, and the pressure propagation equations within the rock matrix and the fracture are given along with their solutions. The exponential expression of the fluid pressure oscillations helps us to transform the one-dimensional fluid pressure propagation equations that are partial differential equations with respect to space x and time t, into ordinary differential equations with respect to space x. The solutions for the pressure propagation equations within the fracture and the rock matrix for fluid pressure oscillations are originally given in Jeong et al. (2011). Section 3.3 gives the derivations of the pressure oscillation equations, and the expressions for calculating the cross-flow rate and the volume of the mobilized oil because of the stimulation. Inspectional analysis of the problem described in Section 3.2 shows that the dimensionless rock matrix and the fracture incremental pressures are functions of the dimensionless independent variables, dimensionless stimulation frequency, dimensionless water injection rate, and dimensionless group representing time scaling factor differences between a flow within the fracture and the rock matrix.

Chapter 4: Example calculation and sensitivity analysis

4.1 INTRODUCTION

The purpose of this chapter is to give example calculations of the fracture, rock matrix incremental pressures, and the cross-flow rate at the interface of the fracture and the rock matrix using the equations derived in Chapter 3. We refer to Figure 3-1 throughout this chapter. The chapter consists of 5 sections. The first section provides the outline of the chapter. The second section gives an example calculation of the fracture and rock matrix incremental pressures because of the stimulation; the cross-flow rate distribution at the fracture and the rock matrix interface; and the volume of the mobilized oil because of the time-harmonic water flooding. The third section performs sensitivity analysis of the fracture incremental pressures, and the cross-flow rate generated by the stimulation. The fourth section gives a comparison of the actual incremental oil production reported in the literature and estimated oil production using the method described in Chapter 3. The last section gives a summary and conclusions.

4.2 EXAMPLE CALCULATION

4.2.1 Example calculation steps

The following steps are taken to calculate the fracture and the rock matrix incremental pressures, and the volume of the mobilized oil because of the stimulation:

1. Apply Equation 3.60 to calculate the complex-valued incremental fracture pressure amplitude distribution with x. $\overline{\mathrm{D}}_{\mathrm{f}}$ and R_{f} are calculated using Equations 3.58 and 3.37, respectively.
2. Apply Equation 3.61 to calculate the real-valued incremental fracture pressure distribution as a function of time and distance. α and ω are calculated using Equations 3.62 and 3.4, respectively.
3. Apply Equation 3.52 to calculate the complex-valued incremental rock matrix pressure amplitude distribution with x and y. $\overline{\mathrm{D}}_{\mathrm{r}}$ is calculated using Equation 3.49.
4. Apply Equation 3.51 to calculate the complex-valued incremental rock matrix pressure distribution, and Equation 3.53 to calculate the real-valued incremental rock matrix pressure distribution with space and time. θ is calculated using Equation 3.54.
5. Apply Equation 3.65 to calculate the complex-valued cross-flow rate amplitude distribution at the interface of the rock matrix and the fracture.
6. Apply Equation 3.64 to compute the complex-valued cross-flow rate distribution, and Equation 3.66 to compute the real-valued cross-flow rate distribution. β is calculated using Equation 3.67.
7. Apply Equation 3.69 to compute the volume of mobilized oil because of the stimulation.

Table 4-1 shows the fracture properties, rock matrix properties, reservoir fluid properties, fracture dimensions, stimulation frequency, injection rate amplitude, and oil fractional flow value used in the example calculation. We use a high oil fractional flow value (0.8), because we assume that initial oil saturation of the rock matrix is high, which means that a significant volume of the rock matrix oil was not swept before the stimulation. Table 4-1 provides the data in English and SI units, whereas the calculation results are given only in SI units.

Fracture properties	**English**	**SI**
Fracture porosity, φ_f	0.05	
Total fracture compressibility, c_{tf}	10^{-5} 1/psi	1.47×10^{-9} 1/Pa
Fracture absolute permeability, k_f	5×10^{5} md	4.94×10^{-10} m2
Fracture water end point real permeability, k^{o}_{rw}	0.8	
Fracture dimensions		
Fracture width, w	0.003 ft	0.001 m
Fracture height, h	32.81 ft	5 m
Fracture length, x_f	65.62 ft	20 m
Rock matrix properties		
Rock matrix porosity, φ_r	0.2	
Total rock matrix compressibility, c_{tr}	10^{-5} 1/psi	1.47×10^{-10} 1/Pa
Rock matrix absolute permeability, k_r	100 md	9.87×10^{-14} m2
Rock matrix oil end point real permeability, k^{o}_{ro}	0.2	
Reservoir fluid properties		
Oil viscosity, μ_o	1 cp	0.001 Pa-s
Water viscosity, μ_w	0.8 cp	0.0008 Pa-s
Stimulation frequency, n	0.1 Hz	
Incremental water injection rate amplitude, $\hat{q}_w$	10 bbl/day	1.84×10^{-5} m^3/s
Oil fractional flow from the rock matrix to fracture, $\bar{f}$	0.8	

Table 4-1: Data used in the example calculation

4.2.2 Incremental fracture pressure distribution

The incremental fracture pressure distribution is calculated using Equation 3.61, where the incremental fracture pressure amplitude, $\widehat{P}_f(x)$ and the phase shift between the real and imaginary values of the incremental fracture pressure amplitude, α are calculated using Equations 3.60 and 3.62, respectively. Figure 4-1 shows the absolute value of the incremental fracture pressure amplitude distribution using the data given in Table 4-1. The figure shows how the incremental fracture pressure attenuates away from the seismic wave source in the injector (Figure 3-1).

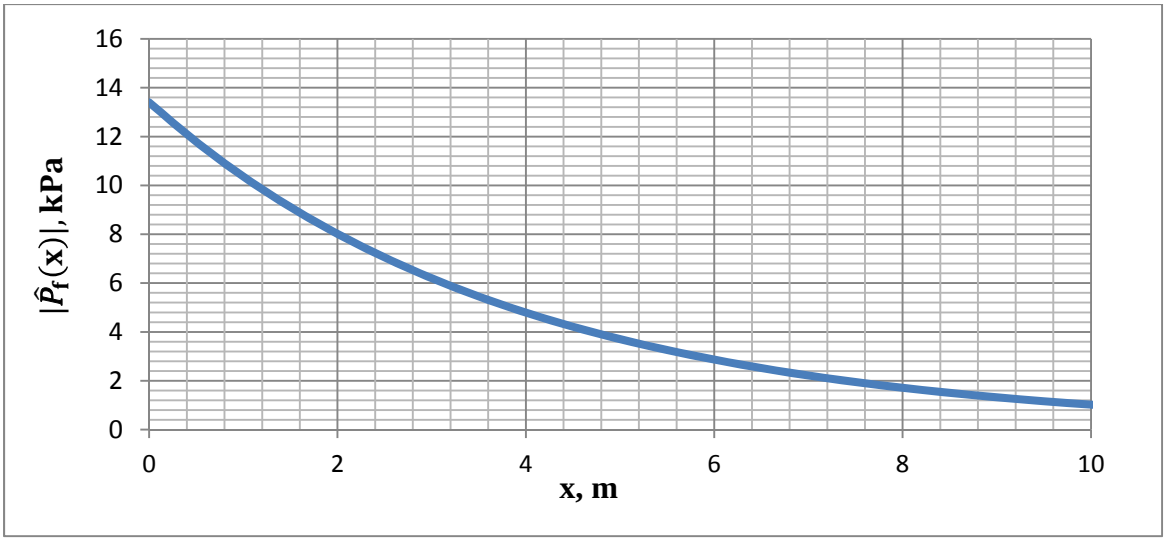

Figure 4-1: Absolute value of the one-dimensional incremental fracture pressure distribution

Once the complex-valued incremental fracture pressure amplitude and phase shift between the real and imaginary values of the fracture incremental pressure amplitude are calculated, we can apply Equation 3.61 to compute the real-valued incremental fracture pressure distribution with time and x. Figure 4-2 shows the incremental fracture pressure

distribution with time at 1, 5, 10, and 20 meters distances from the seismic wave source in the injector.

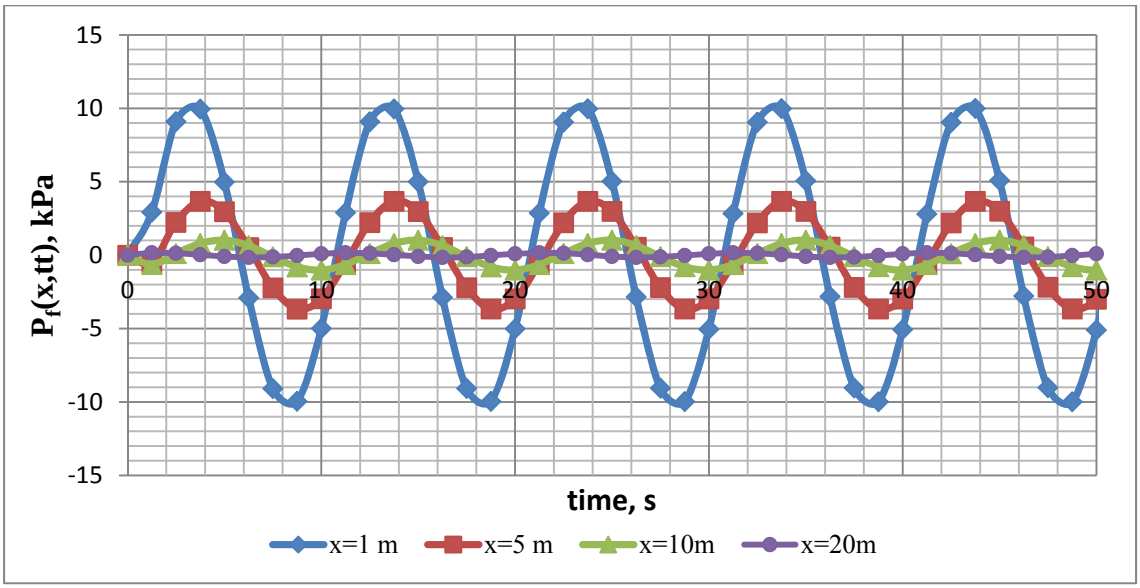

Figure 4-2: Change of incremental fracture pressure with time at 1, 5, 10, 20 m from the injector

Figure 4-3 shows the incremental fracture pressure distribution with x at 1, 2, 3, 6, 7, and 8 seconds of the stimulation. Figures 4-2 and 4-3 show that the incremental fracture pressure can be positive or negative. A positive $P_f(x,t)$ means that the steady-state fracture pressure, $P_{ss}(x)$ was decreased by $P_f(x,t)$, whereas a negative $P_f(x,t)$ means that the steady-state fracture pressure, $P_{ss}(x)$ was decreased by the modulus of $P_f(x,t)$ (Equation 3.5).

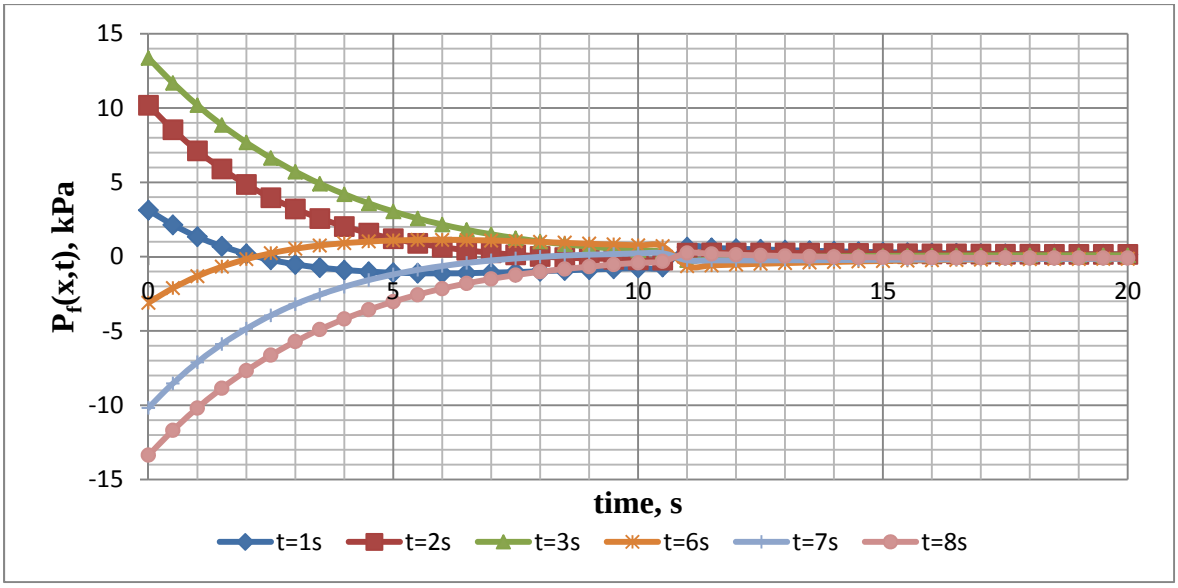

Figure 4-3: Incremental fracture pressure distribution at 1, 2, 3, 6, 7, and 8 seconds of the stimulation

4.2.3 Incremental rock matrix pressure distribution

The real-valued incremental rock matrix pressure amplitude distribution within the two-dimensional rock matrix, $P_r(x, y, t)$ is calculated using Equation 3.53, where the incremental rock matrix pressure amplitude, $\widehat{P}_r(x, y)$ is calculated using Equation 3.52, and the phase shift between the real and imaginary values of $\widehat{P}_r(x, y)$, θ is calculated using Equation 3.54. Figure 4-4 shows distribution of the absolute value of the incremental pressure amplitude within the two-dimensional rock matrix of Figure 3-1b. The rock matrix pressure waves attenuate in both the positive x and y directions from the seismic wave source.

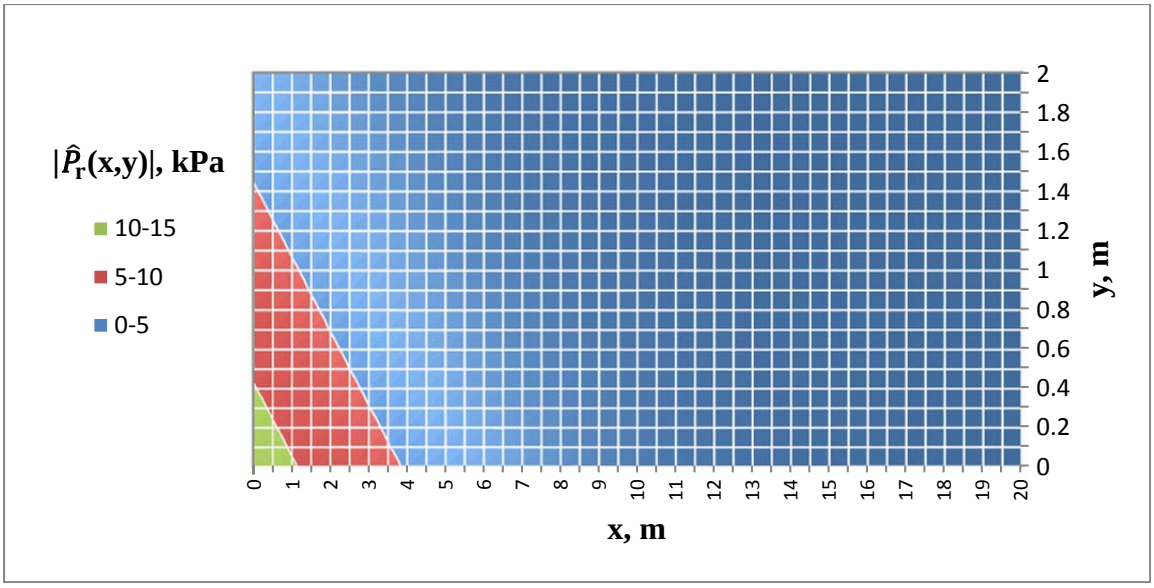

Figure 4-4: Absolute value of the incremental rock matrix pressure amplitude distribution

Figures 4-5 and 4-6 show the distribution of the real values of the incremental rock matrix pressure at t=2 and t=6 seconds respectively. The pressure values are not actual incremental rock matrix pressures, they are only the real parts of the incremental rock matrix pressure $P_r(x,y,t)$. The purpose of Figures 4-6 and 4-7 is to show the cross-flow pressure gradient generated at the interface of the rock matrix and the fracture.

At t=2 seconds, the incremental rock matrix pressure decreases away from the fracture (the positive y direction), which means that there is a flow from the fracture to the rock matrix. It also implies that the incremental rock matrix pressure gradient evaluated at the fracture and the rock matrix interface, $\left.\frac{\partial P_r(x,y,t)}{\partial y}\right|_{y=w/2}$ is negative number (Figure 4-5). The negative pressure gradient makes the cross-flow rate evaluated at the fracture and the rock matrix interface to be positive (Equation 3.63). Thus we call a flow from the fracture to the rock matrix a positive flow.

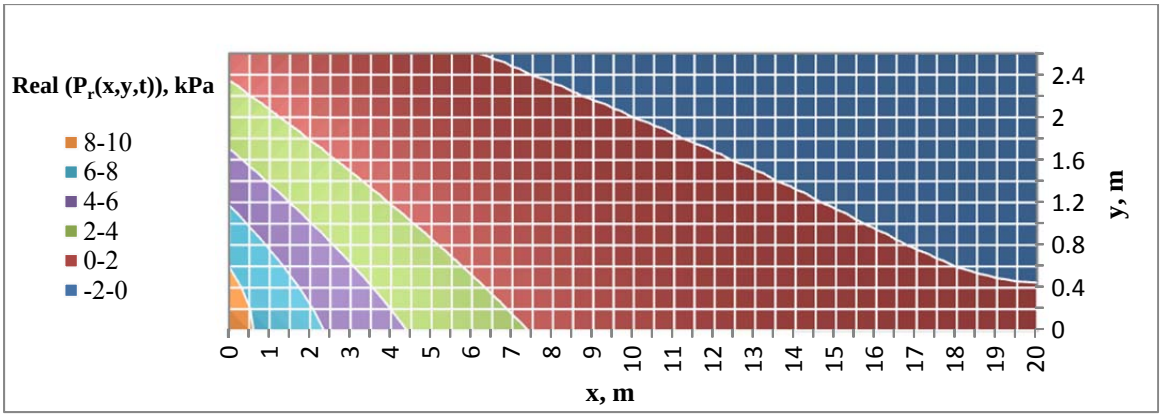

Figure 4-5: Real part of the incremental rock matrix pressure distribution at t=2 seconds

At t=6 seconds, the incremental rock matrix pressure increases away from the fracture (the positive y direction), which means that there is a flow from the rock matrix into the fracture. It also implies that the incremental rock matrix pressure gradient evaluated at the fracture and the rock matrix interface, $\left.\frac{\partial P_r(x,y,t)}{\partial y}\right|_{y=w/2}$ is positive number (Figure 4-6). The positive pressure gradient makes the cross-flow rate evaluated at the fracture and the rock matrix interface to be negative (Equation 3.63). Thus we call a flow from the rock matrix to the fracture a negative flow.

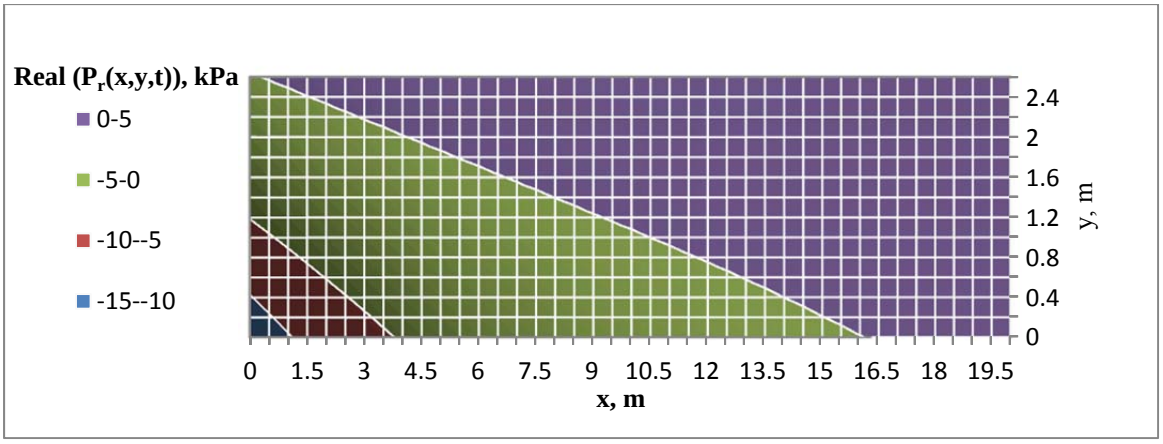

Figure 4-6: Real part of the incremental rock matrix pressure distribution at t=6 seconds

4.2.4 Cross-flow rate

We evaluate the real-valued cross-flow rate at the interface of the fracture and the rock matrix, where y=w/2 and $0 \leq x \leq x_f$ using Equation 3.66, where the cross-flow rate amplitude and the phase shift between the real and imaginary values of the cross-flow rate are calculated using Equations 3.65 and 3.67, respectively. We give the cross flow rate in volumetric flow rate per unit length of the fracture (m^2/s).

Figure 4-7 shows the distribution of the absolute value of the cross-flow rate amplitude. The cross flow rate amplitude decreases with the distance from the injector, x, because of the fracture pressure amplitude attenuation with x.

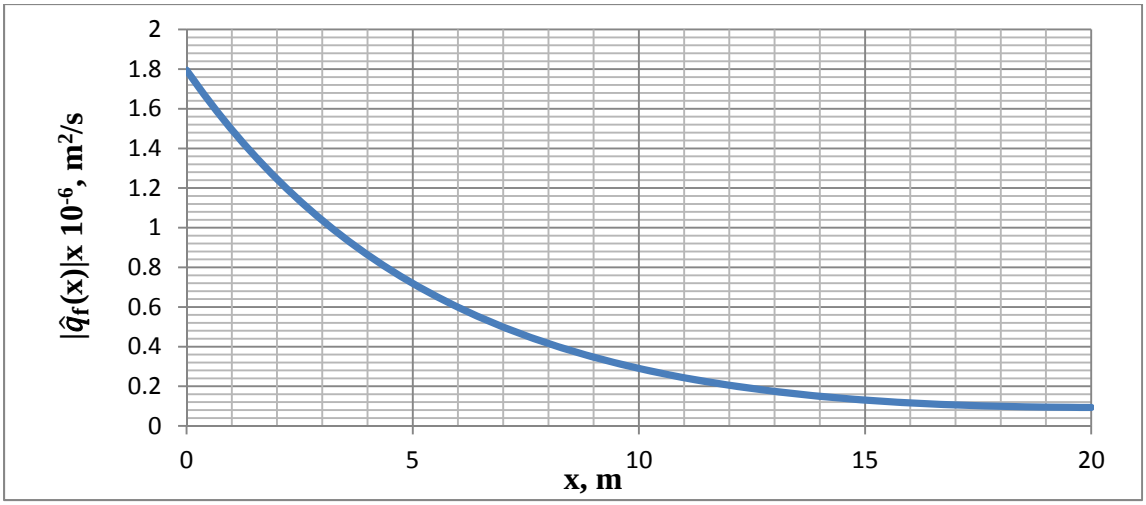

Figure 4-7: Absolute value of the cross-flow rate amplitude distribution with x at the interface of the rock matrix and the fracture

Figure 4-8 shows the real-valued cross-flow rate distribution with time at 1, 5, 10, and 20 meters distances from the seismic wave source, the injector. The cross flow rate can be positive or negative. A positive cross-flow indicates a flow from the fracture to the rock matrix, whereas a negative cross-flow rate indicates a flow from the rock matrix to the fracture.

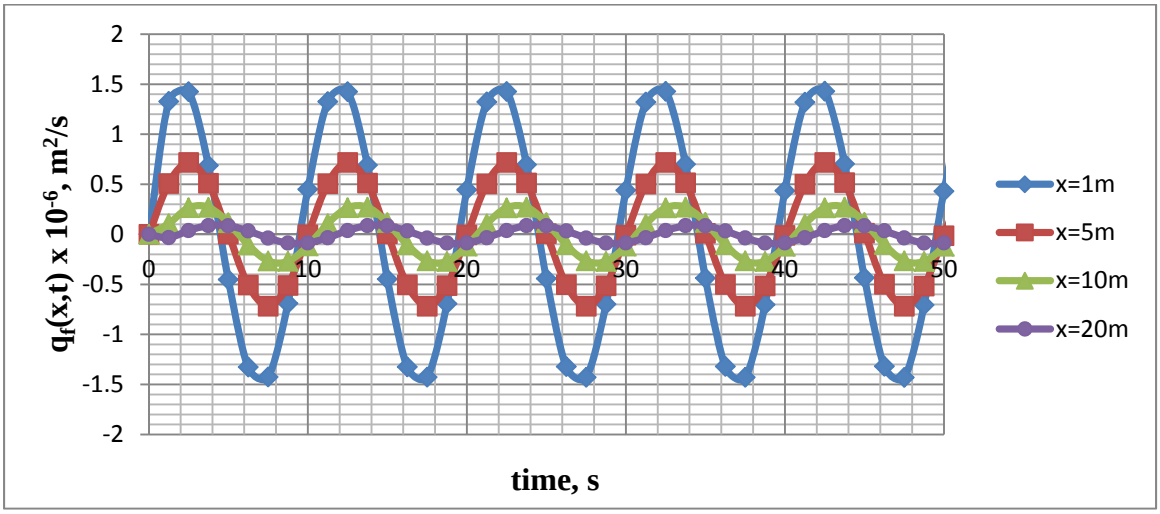

Figure 4-8: Change of cross-flow rate with time at x=1, 5, 10, and 20 meters

4.2.5 Volume of the mobilized oil

Volume of the mobilized oil as a result of the seismic wave stimulation is the integral of the negative cross-flow rate over the stimulation duration and fracture length multiplied by the oil fractional flow from the rock matrix to the fracture (Equation 3.69). We assume that the fractional flow of oil from the fracture to the rock matrix equals to zero, and the fractional flow of oil from the rock matrix to the fracture is constant and equals to 0.8 during one day of stimulation We discuss the fractional flow of oil from the rock matrix to the fracture in Section 3.3.5.3. The volume of the mobilized oil from the reservoir model of Figure 3-1 during one day of the stimulation is 2.42 barrels.

4.3 SENSITIVITY ANALYSIS

In this section, we perform sensitivity analysis of the pressure oscillation equations originally given in Jeong et al. (2011) and again in Chapter 3. We investigate the sensitivity of the fracture incremental pressure, and cross-flow rate to the stimulation frequency, incremental water injection rate amplitude, fracture properties, fracture dimensions, rock matrix properties, oil viscosity, and fractional flow of oil from the rock matrix to the fracture.

4.3.1 Stimulation frequency

The incremental fracture pressure amplitude and the volume of the mobilized oil from the reservoir model of Figure 3-1 for the stimulation frequencies of 0.1, 2, 5, and 10 Hz were investigated in this section. The rock matrix properties, fracture properties,

fracture dimensions, reservoir fluid properties, incremental water injection rate amplitude, and oil fractional flow are the same as used in the example calculation (Table 4-1).

Figure 4-9 shows the incremental fracture pressure amplitude distribution for the aforementioned stimulation frequencies. The higher the stimulation frequency the lower the incremental fracture pressure amplitude. The $\overline{D}_f$ term that expresses the liquid's flow ability through the fracture is directly proportional to the stimulation frequency (Equation 3.58). However, the incremental fracture pressure amplitude is inversely proportional to the $\overline{D}_f$ term (Equation 3.60), which explains why the incremental fracture pressure amplitude decreases with the increased stimulation frequency.

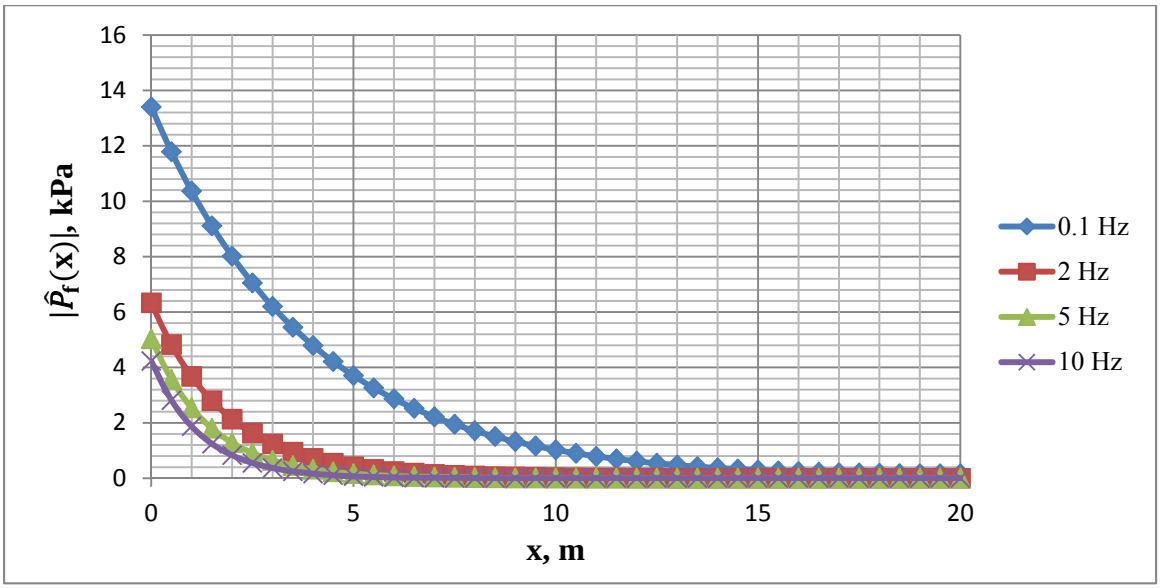

Figure 4-9: Absolute value of the incremental fracture pressure amplitude distribution for stimulation frequencies of 0.1, 2, 5, and 10 Hz

The stimulation frequency affects the cross-flow rate amplitude in two ways (Equation 3.65). Increased stimulation frequency increases the D_r term, which represents

liquid's ability to flow through the rock matrix. On the other hand, increased stimulation frequency decreases the incremental fracture pressure amplitude generated by the stimulation. Thus, the effect is a combination of the changes of D_r and $\widehat{P}_f(x)$. Figure 4-10 shows the cross-flow rate amplitude distribution with x for stimulation frequencies of 0.1, 2, 5, and 10 Hz. The cross-flow rate amplitude is increased near the injector (x is small) with the increased stimulation frequency. However, the cross-flow rate amplitude declines faster for increased stimulation frequencies.

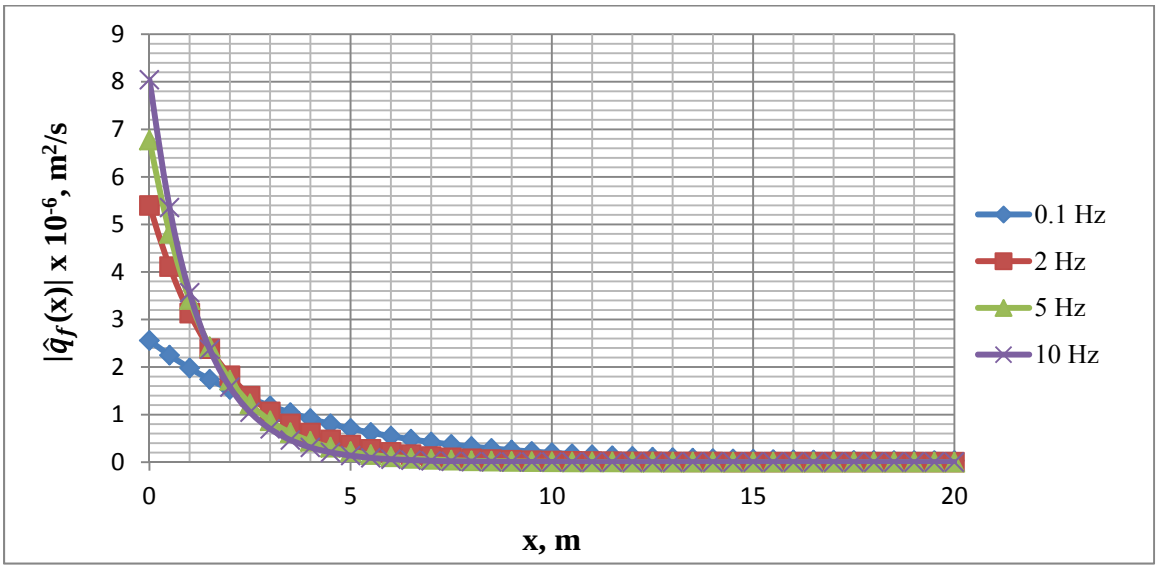

Figure 4-10: Absolute value of the cross-flow rate amplitude distribution for stimulation frequencies of 0.1, 2, 5, and 10 Hz

The volume of the mobilized oil is directly proportional to the area under the cross-flow rate amplitude distribution plot (Figure 4-10). Table 4-2 shows that the volume of the mobilize oil from the reservoir model of Figure 3-1 does not change significantly with the change in the stimulation frequency. In Table 4-2, the volume of mobilized oil was calculated during one day of the stimulation for two reasons: (1) the

initial rate of oil produced by the stimulation can be obtained in the familiar unit of bbl/day; and (2) the fractional flow of oil from the rock matrix to the fracture is assumed to be constant for only small periods of time, the fractional flow term would decrease for a longer stimulation periods. A similar explanation applies to Tables 4-2 to 4-10.

Stimulation frequency, Hz	Stimulation period, day	Volume of mobilized oil, bbl
0.1	1	2.45
2	1	2.48
5	1	2.58
10	1	2.68

Table 4-2: Volume of the mobilized oil for stimulation frequencies of 0.1, 2, 5 and 10 Hz

4.3.2 Incremental water injection rate amplitude

In this section we investigate the sensitivity of the incremental fracture pressure and the cross-flow rate to the incremental injection rate amplitude, $\hat{q}_w$. The incremental fracture pressure distribution for the incremental water injection rate amplitudes of 5, 10, 15 and 20 barrels/day are given in Figure 4-11. The rock matrix, fracture, reservoir fluid properties, fracture dimensions, stimulation frequency, and oil fractional flow are the same as used for the example calculation (Table 4-1). Equations 3.37 and 3.60 show that the incremental fracture pressure amplitude is directly proportion to the incremental water injection rate amplitude, which is also shown in Figure 4-12.

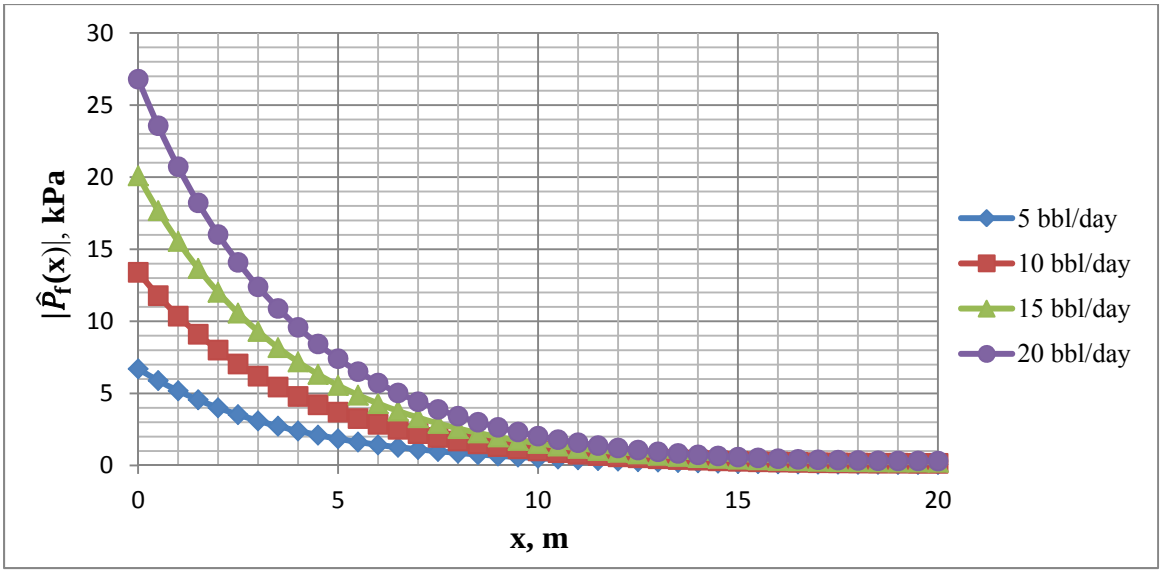

Figure 4-11: Absolute value of the incremental fracture pressure distribution for incremental water injection rate amplitudes of 5, 10, 15 and 20 barrels/day

Figure 4-12 shows the cross-flow rate amplitude distribution for the aforementioned incremental water injection rates. Equation 3.63 shows that the cross-flow rate amplitude is directly proportional to the incremental fracture pressure amplitude.

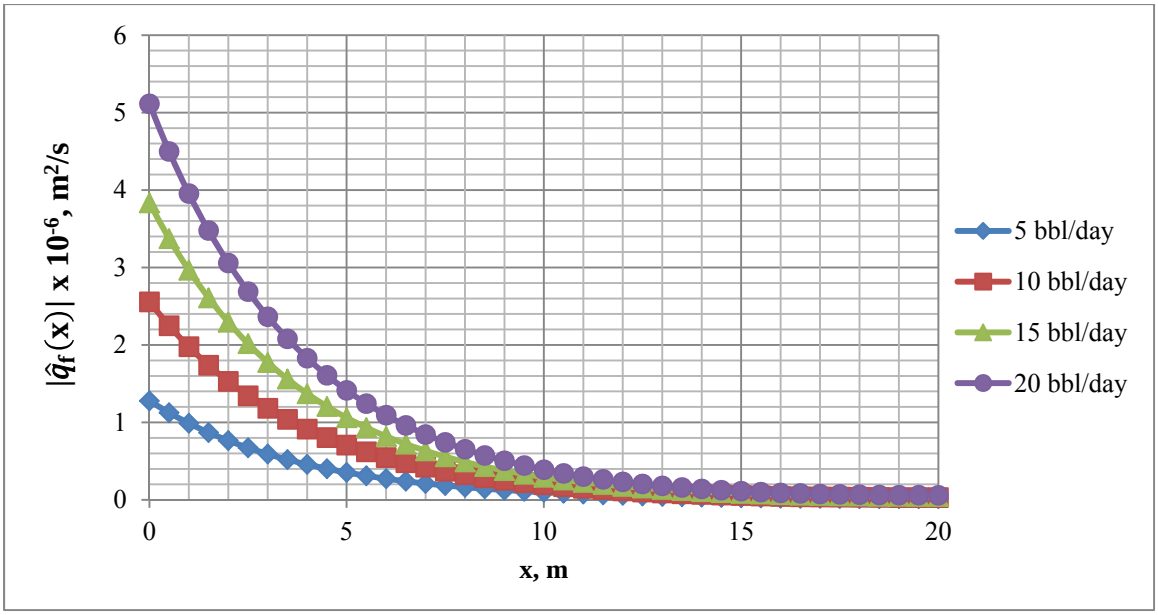

Figure 4-12: Absolute value of cross-flow rate amplitude distribution for incremental water injection rates of 5, 10, 15, and 20 barrels/day

Table 4-3 shows volume of the mobilized oil from the reservoir model of Figure 3-1 for the different incremental water injection rate amplitudes. The volume of the mobilized oil increases with increased incremental water injection rate amplitude.

Incremental water injection rate amplitude, bbl/day	Stimulation period, day	Volume of mobilized oil, bbl
5	1	1.45
10	1	2.43
15	1	3.64
20	1	4.86

Table 4-3: Volume of mobilized oil for incremental water injection rate amplitudes of 5, 10, 15, and 20 barrels/day

4.3.3 Fracture dimensions and properties

4.3.3.1 Fracture dimensions

In this section, we analyze the sensitivity of the incremental fracture pressure and the cross-flow rate to the fracture dimensions of Figure 3-1: fracture height, aperture, and length. The fracture, rock matrix, and reservoir fluid properties, stimulation frequency, incremental water injection rate amplitude, and oil fractional flow are the same as in Table 4-1.

Fracture height. Equations 3.60 and 3.37 show that the incremental fracture pressure amplitude is inversely proportional to the fracture height. It is also shown in Figure 4-13.

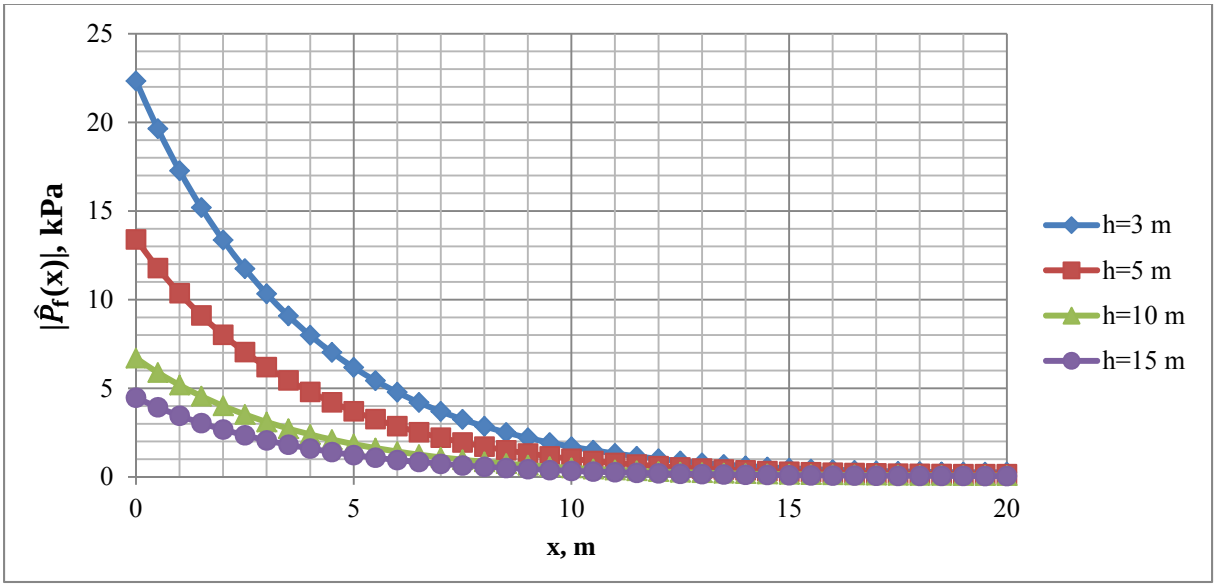

Figure 4-13: Absolute value of the Incremental fracture pressure amplitude distribution for fracture heights of 3, 5, 10, and 20 meters

The volume of the mobilized oil is not affected by the fracture height, because the fracture height decreases the incremental fracture pressure amplitude by the same factor as it increases the cross-flow area.

Fracture aperture. The smaller the fracture aperture the higher the incremental fracture pressure near the injector. The smaller the fracture aperture the faster the incremental fracture pressure amplitude declines with x. These are shown in Figure 4-14.

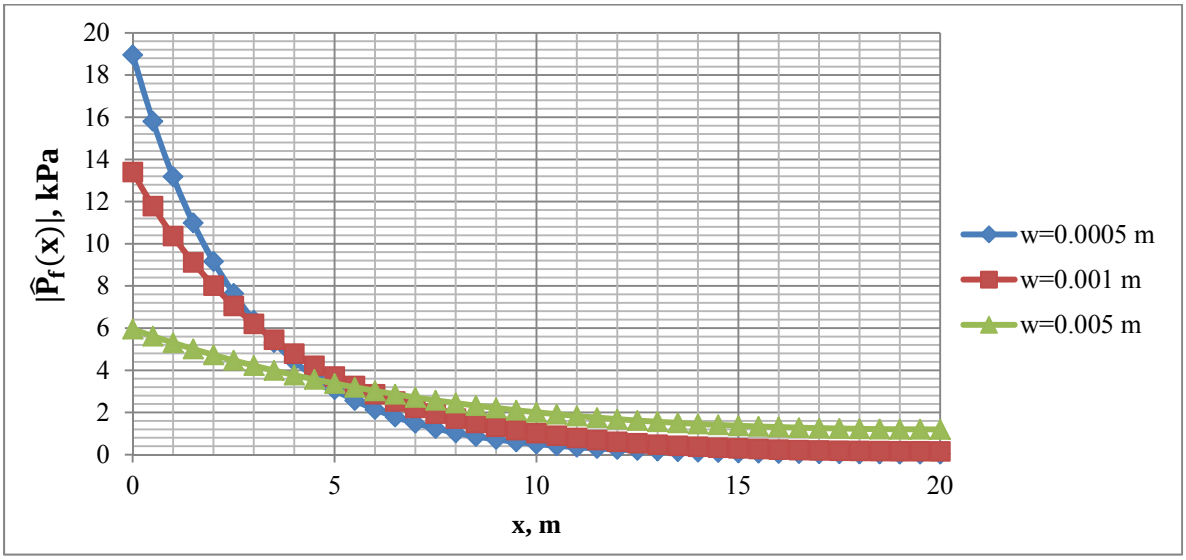

Figure 4-14: Absolute value of fracture incremental pressure distribution for fracture aperture values of 0.0005, 0.001, and 0.005 meters

Figure 4-15 shows the cross-flow rate amplitude distribution with x for the different fracture aperture values. The cross-flow rate amplitude is also greater near the injector, and declines at a higher rate with lower fracture aperture.

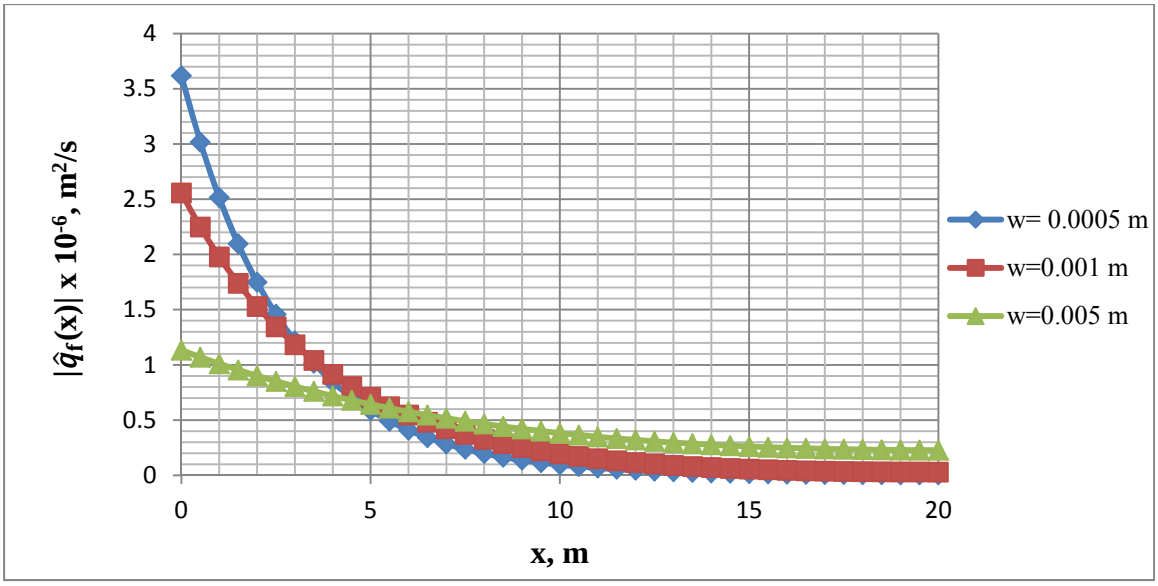

Figure 4-15: Cross-flow rate amplitude distribution for fracture apertures of 0.0005, 0.001, and 0.005 meters

The volume of the mobilized oil is directly proportional to the area under the cross-flow rate amplitude distribution plot (Figure 4-15). Table 4-4 shows the volume of the mobilized oil from the reservoir model of Figure 3-1 for different fracture apertures. The volume of the mobilized oil slightly increases with increased fracture aperture.

Fracture aperture, m	Stimulation period, day	Volume of mobilized oil, bbl
0.0005	1	2.42
0.001	1	2.43
0.005	1	2.45

Table 4-4: Volume of the mobilized oil from the reservoir model of Figure 3-1 for fracture aperture values of 0.0005, 0.001, and 0.005 meters

Fracture length. The incremental fracture and the rock matrix pressures are not affected by the fracture length. The fracture length is directly proportional to the cross-flow area and the volume of the mobilized oil. On the other hand, the incremental

fracture pressures dampens to a very small value after around 15 meters distance from the injector, meaning that fractures longer than 15 meters would not affect the volume of the mobilized oil significantly.

4.3.3.2 Fracture properties

This section performs the sensitivity of the fracture incremental pressure, and the cross-flow rate distribution at the interface of the fracture and the rock matrix of Figure 3-1 to the fracture properties: total fracture compressibility, fracture absolute permeability, and fracture porosity. The rock matrix properties, reservoir fluid properties, fracture dimensions, stimulation frequency, incremental water injection rate amplitude, and oil fractional flow are the same as used for the example calculation (Table 4-1).

Total fracture compressibility. The incremental fracture pressure amplitude does not change significantly with the total fracture compressibility (Figure 4-16). It decreases by 5-30 Pa with increased total fracture compressibility from 0.147 to 7.35 $\frac{1}{\text{GPa}}$.

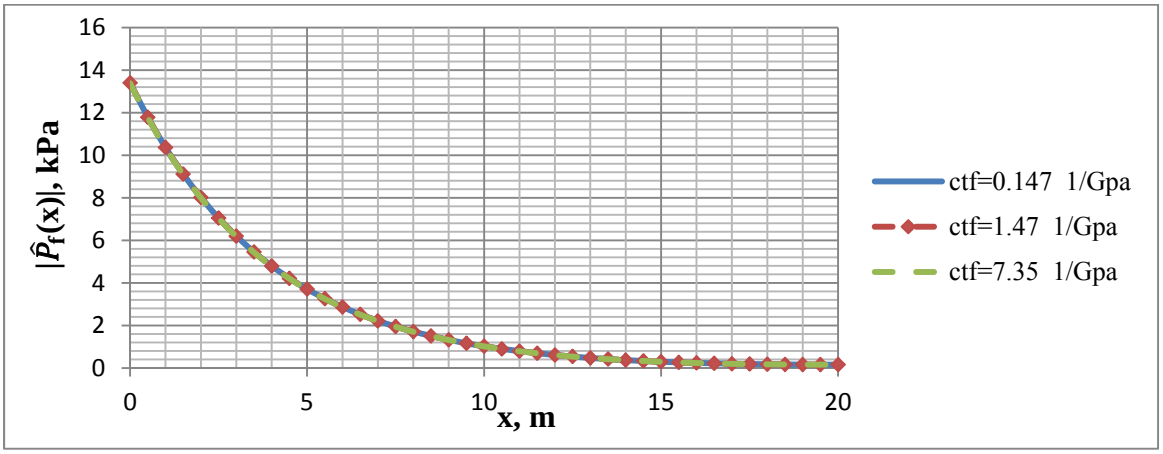

Figure 4-16: Absolute value of the incremental fracture pressure distribution for total fracture compressibility values of 0.147, 14.7, and 7.35 1/GPa.

Figure 4-17 shows that the cross-flow rate amplitude and the volume of the mobilized oil from the reservoir model (Figure 3-1) do not change significantly with the change in the total fracture compressibility.

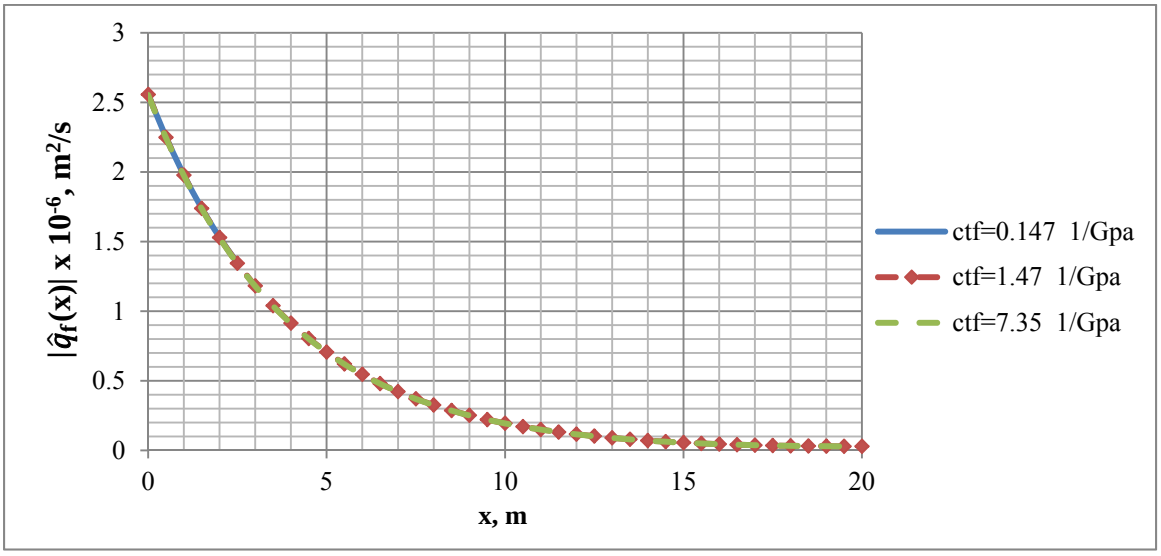

Figure 4-17: Absolute value of the cross-flow rate amplitude distribution for total fracture compressibility values of 0.147, 1.47, and 7.35 1/GPa

Fracture absolute permeability. The incremental fracture amplitude increases near the injector well with increased fracture absolute permeability. However, the incremental fracture pressure declines faster with higher stimulation frequency. Figure 4-18 shows the incremental fracture pressure distribution for the fracture absolute permeability values of 50, 100, 400, and 800 Darcy.

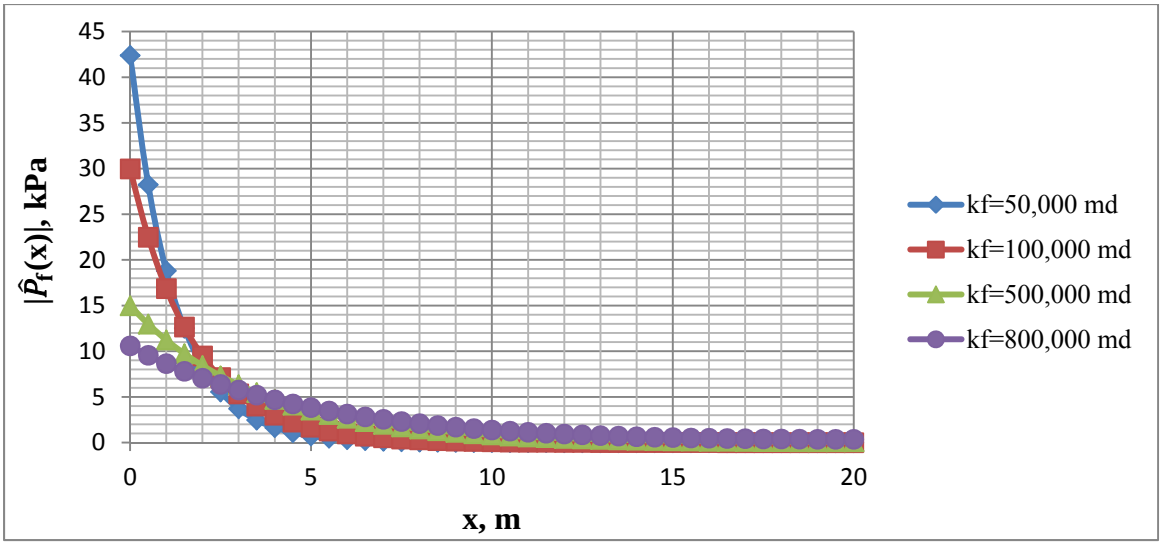

Figure 4-18: Absolute value of the incremental fracture pressure distribution for fracture absolute permeability values of 50, 100, 400, and 800 Darcy

The cross-flow rate amplitude distribution that is directly proportional to the incremental fracture pressure amplitude distribution shows the same behavior (Figure 4-19).

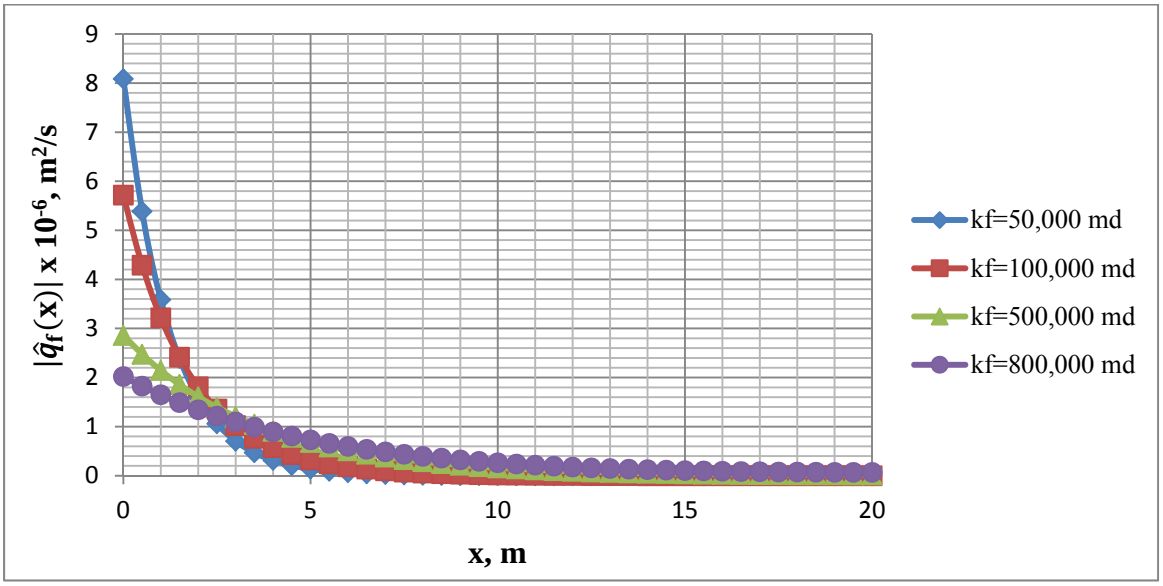

Figure 4-19: Absolute value of the cross-flow rate amplitude distribution for fracture absolute permeability values of 50, 100, 400, and 800 Darcy

Table 4-5 shows that the volume of the mobilized oil does not change significantly with the change in the fracture absolute permeability.

Fracture absolute permeability, Darcy	Stimulation period, day	Volume of mobilized oil, bbl
50	1	2.67
100	1	2.50
400	1	2.42
800	1	2.45

Table 4-5: Volume of the mobilized oil for fracture absolute permeability values of 50, 100, 400, and 800 Darcy

Fracture porosity. Fracture porosity does not have significant impact on the fracture incremental pressure, and the cross-flow rate. Using the data of Table 4-1 and changing the fracture porosity from 0.05 to 0.4 increases the incremental fracture pressure and the volume of the mobilized oil from the reservoir model of Figure 3-1 during 1 day of the stimulation by 40 Pa and 0.01 barrels, respectively.

4.3.4 Rock matrix properties

In this section we investigate the sensitivity of the incremental fracture pressure and the cross-flow rate evaluated at the interface of the fracture and the rock matrix to the rock matrix properties: the total rock matrix compressibility, rock matrix absolute permeability, and rock matrix porosity. The fracture and reservoir fluid properties, fracture dimensions, stimulation frequency, incremental water injection rate amplitude, and oil fractional flow are the same as in the example calculation (Table 4-1).

Total rock matrix compressibility. Figure 4-20 shows that the incremental fracture pressure amplitude decreases with increased total rock matrix compressibility.

The $\overline{D}_f$ term that is defined by Equation 3.58 is increased with the increased total rock matrix compressibility. The incremental fracture pressure amplitude is inversely proportional to the $\overline{D}_f$ term, which explains why the incremental fracture pressure amplitude decreases with increased rock matrix absolute permeability (Equation 3.60).

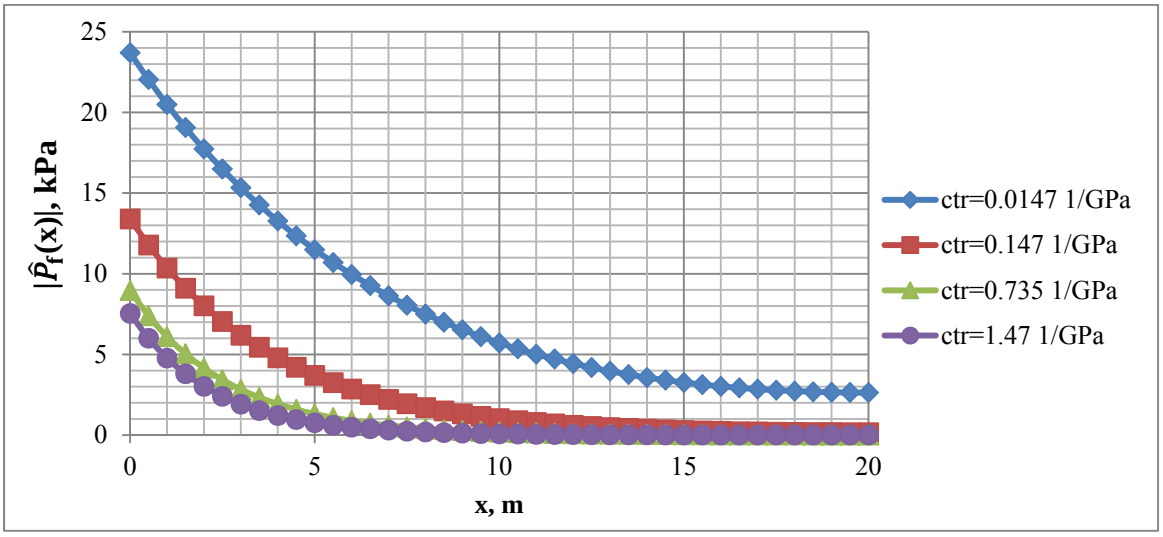

Figure 4-20: Absolute value of the incremental rock matrix pressure distribution for total rock matrix compressibility values of 0.0147, 0.147, 0.735, and 1.47 1/GPa

Furthermore, increased total rock matrix compressibility increases the liquid flow ability through the rock matrix, the D_r term (Equation 3.49). The cross-flow rate amplitude is a function of both $\hat{P}_f(x)$ and the D_r term (Equation 3.63). Near the injector, the cross-flow rate increases with increased total rock matrix compressibility. But it declines at a higher rate with increased total rock matrix compressibility (Figure 4-21).

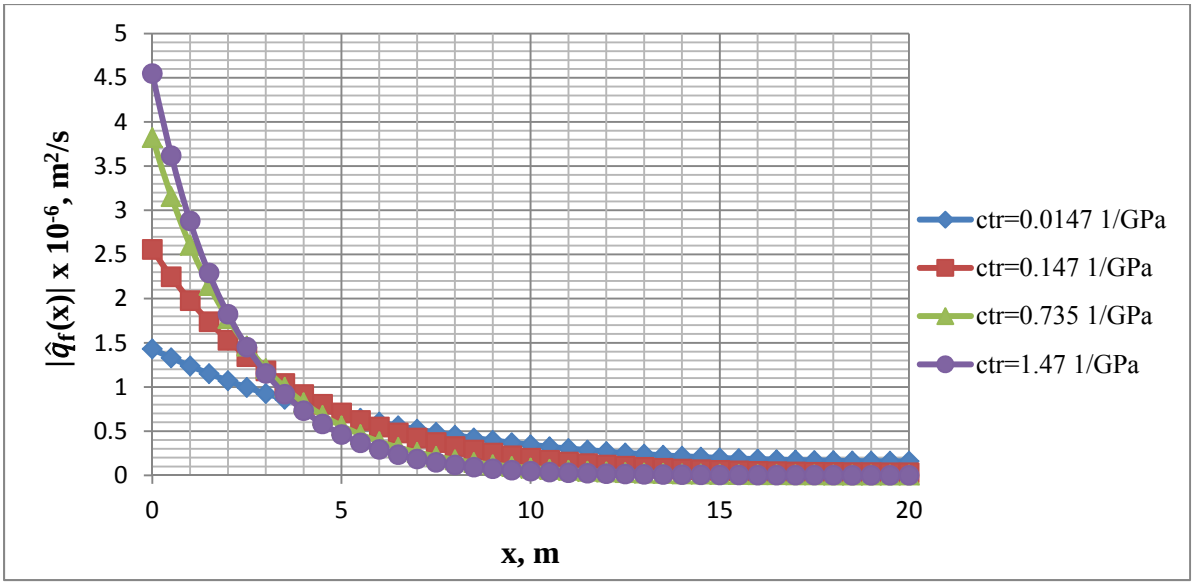

Figure 4-21: Absolute value of the cross-flow rate amplitude distribution for total compressibility values of 0.0147, 0.147, 0.735, and 1.47 1/GPa

Volume of the mobilized oil that is a function of the area under the cross-flow rate amplitude distribution plot does not change significantly with the total rock matrix compressibility (Table 4-6).

Total rock matrix compressibility, 1/GPa	Stimulation period, day	Volume of mobilized oil, bbl
0.0147	1	2.45
0.147	1	2.43
0.735	1	2.43
1.47	1	2.45

Table 4-6: Volume of the mobilized oil for total rock matrix compressibility values of 0.0147, 0.147, 0.735, and 1.47 1/GPa

Rock matrix absolute permeability. Figure 4-22 shows that the incremental fracture pressure amplitude decreases with increased rock matrix absolute permeability. Again, increased rock matrix absolute permeability increases $\overline{D}_f$ term that is inversely proportional to the incremental fracture pressure amplitude (Equation 3.60).

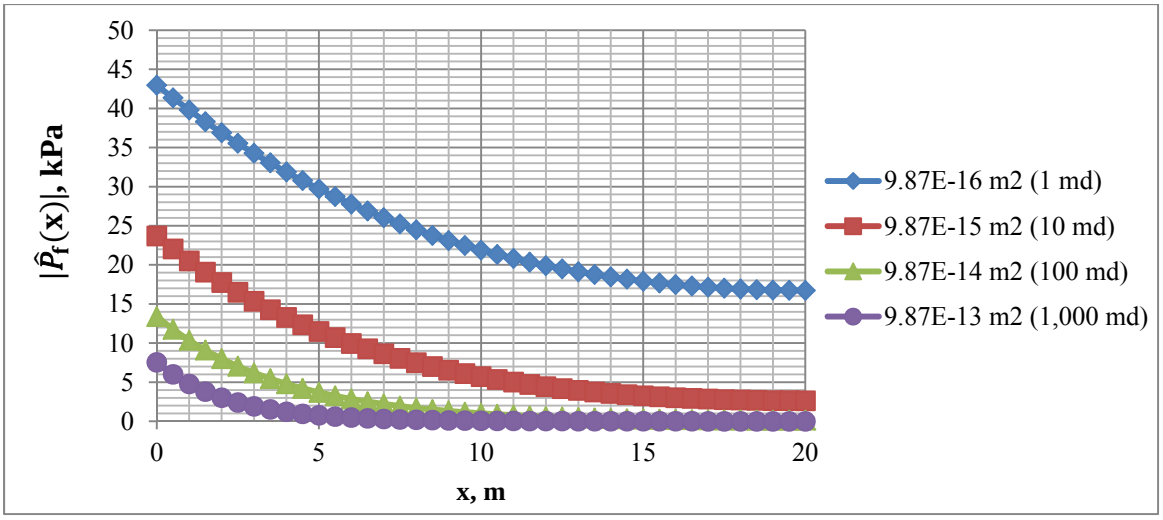

Figure 4-22: Absolute value of the incremental rock matrix pressure distribution for rock matrix absolute permeability values of 1, 10, 100, and 1,000 md

The D_r term increases with the increased rock matrix absolute permeability (Equation 3.49). Near the injector, the cross-flow rate increases with increased rock matrix absolute permeability. But, it declines at a higher rate with increased absolute rock matrix permeability (Figure 4-23).

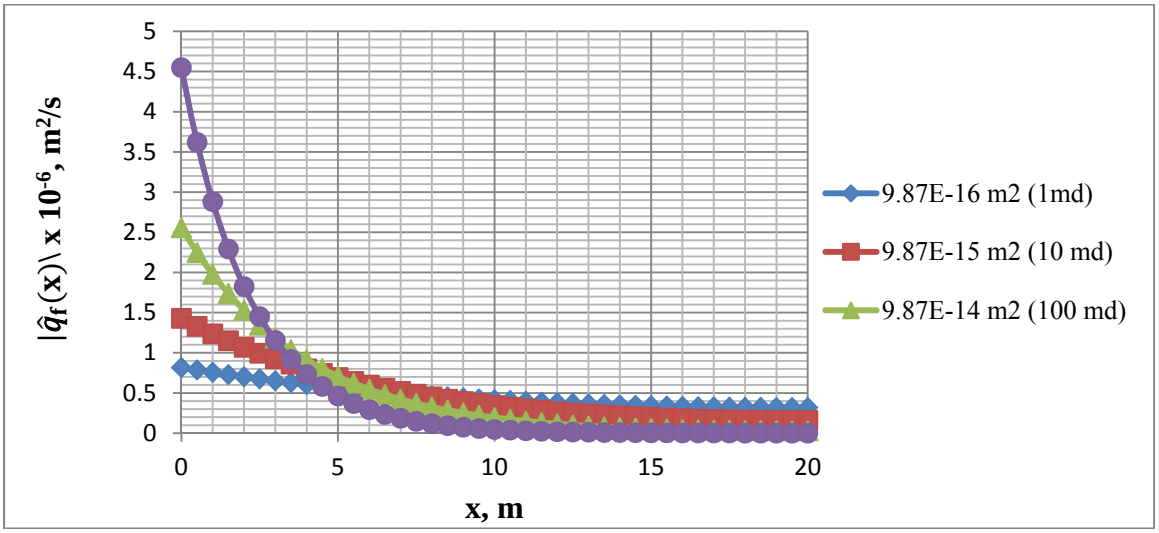

Figure 4-23: Absolute value of the cross-flow rate amplitude distribution for rock matrix absolute permeability values of 1, 10, 100, and 1,000 md

Table 4-7 shows that the volume of the mobilized oil does not change significantly with the rock matrix absolute permeability. The reason is that the area under the cross-flow rate amplitude distribution plot does not change significantly with the change in the rock matrix absolute permeability (Figure 4-23).

Rock matrix absolute permeability	Stimulation period, day	Volume of mobilized oil, bbl
9.87×10^{-16} m^2 (1 md)	1	2.42
9.87×10^{-15} m^2 (10 md)	1	2.43
9.87×10^{-14} m^2 (100 md)	1	2.44
9.87×10^{-13} m^2 (1,000 md)	1	2.44

Table 4-7: Volume of the mobilized oil for rock matrix absolute permeability values of 1, 10, 100, and 1,000 md

Rock matrix porosity. Figure 4-24 shows that the incremental fracture pressure amplitude decreases with increased rock matrix absolute permeability. The $\overline{D}_f$ term increases with the increased rock matrix porosity. The $\overline{D}_f$ term is inversely proportional to the incremental fracture pressure amplitude (Equation 3.60).

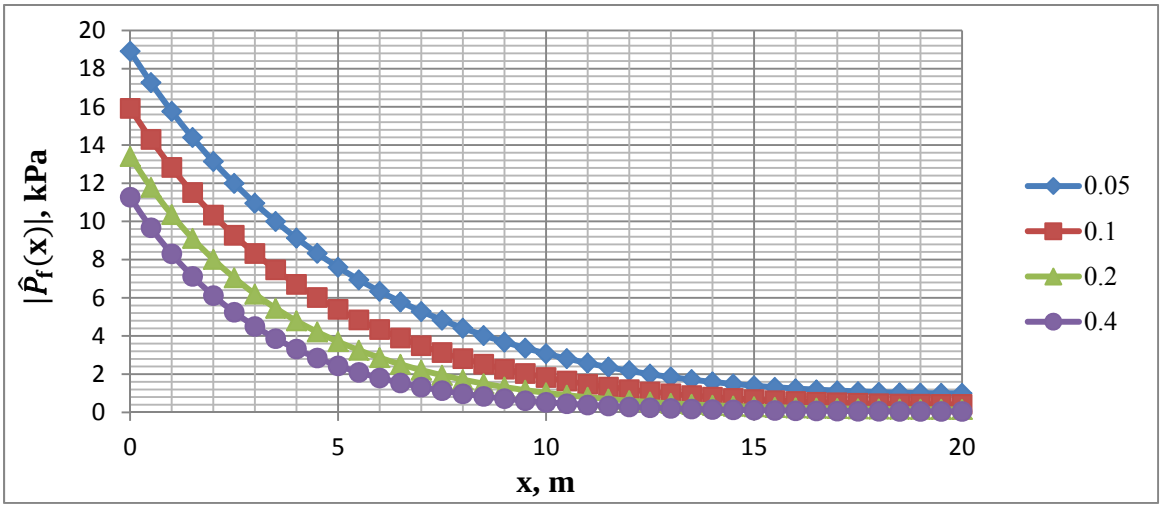

Figure 4-24: Absolute value of the incremental fracture pressure amplitude distribution for rock matrix porosities of 0.05, 0.1, 0.2 and 0.4

Near the injector, the cross-flow rate increases with increased rock matrix porosity, but it declines at a higher rate compared to the lower rock matrix porosity cases (Figure 4-25).

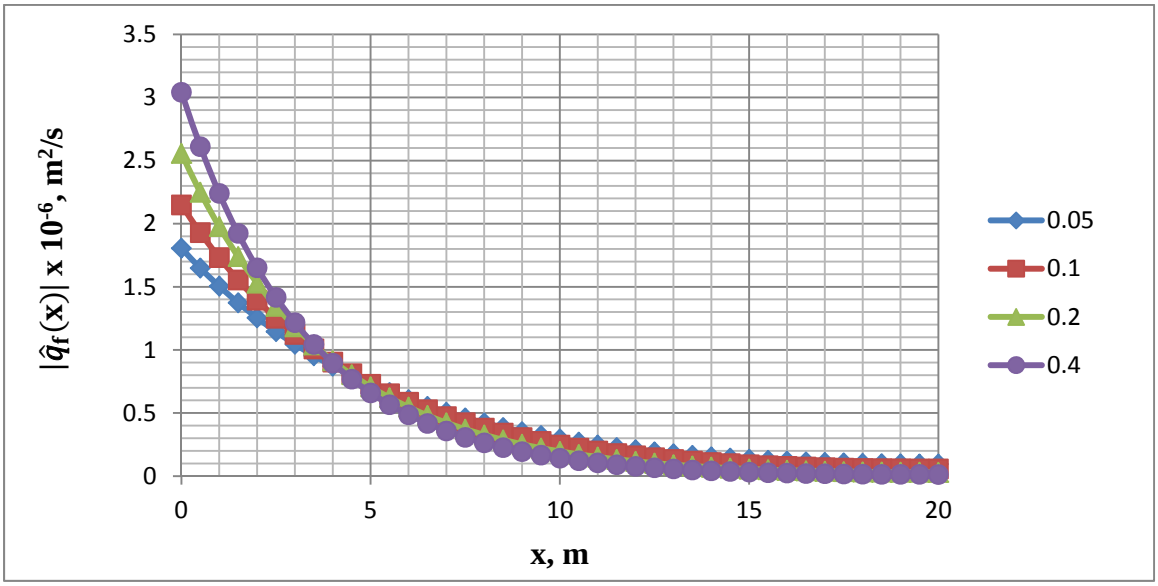

Figure 4-25: Absolute value of the cross-flow rate amplitude distribution for rock matrix porosities of 0.05, 0.1, 0.2, and 0.4

The volume of the mobilized oil does not change significantly with the change in the rock matrix porosity (Table 4-8).

Rock matrix porosity, fraction	Stimulation period, day	Volume of mobilized oil, bbl
0.05	1	2.45
0.1	1	2.44
0.2	1	2.43
0.4	1	2.42

Table 4-8: Volume of the mobilized oil for rock matrix porosity values of 0.05, 0.1, 0.2, and 0.4

4.3.5 Oil viscosity

In this section we analyze the sensitivity of the oil incremental fracture pressure, and cross-flow rate to the oil viscosity. The stimulation frequency, incremental water injection rate amplitude, fracture dimensions, fracture properties, rock matrix properties, and oil fraction flow from the rock matrix to the fracture are the same as used in the example calculation. The incremental fracture pressure amplitude increases with increased oil viscosity (Figure 4-26); the $\bar{D}_f$ term decreases with the increased oil viscosity, which is inversely proportional to the incremental fracture pressure amplitude.

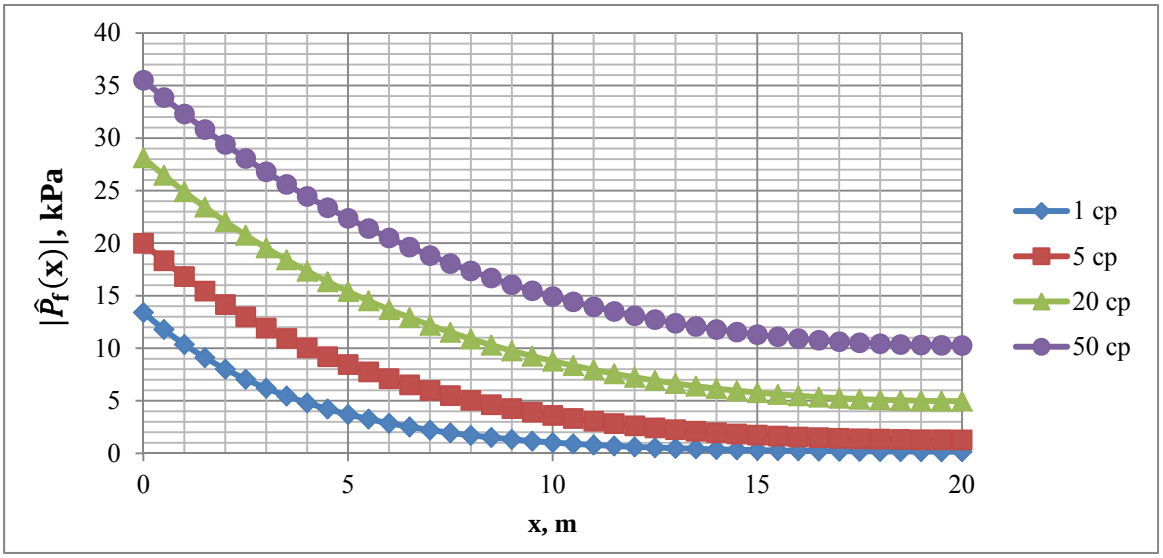

Figure 4-26: Absolute value of the incremental fracture pressure amplitude distribution for oil viscosity values of 1, 5, 20, and 50 cp

The cross-flow rate amplitude increases with increased oil viscosity near the injector, but the decline rate of the cross flow rate with the distance from the injector also increases with increased oil viscosity (Figure 2-27).

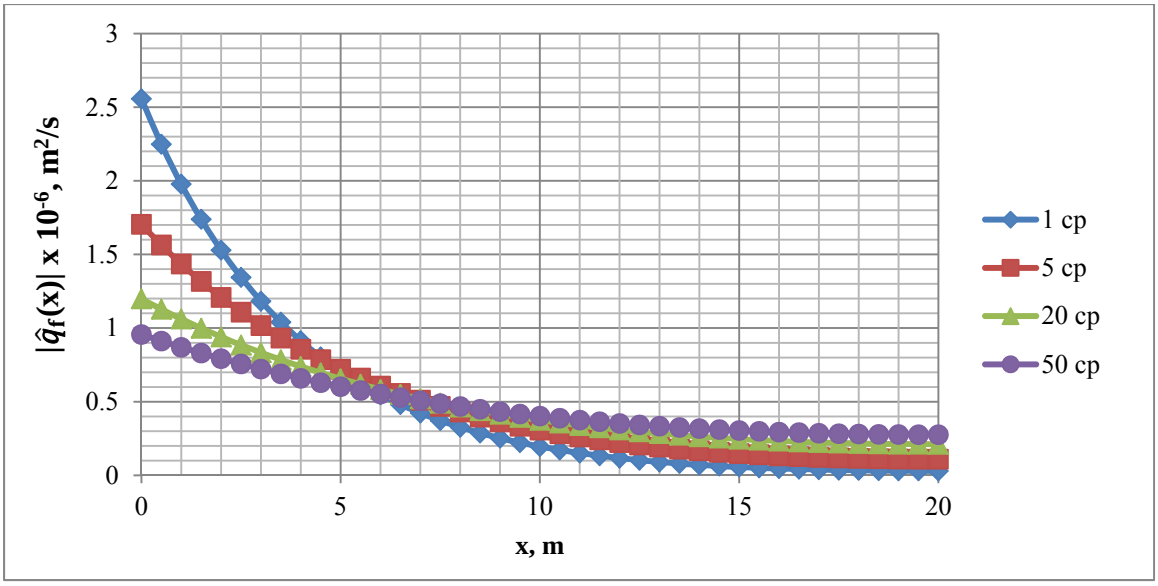

Figure 4-27: Absolute value of the cross-flow rate amplitude distribution for oil viscosity values of 1, 5, 20, and 50 cp.

The volume of the mobilized oil does not change significantly with the investigated oil viscosities (Table 4-9).

Oil viscosity, cp	Stimulation period, day	Volume of mobilized oil, bbl
1	1	2.43
5	1	2.45
20	1	2.45
50	1	2.45

Table 4-9: Volume of the mobilized oil for oil viscosity values of 1, 5, 20, and 50 cp

4.3.6 Fractional flow of oil

We assume that the fractional flow of oil from the rock matrix to the fracture, f^- is constant throughout the stimulation period. We give an analytical work supporting the idea in Section 3.3.5.3. Table 4-10 shows that the fractional flow of oil from the rock matrix to the fracture is directly proportional to the volume of the mobilized oil.

Oil fractional flow	Stimulation period, day	Volume of mobilized oil, bbl
0.4	1	1.21
0.6	1	1.82
0.8	1	2.43
1	1	3.04

Table 4-10: Volume of the mobilized oil for oil fractional flow values of 0.4, 0.6, 0.8, and 1

4.4 COMPARISON WITH THE FIELD DATA

Table 4-11 shows the actual and estimated incremental oil production as a result of seismic wave stimulation for 4 field applications. The actual values were either given in the literature or calculated by integrating the oil production history plots reported in the literature. The estimated values are calculated using the method described in Chapter 3. It was shown in Section 4.3 that the volume of the mobilized oil is only significantly sensitive to the incremental water injection rate amplitude and oil fractional flow from the rock matrix to the fracture. To calculate the estimated values of Table 4-11, we assume that the incremental water injection rate amplitude is 10 bbl/day and the oil fractional flow from the rock matrix to the fracture is constant and equal to 0.6 throughout the stimulation period. Thus, we assume that the volume of the mobilized oil is 2 barrels per day per 2 wells operating in the stimulated area of the example fields (Section 4.2). We realize that the estimated numbers of Table 4-11 are approximate and much dependent on the fracture system of the reservoirs.

Filed name	Actual volume of incremental oil production, bbl	Estmated volume of incremental oil production, bbl
Lost Hills	105,000	96,000
Elk Hills	177,900	28,000
Changirtash-1	1,880	183
Liaohe	900	3,040

Table 4-11: Actual and estimated oil production for 4 field application of seismic EOR. All numbers are approximate

4.5 CONCLUSIONS

Chapter 4 is divided into 2 parts. We refer to the reservoir model described in Figure 3-1 in both parts of this chapter. The first part gives an example calculation of the incremental fracture and rock matrix pressures, the cross-flow rate evaluated at the interface of the fracture and the rock matrix. According to the results, the fracture incremental pressure decreases in the x direction away from the seismic wave source (the injector), and the rock matrix incremental fracture attenuates in both the x and y directions away from the seismic wave source (Figure 3-1b). The cross-flow rate evaluated at the interface of the fracture and the rock matrix also decreases in the x direction. Using the data given in Table 4-1, the volume of the mobilized oil from the reservoir model of Figure 3-1a during 1 day of the stimulation is 2.42 barrels.

The second part performs a sensitivity analysis of the fracture incremental pressure amplitude and the cross-flow rate evaluated at the interface of the fracture and the rock matrix. According to the results, increasing stimulation frequency, decreasing incremental water injection rate, increasing fracture height, increasing rock matrix

absolute permeability, increasing total rock matrix compressibility decreases the incremental fracture pressure amplitude. The volume of the mobilized oil is only significantly affected by the incremental water injection rate amplitude, and the fraction flow of oil from the rock matrix to the fracture. The higher the incremental water injection rate amplitude and oil fractional flow, the higher the incremental oil production because of the stimulation.

Chapter 5: Conclusion

This thesis consists of three major parts.

The first part gives a literature survey on seismic wave based EOR to include pore and reservoir scale production mechanisms suggested in the literature, and field scale application results of the method. Field scale applications of seismic EOR are believed to be promising.

The second part concentrates on one of the reservoir scale possible production mechanisms reported in the literature: cross-flow generation between different permeability layers as a result of fluid pressure oscillations. We describe a fractured reservoir model that is used in all calculations. We also derive pressure oscillation equations originally given in Jeong et al. (2011). We additionally give an analytical expression for calculating the volume of mobilized oil, and investigate fraction flow of oil from the rock matrix to the fracture of Figure 3-1. Lastly, we perform dimensionless analysis to minimize the number of free variables that the rock matrix and the fracture pressures depend on, and to make the problem applicable to any geometrically similar system.

According to the results, the rock matrix and fracture incremental pressures are a function of the dimensionless dependent and independent variables, dimensionless stimulation frequency, dimensionless incremental water injection rate, and a dimensionless group expressing the time scaling factor difference between flow within the fracture and the rock matrix.

In the last part of the thesis, we apply the pressure oscillation equations to calculate incremental fracture and rock matrix pressures. We give example calculations of the incremental fracture and rock matrix pressures, cross-flow rate, and volume of the mobilized oil for a given rock matrix, fracture and reservoir fluid properties, stimulation frequency, incremental water injection rate amplitude and oil fractional flow from the rock matrix to the fracture. We also perform sensitivity analyses of the incremental fracture pressure and cross-flow rate to the stimulation frequency, incremental water injection rate amplitude, fracture dimensions, fracture properties, rock matrix properties, oil viscosity, and fractional flow of oil from the rock matrix to the fracture.

According to the results of the example calculations, the fracture and the rock matrix incremental pressures are in the order of a few tens of kPa, and they attenuate away from the seismic wave source. Using the data given in Table 4-1, the volume of the mobilized oil during one day of the stimulation from the reservoir model of Figure 3.1a is 2.4 barrels. According to the results of the sensitivity analysis, the fracture and rock matrix incremental pressures are sensitive to the stimulations frequency, incremental water injection rate amplitude, fracture height and aperture, total rock matrix compressibility, and rock matrix absolute permeability. The volume of the mobilized oil only changes significantly with the change in the incremental water injection rate amplitude, and oil fractional flow from the rock matrix to the fracture.

Recommendations for future work are to apply the method to a reservoir model with complex fracture system, and to create models for numerical simulators.

Appendix A

Derivation of Equation 3-10

Figure A-1 shows top view of the fracture described in Figure 3-1b.

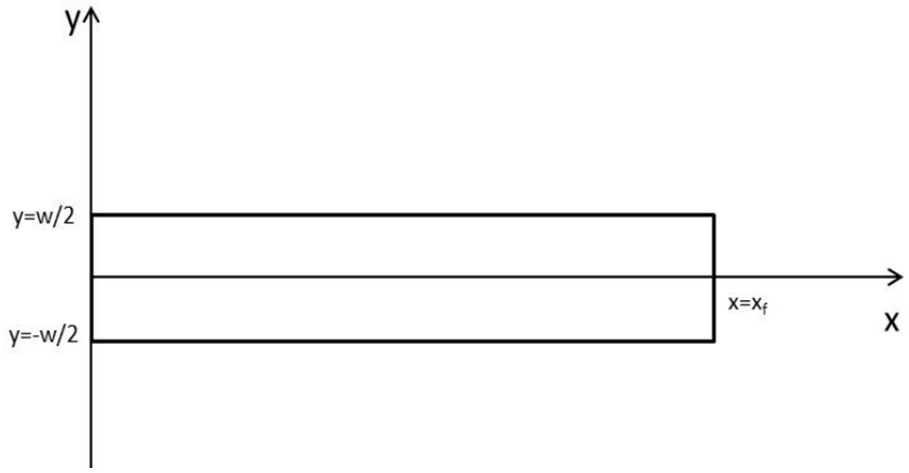

Figure A-1: Top view of the fracture of Figure 3-1b.

To derive Equation 3.10, the following assumptions are made:

- The fracture is homogeneous with isotropic properties
- Fluid properties are constant
- Oil and water phases are flowing
- Oil and water densities are equal
- Capillary pressure is equal to zero (oil and water phase pressures are equal)

The water continuity equation for a flow within a fracture is given below:

$$\frac{\partial(\rho_w \varphi_f S_w)}{\partial t} + \frac{\partial(\rho_w u_{wx})}{\partial x} + \frac{\partial(\rho_w u_{wy})}{\partial y} = 0 \qquad \text{A.1}$$

where ρ_w is water density, φ_f is porosity of the fracture, S_w is the fracture water saturation, u_{wx} is the water phase Darcy velocity in the x direction, and u_{wy} is the water phase Darcy velocity in the y direction. The water continuity equation for a flow within a fracture is given below:

$$\frac{\partial \rho_o \varphi_f S_o}{\partial t} + \frac{\partial \rho_o u_{ox}}{\partial x} + \frac{\partial \rho_o u_{oy}}{\partial y} = 0 \qquad \text{A.2}$$

where ρ_o is oil density, S_o is oil saturation of the fracture, u_{ox} is the oil phase Darcy velocity in the x direction, and u_{oy} is the oil phase Darcy velocity in the y direction.

Combining Equations A.1 and A.2 gives the following:

$$\frac{\partial(\rho_w \varphi_f S_w)}{\partial t} + \frac{\partial(\rho_o \varphi_f S_o)}{\partial t} + \frac{\partial(\rho_w u_{wx})}{\partial x} + \frac{\partial(\rho_w u_{wy})}{\partial y} + \frac{\partial(\rho_o u_{ox})}{\partial x} + \frac{\partial(\rho_o u_{oy})}{\partial y} = 0 \qquad \text{A.3}$$

Applying the product rule of differentiation to the first and second terms of Equation A.3 gives the following:

$$\rho_w S_w \frac{\partial \varphi_f}{\partial t} + \varphi_f S_w \frac{\partial \rho_w}{\partial t} + \rho_w \varphi_f \frac{\partial S_w}{\partial t} + \rho_o S_o \frac{\partial \varphi_f}{\partial t} + \varphi_f S_o \frac{\partial \rho_o}{\partial t} + \rho_o \varphi_f \frac{\partial S_o}{\partial t} + \frac{\partial(\rho_w u_{wx})}{\partial x} + \frac{\partial(\rho_w u_{wy})}{\partial y} + \frac{\partial(\rho_o u_{ox})}{\partial x} + \frac{\partial(\rho_o u_{oy})}{\partial y} = 0 \qquad \text{A.4}$$

Applying the chain rule of differentiation to Equation A.4 gives the following equation:

$$\rho_w S_w \varphi_f \frac{1}{\varphi_f}\frac{d\varphi_f}{dP_{fs}}\frac{dP_{fs}}{\partial t} + \varphi_f S_w \rho_w \frac{1}{\rho_w}\frac{d\rho_w}{dP_{fs}}\frac{dP_{fs}}{\partial t} + \rho_w \varphi_f \frac{\partial S_w}{\partial t} + \rho_o S_o \varphi_f \frac{1}{\varphi_f}\frac{d\varphi_f}{dP_{fs}}\frac{dP_{fs}}{\partial t} + \varphi_f S_o \rho_o \frac{1}{\rho_o}\frac{d\rho_o}{dP_{fs}}\frac{dP_{fs}}{\partial t} + \rho_o \varphi_f \frac{\partial S_o}{\partial t} + \frac{\partial(\rho_w u_{wx})}{\partial x} + \frac{\partial(\rho_w u_{wy})}{\partial y} + \frac{\partial(\rho_o u_{ox})}{\partial x} + \frac{\partial(\rho_o u_{oy})}{\partial y} = 0 \qquad \text{A.5}$$

where P_{fs} is the stimulated fracture pressure. The fracture formation, water and oil compressibility terms are defined below:

$$c_f = \frac{1}{\varphi_f}\frac{d\varphi_f}{dP_{fs}} \tag{A.6}$$

$$c_w = \frac{1}{\rho_w}\frac{d\rho_w}{dP_{fs}} \tag{A.7}$$

$$c_o = \frac{1}{\rho_o}\frac{d\rho_o}{dP_{fs}} \tag{A.8}$$

Substituting Equations A.6-A.8 into Equation A.5 gives the following:

$$\rho_w S_w \varphi_f \left(c_f + c_w\right)\frac{dP_{fs}}{\partial t} + \rho_w \varphi_f \frac{\partial S_w}{\partial t} + \rho_o S_o \varphi_f \left(c_f + c_o\right)\frac{dP_{fs}}{\partial t} + \rho_o \varphi_f \frac{\partial S_o}{\partial t} + \frac{\partial(\rho_w u_{wx})}{\partial x} + \frac{\partial(\rho_w u_{wy})}{\partial y} + \frac{\partial(\rho_o u_{ox})}{\partial x} + \frac{\partial(\rho_o u_{oy})}{\partial y} = 0 \tag{A.9}$$

The water and oil saturations sum to one. Thus, their time derivatives are defined as following

$$\frac{\partial S_o}{\partial t} = -\frac{\partial S_w}{\partial t} \tag{A.10}$$

Substituting Equation A.10 into A.9 and assuming that water and oil densities are equal ($\rho_o = \rho_w$) gives the following equation:

$$\rho_o S_w \varphi_f \left(c_f + c_w\right)\frac{dP_{fs}}{\partial t} + \rho_o S_o \varphi_f \left(c_f + c_o\right)\frac{dP_{fs}}{\partial t} + \frac{\partial(\rho_o u_{wx})}{\partial x} + \frac{\partial(\rho_o u_{wy})}{\partial y} + \frac{\partial(\rho_o u_{ox})}{\partial x} + \frac{\partial(\rho_o u_{oy})}{\partial y} = 0 \tag{A.11}$$

or

$$\rho_o \varphi_f \left(c_f + c_w S_w + c_o S_o\right)\frac{dP_{fs}}{\partial t} + \frac{\partial(\rho_o u_{wx})}{\partial x} + \frac{\partial(\rho_o u_{wy})}{\partial y} + \frac{\partial(\rho_o u_{ox})}{\partial x} + \frac{\partial(\rho_o u_{oy})}{\partial y} = 0 \qquad \text{A.12}$$

The total fracture compressibility, c_{tf} is defined by the following expression:

$$c_{tf} = c_f + S_w c_w + S_o c_o \qquad \text{A.13}$$

Substituting Equation A.13 into A.12 gives the following:

$$\rho_o \varphi_f c_{tf} \frac{dP_{fs}}{\partial t} + \frac{\partial(\rho_o u_{wx})}{\partial x} + \frac{\partial(\rho_o u_{wy})}{\partial y} + \frac{\partial(\rho_o u_{ox})}{\partial x} + \frac{\partial(\rho_o u_{oy})}{\partial y} = 0 \qquad \text{A.14}$$

Integrating Equation A.14 over the fracture width from –w/2 to w/2 gives the following:

$$\int_{-w/2}^{w/2} \rho_o \varphi_f c_t \frac{dP_{fs}}{dt} dy + \int_{-w/2}^{w/2} \frac{\partial \rho_o (u_{wx} + u_{ox})}{\partial x} dy + \int_{-w/2}^{w/2} \frac{\partial(\rho_o u_{wy} + \rho_o u_{oy})}{\partial y} dy = 0 \qquad \text{A.15}$$

$$\rho_o \varphi_f c_t w \frac{d\overline{P}_{fs}}{dt} + w \frac{\partial(\overline{\rho_o u_{wx}} + \overline{\rho_o u_{ox}})}{\partial x} + \rho_0 (u_{wy} + u_{oy})\Big|_{y=w/2} = 0 \qquad \text{A.16}$$

where $\overline{P}_{fs}$, $\overline{\rho_o u_{wx}}$, and $\overline{\rho_o u_{ox}}$ are average valued. We make the following assumptions to carry out the derivation:

$$\overline{P}_{fs} = P_{fs} \qquad \text{A.17}$$

$$\overline{\rho_o u_{ox}} = \rho_o u_{ox} \qquad \text{A.18}$$

$$\overline{\rho_o u_{wx}} = \rho_o u_{wx} \qquad \text{A.19}$$

Substituting Equations A.17-A.19 into Equation A.16 gives the following equation:

$$\rho_o \varphi_f c_t w \frac{dP_{fs}}{dt} + w \frac{\partial\left[\rho_o (u_{wx} + u_{ox})\right]}{\partial x} + \rho_0 (u_{wy} + u_{oy})\Big|_{y=w/2} = 0 \qquad \text{A.20}$$

The total (oil and water) fluid velocity in the x direction is defined below:

$$u_x = u_{wx} + u_{ox} \qquad \text{A.21}$$

$$\rho_o \varphi_f c_t w \frac{dP_{fs}}{dt} + w \frac{\partial(\rho_o u_x)}{\partial x} + \rho_0 \left(u_{wy} + u_{oy}\right)\Big|_{y=w/2} = 0 \qquad \text{A.22}$$

Substituting Darcy's law into the second term of Equation A.22 gives the following:

$$\rho_o \varphi_f c_t \frac{dP_{fs}}{dt} - \lambda_f \rho_o \left(\frac{\partial}{\partial x}\left(\frac{\partial P_{fs}}{\partial x} \right) + \frac{1}{\rho_o} \frac{\partial P_{fs}}{\partial x} \frac{\partial \rho_o}{\partial x} \right) + \rho_0 \left(u_{wy} + u_{oy}\right)\Big|_{y=w/2} = 0 \qquad \text{A.23}$$

where λ_f is mobility of the liquid mixture (water and oil) flowing through the fracture. We assume λ_f is constant and is equal to the water mobility within the fracture at residual oil saturation (Equation 3.11). We use the chain rule and the oil isothermal compressibility equation to make the following changes to the third term of Equation A.23.

$$\frac{1}{\rho_o} \frac{\partial P_{ofs}}{\partial x} \frac{\partial \rho_o}{\partial x} = \frac{1}{\rho_o} \frac{\partial \rho_o}{\partial P_{fs}} \left(\frac{\partial P_{fs}}{\partial x} \right)^2 = c_o \left(\frac{\partial P_{fs}}{\partial x} \right)^2 \qquad \text{A.24}$$

Substituting Equation A.23 into A.23 gives the following:

$$\varphi_f c_t \frac{dP_{fs}}{dt} - \lambda_f \left(\frac{\partial}{\partial x}\left(\frac{\partial P_{fs}}{\partial x} \right) + c_o \left(\frac{\partial P_{fs}}{\partial x} \right)^2 \right) + \left(u_{wy} + u_{oy}\right)\Big|_{y=w/2} = 0 \qquad \text{A.25}$$

The product of the oil isothermal compressibility term and squared pressure gradient in the x direction is a small number and can be neglected. Thus, Equation A.25 becomes

$$\varphi_f c_t \frac{dP_{fs}}{dt} - \lambda_f \frac{\partial^2 P_{fs}}{\partial x^2} + \left(u_{wy} + u_{oy}\right)\Big|_{y=w/2} = 0 \qquad \text{A.26}$$

The total flow velocity in the y direction evaluated at the fracture and the rock matrix interface is defined below:

$$u_y\Big|_{y=w/2} = \left(u_{wy} + u_{oy}\right)\Big|_{y=w/2} \qquad \text{A.27}$$

The total flow rate (volumetric flow rate per unit length of the fracture) is defined by the following equation:

$$u_y\Big|_{y=w/2} = \frac{q_y\Big|_{y=w/2}}{h} = \frac{q_f\Big|_{y=w/2}}{h} \qquad \text{A.28}$$

where h is the fracture height. We call the total flow rate in the y direction evaluated at the interface of the fracture and the rock matrix a cross-flow rate ($q_f(x,t)$). Substituting Equation A.28 into A.26 and rearranging the terms give

$$\frac{\varphi_f c_t}{\lambda_f}\frac{dP_{fs}(x,t)}{dt} = \frac{\partial^2 P_{fs}(x,t)}{\partial x^2} - \frac{q_f(x,t)\Big|_{y=w/2}}{\lambda_f h} \qquad \text{A.29}$$

$P_f(x,t)$ is the stimulated fracture pressure and defined by Equation 3.5. Substituting the stimulated fracture pressure term of Equation A.29 with Equation 3.5 gives Equation 3.10 we use in Chapter 3.

$$\frac{\varphi_f c_t}{\lambda_f}\frac{dP_f(x,t)}{dt} = \frac{\partial^2 P_f(x,t)}{\partial x^2} - \frac{q_f(x,t)\Big|_{y=w/2}}{\lambda_f h} \qquad 3.10$$

Appendix B

Derivation of Equation 3.70

The continuity equation for a flow of an oil phase within the two-dimensional rock matrix of Figure 3-1 is given below:

$$\frac{\partial(\rho_o \varphi_r S_o)}{\partial t} + \frac{\partial(\rho_o u_{ox})}{\partial x} + \frac{\partial(\rho_o u_{oy})}{\partial y} = 0 \qquad \text{B.1}$$

where ρ_o is oil density, φ_r is porosity of the rock matrix, S_o is the two-dimensional rock matrix oil saturation, u_{ox} is the oil phase Darcy velocity in the x direction, and u_{oy} is the oil phase Darcy velocity in the y direction. Applying product rule of differentiation to Equation B.1 and dividing both sides of the equation by ρ_o gives the following results:

$$\varphi_r \frac{\partial S_o}{\partial t} + S_o \frac{\partial \varphi_r}{\partial t} + \frac{S_o \varphi_r}{\rho_o} \frac{\partial \rho_o}{\partial t} + \frac{u_{ox}}{\rho_o} \frac{\partial \rho_o}{\partial x} + \frac{\partial u_{ox}}{\partial x} + \frac{u_{oy}}{\rho_o} \frac{\partial \rho_o}{\partial y} + \frac{\partial u_{oy}}{\partial y} = 0 \qquad \text{B.2}$$

Applying chain rule of differentiation to Equation B.2 gives

$$\varphi_r \frac{\partial S_o}{\partial t} + S_o \varphi_r \frac{1}{\varphi_r} \frac{\partial \varphi_r}{\partial P_{rs}} \frac{\partial P_{rs}}{\partial t} + S_o \varphi_r \frac{1}{\rho_o} \frac{\partial \rho_o}{\partial P_{rs}} \frac{\partial P_{rs}}{\partial t} + u_{ox} \frac{1}{\rho_o} \frac{\partial \rho_o}{\partial P_{rs}} \frac{\partial P_{rs}}{\partial x} + \frac{\partial u_{ox}}{\partial x} + u_{oy} \frac{1}{\rho_o} \frac{\partial \rho_o}{\partial P_{rs}} \frac{\partial P_{rs}}{\partial y} + \frac{\partial u_{oy}}{\partial y} = 0 \qquad \text{B.3}$$

where $P_{rs}(x, y, t)$ is the toe-dimensional stimulated rock matrix pressure The oil and rock matrix formation isothermal compressibility terms are defined below:

$$c_o = \frac{1}{\rho_o} \frac{\partial \rho_o}{\partial P_{rs}} \qquad \text{B.4}$$

$$c_r = \frac{1}{\varphi_r} \frac{\partial \varphi_r}{\partial P_{rs}} \qquad \text{B.5}$$

where c_o and c_r are the oil and formation isothermal compressibilities. Identifying the compressibility terms of Equation B.3 gives the following:

$$\varphi_r \frac{\partial S_o}{\partial t} + S_o \varphi_r c_r \frac{\partial P_{rs}}{\partial t} + S_o \varphi c_o \frac{\partial P_{rs}}{\partial t} + u_{ox} c_o \frac{\partial P_{rs}}{\partial x} + \frac{\partial u_{ox}}{\partial x} + u_{oy} c_o \frac{\partial P_{rs}}{\partial y} + \frac{\partial u_{oy}}{\partial y} = 0 \qquad \text{B.6}$$

Under a small compressibility assumption the 2nd, 3rd, 4th, and 5th terms of Equation B.6 can be neglected. Thus, Equation B.6 becomes:

$$\varphi_r \frac{\partial S_o}{\partial t} + \frac{\partial u_{ox}}{\partial x} + \frac{\partial u_{oy}}{\partial y} = 0 \qquad \text{B.7}$$

u_{ox} and u_{oy} are defined by Darcy's equation:

$$u_{ox} = \frac{k_r k_{ro}}{\mu_o} \frac{\partial P_{rs}(x,y,t)}{\partial x} \qquad \text{B.8}$$

$$u_{oy} = \frac{k_r k_{ro}}{\mu_o} \frac{\partial P_{rs}(x,y,t)}{\partial y} \qquad \text{B.9}$$

where k_r is the rock matrix absolute permeability, k_{ro}^{o} is the oil end point relative permeability of the rock matrix, and μ_o is the oil viscosity. Substituting velocity terms of Equation B.7 with Equations B.8 and B.9 gives the following equation for the oil saturation change with time within of the two-dimensional rock matrix:

$$\frac{\partial S_o(x,y,t)}{\partial t} = \frac{k_r k_{ro}}{\varphi \mu_o} \left(\frac{\partial^2 P_{rs}(x,y,t)}{\partial x^2} + \frac{\partial^2 P_{rs}(x,y,t)}{\partial y^2} \right) \qquad \text{B.10}$$

$P_{rs}(x,y,t)$ is defined by Equation 3.18. Taking derivative of $P_{rs}(x,y,t)$ with respect to x and y and substituting in Equation B.10 gives Equation 3.70 we use in Chapter 3.

$$\frac{\partial S_o(x,y,t)}{\partial t} = \frac{k_r k_{ro}}{\varphi \mu_o} \left(\frac{\partial^2 P_r(x,y,t)}{\partial x^2} + \frac{\partial^2 P_r(x,y,t)}{\partial y^2} \right) \qquad 3.70$$

where $P_r(x, y, t)$ is the incremental rock matrix pressure generated by the stimulation, time-harmonic water flooding.

References

Ashiepkov, J. S. 1989. Percolation characteristics of inhomogeneous porous media in seismic field. Soviet Mining Science, no. 5, p. 104-109.

Barabanov, V. L. and Pavlov, M. V. 2009. Increasing oil production from depleted fields through seismic stimulation. First Break, vol. 27, p. 97-102.

Belonenko, V. N., Miclyaev, M. I., and Goryunov, A. V. 1996. Vibroseismic technology of hydrocarbon yield and analogies of the Australian Pacific region and CIS. Oil and Gas Australia, July 1996.

Beresnev, I. A., and Johnson P. A. 1994. Elastic-wave stimulation of oil production: A review of methods and results. Geophysics, vol. 59, no. 6, p. 1000-1017.

Beresnev, I. A. 2006. Theory of vibratory mobilization on nonwetting fluids entrapped in pore constrictions. Geophysics, vol. 75, no. 6, p. N47-N56.

Cinco, H. L., Samaniego, F. V., and Dominquez, N. A. 1978. Transient pressure behavior for a well with a finite-conductivity vertical fracture. Paper SPE 6014 was presented at the SPE-AIME 51st Fall Technical Conference and Exhibition held in New Orleans, 3-6 October, 1976.

Duhon, R. D. and Campbell, J. M. 1965. The effect of ultrasonic energy on the flow of fluids in porous media. Paper SPE 1316 was presented at the Second Annual Eastern Regional Meeting of the SPE of AIME held in Charleston, West Va, 4-5 November, 1965.

Eckel, E. B. 1970. The Alaska earthquake March 27, 1964: lessons and conclusions. Geological survey professional paper 546.

Guo, X., Du, Z., Li, G., and Shu, Z. 2004. High frequency vibration recovery enhancement technology in the heavy oil fields of China. Paper SPE 86956 was presented at the SPE International Thermal Operations and Heavy Oil Symposium and Western Regional Meeting held in Bakersfliedl, Califormia, US, 16-18 March 2004.

Hamidi, H., Rafati, R., Junin, R. B., and Manan, M. A. 2012. A role of ultrasonic frequency and power on oil mobilization in underground petroleum reservoirs. Journal of Petroleum Exploration and Production Technology, p. 29-36.

Huh, C. 2006. Improved oil recovery by seismic vibration: a preliminary assessment of possible mechanisms. Paper SPE 103870 was presented at the first International Oil Conference and Exhibition in Mexico held in Cancun, Mexico, 31 August-2 September 2006.

Jeong, C., Huh, C., and Kallivokas, L. F. 2011. On the feasibility of inducing oil mobilization in existing reservoirs via wellbore harmonic fluid action. Journal of Petroleum Science and Engineering 76, p. 116-123.

Jeong, C. 2011. On an inverse-source problem for elastic wave-based enhanced oil recovery. Ph.D. Dissertation, the University of Texas at Austin.

Kostrov, S. A. and Wooden W. O. 2002. Mechanisms, field suitability, and case studies for enhancement of oil recovery and production using in-situ seismic stimulation. This paper was presented at the 16th International Symposium on Nonlinear Acoustics, Moscow, 9-23 August, 2002.

Kostrov, S. and Wooden, W. 2005. In situ seismic stimulation shows promise for revitalizing mature fields. Oil & Gas Journal, 18 April, 2005.

Kostrov, S. and Wooden, W. 2008. Possible mechanisms and case studies for enhancement of oil recovery and production using in-situ seismic stimulation. Paper SPE 114025 was prepared for presentation at the SPE Improved Oil Recovery Symposium held in Tulsa, OK, US, 19-23 April 2008.

Kouznetsov, O. L., Simkin, G. V., Chilingar, G. V., and Katz, S. A. 1998. Improved oil recovery by application of vibro-energy to waterflooded sandstones. Journal of Petroleum Science and Engineering 19, p. 191-200.

Kurlenya, M. V. and Serdyukov, S. V. 1999. Reaction of fluids of an oil-producing stratum to low-intensity vibro-seismic action. Journal of Mining Science, vol. 35, no. 2, p.113-119.

Lopukhov, G. P., and Nikolaevskii, V. N. 1995. The role of acoustic emission at vibroseismic stimulation of waterflooded oil reservoirs. The paper was presented at the 8th European IOR symposium, Vienna, Austria, 15-17 May, 1995.

Marshall, J., Kostrov, S., and Wooden, B. 2011. Seismic stimulation improves production from West Texas carbonate. Oil & Gas Journal, December 5, 2011.

Medlin, W. L., Masse, L., and Zumwalt, G. L. 1983. Method for recovery of oil by means of a gas drive combined with low amplitude seismic excitation. U.S.A. Patent 4 417 621.

Nikolaevskiy, V. N., Lopukhov, G. P., Liao, Y., and Economides M. J. 1996. Residual oil reservoir recovery with seismic vibrations. SPE Production & Facilities, May 1996.

Osika, D. G. 1981. Fluid regime of seismically active regions (Fluidniy rejim seismicheski-aktivnikh oblastey). Nauka Press (in Russian).

Parker, G. G. and Stringfield V. T. 1950. Effects of earthquakes, trains, tides, winds, and atmospheric pressure changes on water in the geologic formations of southern Florida. Economic Geology, vol. 45, p. 441-460.

Pride, S. R., Flekkoy, E. G., and Aursjo, O. 2008. Seismic stimulation for enhanced oil recovery. Geophysics, vol. 73, no. 5, September-October 2008, p. O23-O35.

Roberts, P. M., Sharma, A., Uddameri, V., Monagle, M, Dale, D. E., and Steck, L. K. 2001. Enhanced DNAPL transport in a sand core during dynamic stress stimulation. Environmental Engineering Science, vol. 18, no. 2, p. 67-80.

Roberts, P. M., Esipov I. B., and Majer E. L. 2003. Elastic wave stimulation of oil reservoirs: promising EOR technology? The Leading Edge, May 2003.

Roberts, P. M. and Abdel-Fattah, A. I. 2009. Seismic stress stimulation mobilizes colloids trapped in a porous rock. Earth and Planetary Science Letters 284, p. 538-543.

Serdyukov, S. V. and Kurlenya, M. V. 2007. Mechanism of oil production stimulation by low-intensity seismic fields. Acoustical Physics, vol. 53, no. 5, p. 618-628.

Simkin, E. M. and Surguchev, M. L. 1991. Advanced vibroseismic technique for water flooded reservoir stimulation, mechanism and field tests results. This paper was presented at the 6th European IOR Symposium held in Stavanger, Norway, 21-23 May, 1991.

Shook, M., Li, D., and Lake, L. W. 1992. Scaling immiscible flow through permeable media by inspectional analysis. In situ, 16 (4), p. 311-349.

Smirnova, M. N. 1968. Effect of earthquakes on the oil yield of the Gudermos field (Northeastern Caucasus). Isvestiya Academy of Sciences, USSR, Fizika Zemli (Physics of the Solid Earth), no. 12, 71-76.

Steinbrugge, K. V. and Moran, D. F. 1954. An Engineering study of the Sothern California Eurthquake of July 21, 1952 and its aftershocks. Bulletin of the seismological society of America, vol. 44, April, 1954.

Van der Bas, F., de Rouffignac, E., Zuiderwijk, P., and van Batenburg, D. 2004. Near wellbore stimulation by acoustic waves. Paper SPE 88767 was presented at the 11th Abu Dhabi International Petroleum Exhibition and Conference held in Abu Dhabi, UAE, 10-13 October, 2004.

Voytov, G. I., Osika, D. G., Grechukhina, T. G., and Plotnikov, I. A. 1972. Some geological and geochemical consequences of the Daghestan earthquake of May 14, 1970. Transactions of USSR Academy of Sciences, Earth Sciences Sections, 202, 576-579.

Walsh, M. P. and Lake, L. W. 2003. A generalized approach to primary hydrocarbon recovery. Elsevier, Amsterdam, The Netherlands, 2003.

White, J. E., Mikhaylova, N. G., and Lyakhovitskiy, F. M. 1975. Low-frequency seismic waves in fluid-saturated layered rocks. Earth Physics, no. 10, p. 44-52.

Zhu, T., Xutao, H., and Vajjha, P. 2005. Dawnhole harmonic vibration oil-displacement system: a new IOR tool. Paper SPE 94001 was presented at the SPE Western Regional Meeting held in Irvine, CA, US, 30 March-1 April, 2005.